UNIVERSITY *of the*
WESTERN CAPE

Green synthesis of novel nanostructured silicon semiconductor thin film material from sugarcane bagasse ash for solar energy materials.

by

Ntalane Sello Seroka
Student no (3754640)

A PhD thesis
Submitted to the Department of Chemical Science
University of Western Cape
Faculty of Science

In Fulfilment of the Requirements
For a Doctoral Degree in Chemistry
November 2022

Supervised by Prof. Lindiwe. E. Khotseng
Co-Supervised by Dr. Raymond. T Taziwa

UNIVERSITY *of the*
WESTERN CAPE

AFFIDAVIT: MASTER AND DOCTORAL STUDENTS
TO WHOM IT MAY CONCERN

This serves to confirm that I__Ntalane Sello Seroka_____
Full Name(s) and Surname

ID Number/ Passport___9309155641083_____

Student number__3754640____ enrolled for the Qualification _Doctoral degree in Chemistry__

_____

in the Faculty of Science

Herewith declare that my academic work is in line with the Plagiarism Policy of the University of the Western Cape with which I am familiar.

I further declare that the work presented in the ____Thesis____ is authentic and original unless clearly indicated otherwise and in such instances full reference to the source is acknowledged and I do not pretend to receive any credit for such acknowledged quotations, and that there is no copyright infringement in my work. I declare that no unethical research practices were used or material gained through dishonesty. I understand that plagiarism is a serious offence and that should I contravene the Plagiarism Policy notwithstanding signing this affidavit, I may be found guilty of a serious criminal offence (perjury) that would amongst other consequences compel the University of Johannesburg to inform all other tertiary institutions of the offence and to issue a corresponding certificate of reprehensible academic conduct to whomever requests such a certificate from the institution.

Signed at Cape Town _University of the Western Cape_____ on this _30__ of _November_____ 2022

Signature __ 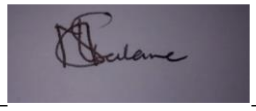 _____ Print name _Ntalane Sello Seroka___

STAMP: COMMISSIONER OF OATHS
Affidavit certified by a Commissioner of Oaths
This affidavit conforms with the requirements of the JUSTICES OF THE PEACE AND COMMISSIONERS OF OATHS ACT 16 OF 1963 and the applicable Regulations published in the GG GNR 1258 of 21 July 1972; GN 903 of 10 July 1998; GN 109 of 2 February 2001 as amended.

Dedication

I would like to dedicate this PhD degree to my parents, my father, David Makgwahleng Seroka, Brother Ntalane Cedric Molatudi and Sister(s) Mashego Khutsiso Seroka, Leseilane Salphina Molatudi, Ramakgahele Merriam Molatudi and Sethogola Dineo Seroka and my late mother, Linah Phaswane Seroka and my late brother Matsoshe Daniel Seroka for their loving support throughout my studies, and all the disadvantaged people in South Africa with no access to electricity.

Acknowledgements

I want to start by thanking God for providing me with the safety, power, and knowledge necessary to finish my studies. I also like to thank the organizations and people listed below:

- I would like to thank Prof. Lindiwe E. Khotseng and Dr. Raymond for their guidance, encouragement and counsel throughout the entire period of my research work. I am also indebted to my supervisors, and whose passion for their work inspired me to take my own passions seriously. I also give a special thanks to my best friend Auldrin Matlou, younger brother Godney Molatudi, big brother Ngwanatau Repshana Seroka , sister Lucia (Pheladi) Seroka and fiancée Maredi Balemira for their exceptional love and support during the period of my studies.

- I would also like to extend my heartfelt gratitude of appreciation to my supervisors Prof Lindiwe E. Khotseng, and Dr Raymond Taziwa, for their support and guidance during my research study.

- I am grateful to the National Research Foundation (NRF) of South Africa, Tertiary Institution Support Programme (TESP) and HySA Systems for their financial support during my studies at the University of the Western Cape.

- I would like to thank my family; my father, David Makgwahleng Seroka and my late mother, Linah Phaswane Seroka, my late brother Daniel Seroka, Khutsiso Seroka and Dineo Seroka for their love, patience and support during my studies at University of the Western Cape (UWC).

- Last but not least, I thank the technical staff of the Department of Chemistry, University of the Western Cape, Walter Sisulu University University of Cape Town and Ithemba labs for assistance with their facilities for use of research instruments. I thank the University of the Western Cape and its Department of Chemistry for presenting me with an opportunity to pursue my Doctoral studies.

Finally, maternal instincts, mother and supervision of Professor Lindiwe Khotseng when it was not fashionable to do so, she went extra mile in making sure I undertake the study with high emotional intelligence and support as a mother would to her Son, I am forever indebted.

Appendix

Presentations and Publications

In partial fulfilment of university regulations, the work presented in this thesis has been presented at conference(s) and submitted for publication in an international peer-reviewed scientific journal.

The PhD student Ntalane Sello Seroka was able to invent and pioneer the environmentally friendly synthesis of silica from sugarcane bagasse ash. The invention was published in the Conversation newsletter, which is a network of not-for-profit media outlets publishing news stories and research reports online with accompanying expert opinion and analysis. The study reported on the greener method of extracting silica using harmless chemicals that are easy to handle and eco-friendly. The method rivals the use of conventional strong and harsh chemicals to extract silica from sugarcane bagasse ash. It was novel, and it was published in a nanomaterials journal for the first time.

THE CONVERSATION

Academic rigour, journalistic flair

Search analysis, research, academics...

COVID-19 Arts + Culture Business + Economy Education Environment + Energy Health + Medicine Politics Science + Technology TC Afrique

Silicon is used in construction, microchips and more – 'green' methods could help extract it from sugarcane waste

Published: October 18, 2022 5.29pm SAST

When sugarcane bagasse is burned, the ash contains silica. The race is on to extract this for various uses. Geoff Sperring/Shutterstock

Email
Twitter 1
Facebook 26
LinkedIn
Print

In some parts of South Africa's Mpumalanga and KwaZulu-Natal provinces, sugarcane fields stretch as far as the eye can see. The crop is more than just a treat for those with a sweet tooth: in 2017 the country's sugar industry had an estimated value of more than R12 billion; of this, sugarcane production alone was worth R5.1 billion.

Authors

Lindiwe Khotseng
Professor, University of the Western Cape

Ntalane Sello
PhD Candidate, University of the Western Cape

Disclosure statement

Lindiwe Khotseng works for the University of the Western Cape. She receives funding from National Research Foundation (NRF) and Tertiary Education Support Program (TESP).

Ntalane Sello does not work for, consult, own shares in or receive funding from any company or organisation that would benefit from this article, and has disclosed no relevant affiliations beyond their academic appointment.

Partners

UNIVERSITY of the WESTERN CAPE

University of Western Cape provides support as a hosting partner of The Conversation AFRICA.

Attended Conferences

- A One Day Technical Seminar On Emerging Photovoltaic Technology and Green Hydrogen for Decarbonisation (EPTGH-22), 15 October 2022, online, Singapore.
- Seroka, N.S., Taziwa, R. and Khotseng, L. Conversion of Biomass into Valuable Silicon Material for Solar Energy Application. (*Oral presentation*), Global Conference on Renewable and Non Renewable Energy & Global Conference on Materials Science and Engineering, November 07-08, 2022 | Valencia, Spain

- Radio interview on SAFM 30 January 2023 (Silicon from sugarcane bagasse for microchips)

Publications

- Seroka, N.S., Taziwa, R. and Khotseng, L., 2022. Solar Energy Materials-Evolution and Niche Applications: A Literature Review. *Materials*, *15*(15), p.5338.
- Seroka, N.S., Taziwa, R.T. and Khotseng, L., 2022. Extraction and synthesis of silicon nanoparticles (SiNPs) from sugarcane bagasse ash: A Mini-Review. *Applied Sciences*, *12*(5), p.2310.
- Seroka, N.S., Taziwa, R. and Khotseng, L., 2022. Sugar Cane Bagasse Ash: An Agricultural Residue with Potential Rubber Filler Applications. (Book Chapter)
- Seroka, N.S., Taziwa, R. and Khotseng, L., 2022. Green synthesis of crystalline Silica from Sugarcane Bagasse Ash: Physico-chemical properties. *Nanomaterials*, *12*(13), p.2184. (Impact factor:5.7).
- Seroka, N.S., Taziwa, R. and Khotseng, L., 2023. Nanostructured Silicon Derived from an Agricultural Residue Bagasse Ash via Magnesiothermic Reduction Method. *Coatings*, *13*(2), p.221. (Impact factor:3.12).

Open Access Review

Extraction and Synthesis of Silicon Nanoparticles (SiNPs) from Sugarcane Bagasse Ash: A Mini-Review

by Ntalane Sello Seroka [1,*], Raymond T. Taziwa [2] and Lindiwe Khotseng [1]

[1] Department of Chemistry, University of the Western Cape, Robert Sobukwe Rd., Private Bag X17, Bellville 7535, South Africa

[2] Department of Applied Science, Faculty of Science Engineering and Technology, Walter Sisulu University, Old King William Town Road, Potsdam Site, East London 5200, South Africa

* Author to whom correspondence should be addressed.

Academic Editor: Anming Hu

Appl. Sci. **2022**, *12*(5), 2310; https://doi.org/10.3390/app12052310

Received: 14 January 2022 / Revised: 1 February 2022 / Accepted: 14 February 2022 / Published: 23 February 2022

Abstract

This current study reviews the utilization of the traditional extraction methods and latest findings in extraction of silica from agricultural wastes, in particular, sugarcane bagasse, using inorganic acids to produce nano-silicon. The three key processes discussed in detail include electrochemical, ball milling, and sol–gel processes. The sugarcane bagasse has been identified as the cheapest source of producing silica from the potential raw material for the preparation of nano-silicon. The acid-base extraction and precipitation methodology involves the use of bases like sodium hydroxide (NaOH) and potassium hydroxide (KOH), and acids such as hydrofluoric acid (HF), sulphuric acid (H_2SO_4), nitric acid (HNO_3), and hydrochloric acid (HCl) for the treatment of the ash. Sugarcane bagasse has notably emerged as an excellent and sustainable source of both tailored silica particles and bioenergy production. The ability to manipulate the engineered silica particles at the nano-level from sugarcane bagasse-based silica is explained in detail. Silica is a significant raw material with various industrial applications, with much research underway to extract it efficiently from industrial agro-waste, such as sugarcane bagasse. The production of highly pure silicon nanoparticles from sugarcane bagasse ash will serve as an important synthetic route in lowering the manufacturing costs and providing a low-cost polycrystalline silicon semiconductor for niche application in thin film solar technology. View Full-Text

Keywords: sugarcane; silica; SiNPs; silicon; green technology

OPEN ACCESS PEER-REVIEWED CHAPTER - ONLINE FIRST

Sugar Cane Bagasse Ash: An Agricultural Residue with Potential Rubber Filler Applications

WRITTEN BY

Ntalane S. Seroka, Raymond Taziwa and Lindiwe Khotseng

Submitted: June 2nd, 2022 , Reviewed: September 12th, 2022 , Published: November 9th, 2022

DOI: 10.5772/intechopen.108020

FROM THE EDITED VOLUME

Rubber Materials [Working Title]

Associate Prof. Gülşen Akın Evingür and Dr. Önder Pekcan

Abstract

South Africa produces approximately 7 million tons of sugarcane bagasse annually as an agricultural residue, which is treated as waste and its disposal is known to have negative impacts on the environment. To lessen reliance on petroleum and polymers, consideration is given on use of sugarcane bagasse ash as substitute materials for the development of fillers for rubber and other large-scale commodity polymers. This work reports on the mechanical, physiochemical, and structural properties of sugarcane bagasse ash to define the compatibility with the specific polymers that will pave way to the engineering of composites to utilize the potential benefits of these residue-derived fillers. The structural and morphological properties of the untreated and treated sugarcane bagasse ash were performed using XRD, FTIR, and SEM-EDX, respectively. The obtained results confirmed the successful treatment of the sugarcane bagasse ash. The study was successful in showing that sugarcane bagasse ash as potential filler in rubber polymer matrix is a natural resource of silica, which is sustainable and cost-effective, thus should be harnessed for industrial purposes in South Africa.

Keywords

sugarcane bagasse ash(SCBA) | fillers | rubber materials | composites | eco-friendly

Open Access Article

Green Synthesis of Crystalline Silica from Sugarcane Bagasse Ash: Physico-Chemical Properties

by Ntalane S. Seroka [1,*], Raymond Taziwa [2] and Lindiwe Khotseng [1,*]

[1] Department of Chemistry, University of the Western Cape, Robert Sobukwe Rd, Private Bag X17, Bellville 7535, South Africa

[2] Department of Applied Science, Faculty of Science Engineering and Technology, Walter Sisulu University, Old King William Town Road, Potsdam Site, East London 5200, South Africa

* Authors to whom correspondence should be addressed.

Academic Editor: Manolis Stratakis

Nanomaterials **2022**, *12*(13), 2184; https://doi.org/10.3390/nano12132184

Received: 18 May 2022 / Revised: 17 June 2022 / Accepted: 22 June 2022 / Published: 25 June 2022

Abstract

Sugarcane bagasse South Africa is an agricultural waste that poses many environmental and human health problems. Sugarcane bagasse dumps attract many insects that harm the health of the population and cause many diseases. Sugarcane ash is a naturally renewable source of silica. This study presents for the first time the extraction of nanosilica from sugar cane bagasse ash using L-cysteine hydrochloride monohydrate acid and Tetrapropylammonium Hydroxide. The structural, morphological, and chemical properties of the extracted silica nanoparticles was cross examined using XRD, FTIR, SEM, and TGA. SEM analysis presents agglomerates of irregular sizes. It is possible to observe the structure of nanosilica formed by the presence of agglomerates of irregular shapes, as well as the presence of some spherical particles distributed in the structure. XRD analysis has revealed 2θ angles at 20, 26, 36, 39, 50, and 59 which shows that each peak on the xrd pattern is indicative of certain crystalline cubic phases of nanosilica, similar to results reported in the literature by Jagadesh et al. in 2015. The crystallite size estimated by the Scherrer equation based on the aforementioned peaks for ca-silica and L-cys-silica for the extracted particles had an average diameter of 26 nm and 29 nm, respectively. Furthermore, it showed a specific surface area of 21.6511 m^2/g and 116.005 m^2/g for ca-silica and L-cys silica, respectively. The Infrared (IR) spectra showed peaks at 461.231 cm^{-1}, 787.381 cm^{-1} and 1045.99 cm^{-1} which corresponds to the Si~O~Si bending vibration, the Si~O~Si stretch vibration, and the Si~O~Si stretching vibration, respectively. This confirms the successful extraction of nanosilica from sugar cane bagasse ash. TGA analysis has revealed that the as received sugarcane bagasse has high loss on ignition (LOI) of 18%, corresponding to the presence of the unburnt or partial burnt particles, similar to results reported by Yadav et al. This study has shown that sugar cane bagasse ash is a natural resource of silica which should be harnessed for industrial purposes in south Africa. View Full-Text

Keywords: **green synthesis; silica; tetrapropylammonium hydroxide; citric acid; L-cysteine hydrochloride monohydrate; sugarcane bagasse ash**

coatings

Submit to this Journal

Review for this Journal

Edit a Special Issue

Article Menu

Academic Editors

Mehmet Yilmaz

Nagabandi Jayababu

Subscribe SciFeed

Recommended Articles

Related Info Link

More by Authors Links

Article Views 426

Table of Contents

- Abstract
- Introduction

Open Access Article

Nanostructured Silicon Derived from an Agricultural Residue Bagasse Ash via Magnesiothermic Reduction Method

by Ntalane S. Seroka [1,*], Raymond Taziwa [2] and Lindiwe Khotseng [1,*]

[1] Department of Chemistry, University of the Western Cape, Robert Sobukwe Road, Private Bag X17, Bellville 7535, South Africa

[2] Department of Applied Science, Faculty of Science, Engineering and Technology, Walter Sisulu University, Old King William Town Road, Potsdam Site, East London 5200, South Africa

* Authors to whom correspondence should be addressed.

Order Article Reprints

Received: 15 December 2022 / Revised: 12 January 2023 / Accepted: 14 January 2023 / Published: 17 January 2023

(This article belongs to the Special Issue Nanoparticles for Energy, Sensing and Biomedical Applications)

Download Browse Figures Versions Notes

Abstract

This study presents the magnesiothermic reduction of silica into silicon. This reduction process occurs at a lower reaction temperature than its carbothermal counterpart. Furthermore, silica was extracted from sugarcane bagasse ash via a thermo-chemical treatment method using, for the first time, L-cysteine chloride monohydrate and used as a precursor in the production of silicon using magnesiothermic reduction. The as-synthesized nanocrystalline silicon's physicochemical properties were investigated using XRD, Raman, FTIR, BET, and SEM. A peak at 2 of 28.2 with a crystallite size of 32 nm was discovered using X-ray diffraction spectroscopy. The pronounced peak around 518 cm^{-1} was observed from the Raman spectrum, characteristic of crystalline silicon. The FTIR analysis showed two sharp peaks at 446 cm^{-1} and 1056 cm^{-1}, indicative of the Si-O rocking mode and Si-O-Si stretching mode functional groups present. N_2 physisorption at 77 K reveals that the surface area, pore volume, and pore diameter of the as-synthesized silicon were 73 m^2/g, 0.23 cm^3/g, and 12 nm, respectively. In this study, we were able to produce silicon from silica extracted from SCBA using the magnesiothermic reduction method in a tube furnace, which has potential for thin-film solar cells.

Keywords: sugarcane bagasse ash; silica; magnesiothermic reduction; silicon; solar cell

Nomination(s)


Global Young Scientists Summit 2023
Congratulations on being selected as a Viewer for GYSS 2023!
Excite | Engage | Enable
Dear Sello, congratulations on being selected as a Viewer in the Global Young Scientists Summit (GYSS) 2023 from 17 - 20 January 2023.
You will have the opportunity to join in all of the virtual sessions happening LIVE in Singapore. Look forward to an exciting lineup of plenary lectures and panel discussions, led by some of the top minds around the world.

Acronyms

Al	Aluminium
A	Amps
Ag	Silver
FTIR	Fourier Transform Infrared Spectroscopy
XRD	X-ray diffraction spsectroscopy
UV/Vis	Ultraviolet-visible spectrophotometer
SEM	Scanning electron microscope
TEM	Transmission electron microscope
EDX	Energy dispersive x-ray spectroscopy
BET	Brunauer–Emmett–Teller
TGA	Thermogravimetric analysis
XRF	X-ray fluorescence spectroscopy
E-beam	Electron-beam
PVD	Physical vapour deposition
FF	Fill factor
Voc	Open circuit Voltage
Jsc	Short circuit current density
SiNPs	Silicon Nanoparticles
SCBA	Sugar cane Bagasse Ash
J_{sc}	Short circuit current density
mg/L	Milligrams per litre
Mg	Magnesium
mW	Milliwatts
Np	Nanoparticles
Pmax	Maximum Power
%	Percentage
Si	Silicon
SiSC	Silicon solar cell
V	Volts
PCE	Power Conversion Efficiency
Nc-Si	Nanocrystalline silicon

Abstract

The sun is considered the most abundant source of renewable and clean energy. With silicon being the most common element used for the direct conversion of solar energy into electrical energy, solar cells have, over the years, been the corresponding technology to the problem of energy on our planet. This technology is most common in aerospace applications. Nonetheless, the application in terrestrial areas is currently hampered by the high cost of photovoltaic modules. Therefore, the study focuses on the extraction and synthesis of silicon nanostructures from sugarcane bagasse ash. Notably, silicon is found in this feedstock in the form of silicic acid and predominantly as silica. The study's main goal could be achieved through the sustainable extraction of silica from sugarcane bagasse ash and subsequent transformation into nanostructured silicon.

Agricultural wastes are considered one of the most promising sources of silica. It essentially contains other minerals, including amorphous silica, which can be readily purified by dissolving in an alkaline solution. In addition, there are several reserves large enough across the globe to get the silica at a reduced cost.
The appealing properties of photovoltaic technology have fuelled the need for a transition away from fossil fuel-based energy sources. Consequently, the energy produced from photovoltaics is technologically feasible (economically viable), environmentally benign, sustainable, and socially equitable.

To investigate the structural characteristics of these solid-state materials, X-ray diffraction spectroscopy, Fourier transform infrared (FTIR) spectroscopy, Raman spectroscopy, and transmission electron microscopy studies were conducted. The optical properties were studied via UV and Vis to determine the band gap and confirm the doping process of silicon. The IR spectra was able to confirm the key functional groups present in the extracted sample(s) as silica due to the presence of Si-O-Si groups. To evaluate the successful synthesis of silica, XRD was used, and characteristic peak(s) of a highly crystalline nature were observed for the silica sample. Silica samples were then reacted with magnesium (Mg) in an inert atmosphere of nitrogen in a tube furnace for a duration of 4 hours at 700 ℃, due to Mg's melting point of around 650 ℃.

The sugarcane bagasse ash (scba) nano silicon was also confirmed via FTIR, XRD studies. And, complimentary studies were further performed using scanning electron microscope (SEM) coupled with energy dispersive x-ray (EDX) for elemental composition and mapping, essentially supported results already conducted.

According to this study, sugarcane bagasse ash contains highly crystalline silica, which may be affected by leaching. The extracted crystallite size ca-silica and L-cys-silica had an average diameter of 26 nm and 29 nm, respectively, as well as specific surface areas of 21.6511 m^2/g and 116.005 m^2/g for ca-silica and L-cys silica, respectively. Peaks in the FTIR spectra were found at 461.231 cm^{-1}, 787.381 cm^{-1}, and 1045.99 cm^{-1}, corresponding to the $Si-O-Si$ bending vibration, $Si-O-Si$ stretch vibration, and $Si-O-Si$ stretching vibration, respectively. The nanosilicon nanoparticles were successfully synthesized using biosilica extracted from sugarcane bagasse ash (SCBA). Nano-physical silicon's properties and quantitative elemental composition were investigated. As-synthesized silicon had surface area, pore volume, and pore diameter of 74 m^2/g, 0.23 cm^{-1}, and 12 nm, respectively. A frequency downshift is caused by a decrease in particle size as a result of particle surface oxidation, according to Raman spectroscopy. The FTIR spectrum confirms the increase in oxidation of the particles during deionized water washing, with peaks at 446 cm^{-1} and 1056 cm^{-1} corresponding to rocking and stretching modes, respectively. According to the morphological, textural, and structural properties determined in this study, the as-produced material has highly rich silicon with a well-defined crystalline structure of 32 nm diameter.

A typical silicon solar cell was inspired for this study, whereby it consists primarily of n-type and p-type layers, and rear contact as metallic silver (Ag). The anode was the ITO coated glass substrates which can be a dual layer as transparent conductive oxide (TCO) layer and hole transporting layer while the back contact was Ag. Metallic silver was chosen because it does not diffuse easily on the positive layer to avoid creating heavily doped positive layer. The results obtained in this study (0.01%) were significantly low for crystalline silicon solar cells with an efficiency of more than 25%.

Keywords: Sugarcane bagasse, silica, silicon, solar energy materials.

TABLE OF CONTENTS

LIST OF FIGURES

LIST OF TABLES

Table ***Description*** ***Page***

Chapter 1

1 Introduction

Due to the world's continuously growing population, which still produces electricity from non-renewable energy sources, energy consumption has become a major worry throughout the years. Fossil fuels, which are non-renewable sources, are currently used to produce most of the energy used in the world, along with detrimental industrial byproducts such greenhouse gases [1]. As a result, they damage the ecosystem and pollute the air and atmosphere (microorganisms). A threat to the value of human life is also present. In addition, the majority of industries need enough electricity to function at their best for the foreseeable future [1, 2].

As a result, the global community desires an immediate and promising alternative for the production of electricity that is both promising and sustainable. Notably, as non-renewable energy sources become depleted, photovoltaic technologies are being recognized as the best solution for dealing with and meeting the ever-increasing energy demand and consumption. Solar and wind power generation have received a lot of attention due to the rising demand for clean and renewable energy because they rely on the sun and wind [3, 4].

One of the most extensively researched and debated areas in energy politics has been harnessing the sun's energy to produce electricity [4]. Solar technology is currently dominated by silicon-based materials, which account for approximately 80-90% of PV modules and have proven to be a reliable technology in this field. Furthermore, silicon is the primary material used in bulk (1st generation), thin film (2nd generation), and nano-structured (3rd generation) photovoltaic solar cells [5, 6].

Since silicon dominates the PV market and is directly extracted from raw materials, the price of silicon wafers and the lengthy energy payback period are the key constraints. Due to the low absorption of Si material, improvements have been made for this technology to lower the cost. Despite this, ion implantation and other Si fabrication procedures are still pricy and challenging [7, 8].

Environmentally friendly and capable of producing electrical energy at a lesser cost are photovoltaics. Due to their low material consumption and increasing efficiency, thin-film solar cells are appealing options in the field of photovoltaics. Silicon (Si), copper indium gallium selenide (CIGS), and star absorber materials like cadmium telluride are examples of thin film technologies that have undergone substantial study and are still being researched (CdTe). Although crystalline silicon solar cells presently hold a market share of more than 55%, CIGS and CdTe technologies' module efficiencies are approximately on par with those of crystalline solar cells [9, 10].

Thin films have numerous advantages, including low material consumption, production flexibility, energy payback time, and cost effectiveness. Despite the above-mentioned property (power conversion from these devices with a massive amount of sun energy), photovoltaic devices still produce about 30% or less of the electricity they consume from roughly 80–90% of the sun's energy [10].

The main focus when it comes to new materials for thin film technology is on perovskites for solar technology. In this study, i suggest employing sugarcane bagasse ash (SCBA), an unique nanostructured silicon semiconductor thin film raw material, for solar energy materials. At the moment, SCBA serves as the primary energy source for fuel in boilers that generate electricity.

According to recent research, SCBA is high in mineral content, including silicon, iron, and other minerals. Silicon is found primarily in the form of silicic acid and accounts for approximately 380 kg/ha of silicon composition in a 12-month-old crop. It is worth noting that pure silicon can be obtained from silicate (), which has been reported to be biocompatible and environmentally friendly [11-33].

Furthermore, it is worth noting that residual sugarcane bagasse (RSB) can also be to produce megasse, which is a specific type of paper. Among the various applications in electricity generation, gas generation, charcoal briquettes, pulp, paper, and concrete production, RSB remains the most utilized and preferred method. Sugarcane compositions reveal that silicon is the most absorbed mineral content, which is predominantly in the form of silicic acid (H_4SiO_4) [14–16].

It has been reported that natural silica is safe to handle and can be extracted easily and cheaply from a variety of sources. The fate and inadequate disposal of bagasse pose a challenge to the environment [14].

After careful consideration, we chose this feedstock, sugarcane bagasse, as a sustainable source to produce green nanostructured silicon semiconductor thin film suitable for solar energy materials. Thus, the work is termed *"the conversion of waste to wealth.*"

1.1. Problem statement

Knowledge gap:

Due to the rising demand for clean energy production and storage, energy storage systems (ESS) have gained considerable momentum due to concerns over technological advancement and the impact on the environment. Therefore, in the 21st century, these areas have led to the desire to search for alternative sources of renewable energy. Currently, non-renewable energy sources pose a threat to electrical energy generation, which is dominated by fossil fuels because of the continuous increase in energy demand. Fossil fuels are the main contributors to global warming with CO_2 emissions, which has made them the limiting issue in global energy politics [17].

Henceforth, the use of energy produced from wind and solar resources tends to be variable and uncontrollable, despite their abundance and readily available nature. Presently, an approach to combat energy-related issues is to use electrical energy storage (EES), especially storing energy in excess and releasing it whenever required. It is worth noting that it requires a very compatible and sustainable, highly efficient solar cell. Therefore, the development of cost-effective solar cells that can be vastly used in terrestrial areas could be an efficient tool to combat the ever-increasing energy demand [17, 18].

The use of raw materials to get energy would be beneficial and a scientific contribution to knowledge.

1.2. Rationale and motivation of the study

Since the dawn of humanity, people have utilized and relied on renewable sources of energy to survive: wood for cooking and heating, wind and water for milling grain, and solar for lighting fires. Additionally, about 150 years ago, people developed the technology to extract energy from the ancient fossilized remains of plants and animals. These super-rich but limited energy sources (coal, oil, and natural gas) eventually and quickly replaced wood, wind, solar, and water as the primary fuel sources [19].

Coal, nuclear energy, oil, and natural gas are non-renewable energy sources that are in short supply. This is typically caused by how slowly they are replaced. Renewable resources are naturally renewed over a brief period. Solar, wind, water (hydro), biomass, and geothermal energy are the top five sources of renewable energy. As a result, the process of extracting energy from the aforementioned energy sources has been well researched over time. Thus, customized synthetic approaches for a variety of materials have been developed to reduce the cost of the finished good [20–22].

The synthesis of silicon wafer for solar technology is an expensive technology, which ultimately makes silicon-based solar cells more expensive. The costs limit their terrestrial use to some extent. However, this can be overcome by resorting to newer methods and cheaper raw materials for the synthesis of silicon-based solar devices. As the global urgency to combat the energy crisis has grown, an efficient transition from conventional electricity generation to non-renewable energy sources has occurred [23-26].

Therefore, synthesis of silicon thin films from raw materials such as biomass (an industrial term for industrial wastes) is possible. This will add value by lowering costs and increasing the widespread effective use of environmentally friendly materials. The main motivation for using Si is that it is an abundant mineral resource, irrespective of geopolitical issues. Additionally, Si solar cells have fewer toxicity issues than other heavy-metal-based devices, *i.e.*, CdTe [27, 28].

Due to the trade-off between cost and efficiency of currently available solar cells, the solar cell markets are still lagging. Although state-of-the-art silicon solar cells have already made

it to commercialization, they still suffer from high manufacturing costs, a scarcity of silicon, and complex fabrication processes. Second to the silicon solar cells in terms of solar-to-electricity conversion efficiency are organic solar cells, which have high manufacturing costs, material loss during fabrication, and narrow absorption wavelengths.

1.3. Aims and Objectives of the study

Towards the development of novel nanostructured silicon semiconductor thin film (TF) for solar energy materials. A plausible approach to the research would be to create an effective and efficient p-n junction thin film cell made of p- and n-doped SiNPs with different band gaps in order to target the entire solar spectrum and thus have a high energy harvesting potential. Thus, the aim was achieved through the execution of the following objectives:

- Detailed review on current solar energy materials and their niche applications.
- Review on extraction of silicon derived from sugarcane bagasse ash.
- Green synthesis of nanosilica from sugarcane bagasse ash.
- Reduction of nanosilica into nanostructures silicon via magnesiothermic reaction.
- The prepared Silica, SiNPs and thin films were characterised using techniques such as; Transmission Electron Microscope (TEM) and Scanning Electron Microscopy (SEM), Atomic Force Microscopy (AFM) and Ultraviolet visible (UV-vis) spectroscopy.

- The purity of the prepared SiNPs was evaluated using spectroscopic and microscopic analysis.
- Fabrication of nanostructured silicon thin films on ITO glass substrates using e-beam PVD technique

- Optical and structural properties were determined using UV/Vis, PL and Raman spectroscopy, respectively.
- The power conversion efficiency (PCE) was determined by illuminating the cells with simulated sunlight AM1.5 with specific voltage and measuring current output.

1.4. Overview of this work

A thorough review of the literature is given in **Chapter 2** on specific features, such as the advantages and prospects of the first generations of solar cells made of mono- and polycrystalline silicon. A review of the second generation of solar cells, including amorphous silicon and thin-film solar cells, is also included in **Chapter 2**. The third generation of solar cells, as well as the development of photovoltaic materials such as polymers, perovskites, quantum dots, and dye-synthesized materials, are covered in detail in this chapter.

Chapter 3 provides the detailed experimental procedures utilized in the preparation of silicon nanostructures**. Chapter 3** also provides a step-step procedure used in the extraction of silicon. A theoretical background on the analytical instruments used to evaluate the morphological, structural, elemental, and electrical properties of the prepared nanostructures is briefly provided in **Chapter 3. Chapter 3** also details the actual techniques employed in the cross-examination of the nanostructured materials.

A novel method for preparing silica nanostructures is presented in **Chapter 4**. This is based on a paper titled "Green synthesis of crystalline silica from sugarcane bagasse ash: physico-chemical properties." The morphological, elemental, structural, and thermogravimetric properties of silicon nanostructures prepared for the first time from sugar cane bagasse ash using L-cysteine hydrochloride monohydrate acid and tetrapropylammonium hydroxide are presented and discussed in **Chapter 4.**

Chapter 5: describes a magnesiothermic reduction technique of silica into nanostructured silicon. The structural, morphological, elemental, and textural qualities are presented in **Chapter 5**. These characteristics demonstrated the sustainability of sugarcane bagasse ash as a silicon source.

Chapter 6: This chapter discusses the fabrication and characterization of thin films of doped silicon nanostructures, as well as the optical, morphological, and electrical properties of the devices. An e-beam physical vapor deposition technique is used to deposit these thin films on ITO glass substrates.

Chapter 7: Conclusions are drawn in Chapters 4, 5, and 6 based on interpreted data and in-depth analysis. This section also includes recommendations and future research.

Appendix: The list of the research outputs as results of the work done by the PhD candidate.

1.5. References

[1] Scrosati, B. and Garche, J., 2010. Lithium batteries: Status, prospects and future. *Journal of power sources*, *195*(9), pp.2419-2430.

[2] Aberle, A.G., 2009. Thin-film solar cells. *Thin solid films*, *517*(17), pp.4706-4710.

[3] Green, M.A., Emery, K., Hishikawa, Y., Warta, W. and Dunlop, E.D., 2015. Solar cell efficiency tables (Version 45). *Progress in photovoltaics: research and applications*, *23*(1), pp.1-9.

[4] Lee, T.D. and Ebong, A.U., 2017. A review of thin film solar cell technologies and challenges. *Renewable and Sustainable Energy Reviews*, *70*, pp.1286-1297.

[5] Wolden, C.A., Kurtin, J., Baxter, J.B., Repins, I., Shaheen, S.E., Torvik, J.T., Rockett, A.A., Fthenakis, V.M. and Aydil, E.S., 2011. Photovoltaic manufacturing: Present status, future prospects, and research needs. *Journal of Vacuum Science & Technology A: Vacuum, Surfaces, and Films*, *29*(3), p.030801.

[6] Guo, Q., Ford, G.M., Yang, W.C., Walker, B.C., Stach, E.A., Hillhouse, H.W. and Agrawal, R., 2010. Fabrication of 7.2% efficient CZTSSe solar cells using CZTS nanocrystals. *Journal of the American Chemical Society*, *132*(49), pp.17384-17386.

[7] Luque, A. and Hegedus, S. eds., 2011. *Handbook of photovoltaic science and engineering*. John Wiley & Sons.

[8] Catchpole, K.R., McCann, M.J., Weber, K.J. and Blakers, A.W., 2001. A review of thin-film crystalline silicon for solar cell applications. Part 2: Foreign substrates. *Solar Energy Materials and Solar Cells*, *68*(2), pp.173-215.

[9] Wang, W., Winkler, M.T., Gunawan, O., Gokmen, T., Todorov, T.K., Zhu, Y. and Mitzi, D.B., 2014. Device characteristics of CZTSSe thin-film solar cells with 12.6% efficiency. *Advanced Energy Materials*, *4*(7), p.1301465.

[10] Shah, A., Torres, P., Tscharner, R., Wyrsch, N. and Keppner, H., 1999. Photovoltaic technology: the case for thin-film solar cells. *science*, *285*(5428), pp.692-698

[11] Pandey, A., Soccol, C.R., Nigam, P. and Soccol, V.T., 2000. Biotechnological potential of agro-industrial residues. I: sugarcane bagasse. *Bioresource technology*, *74*(1), pp.69-80.

[12] Savant, N.K., Korndörfer, G.H., Datnoff, L.E. and Snyder, G.H., 1999. Silicon nutrition and sugarcane production: a review. *Journal of plant nutrition*, *22*(12), pp.1853-1903.

[13] Norsuraya, S., Fazlena, H. and Norhasyimi, R., 2016. Sugarcane bagasse as a renewable source of silica to synthesize santa barbara amorphous-15 (SBA-15). *Procedia Eng*, *148*, pp.839-846.

[14] Canilha, L., Chandel, A.K., Suzane dos Santos Milessi, T., Antunes, F.A.F., Luiz da Costa Freitas, W., das Graças Almeida Felipe, M. and da Silva, S.S., 2012. Bioconversion of sugarcane biomass into ethanol: an overview about composition, pretreatment methods, detoxification of hydrolysates, enzymatic saccharification, and ethanol fermentation. *Journal of Biomedicine and Biotechnology*, *2012*.

[15] Nikodinovic-Runic, J., Guzik, M., Kenny, S.T., Babu, R., Werker, A. and Connor, K.E., 2013. Carbon-rich wastes as feedstocks for biodegradable polymer (polyhydroxyalkanoate) production using bacteria. In *Advances in applied microbiology* (Vol. 84, pp. 139-200). Academic Press.

[16] Norsuraya, S., Fazlena, H. and Norhasyimi, R., 2016. Sugarcane bagasse as a renewable source of silica to synthesize santa barbara amorphous-15 (SBA-15). *Procedia Eng*, *148*, pp.839-846.

[17] Scrosati, B. and Garche, J., 2010. Lithium batteries: Status, prospects and future. *Journal of power sources*, *195*(9), pp.2419-2430.

[18] Paravasthu, R., 2012. Synthesis and characterization of lithium-ion cathode materials in the system (1-xy) LiNi1/3Mn1/3Co1/3O2· xLi2MnO3· yLiCoO2. *2000-2019-CSU Theses and Dissertations*.

[19] Tahvonen, O. and Salo, S., 2001. Economic growth and transitions between renewable and nonrenewable energy resources. *European Economic Review*, *45*(8), pp.1379-1398.

[20] Demirbas, A., Sahin-Demirbas, A. and Hilal Demirbas, A., 2004. Global energy sources, energy usage, and future developments. *Energy Sources*, *26*(3), pp.191-204.

[21] Shafiee, S. and Topal, E., 2009. When will fossil fuel reserves be diminished? *Energy policy*, *37*(1), pp.181-189.

[22] Stein, E.W., 2013. A comprehensive multi-criteria model to rank electric energy production technologies. *Renewable and Sustainable Energy Reviews*, *22*, pp.640-654.

[23] De Wolf, S., Descoeudres, A., Holman, Z.C. and Ballif, C., 2012. High-efficiency silicon heterojunction solar cells: A review. *green*, *2*(1), pp.7-24.

[24] Chopra, K.L., Paulson, P.D. and Dutta, V., 2004. Thin-film solar cells: an overview. *Progress in Photovoltaics: Research and applications*, *12*(2-3), pp.69-92.

[25] Pagliaro, M., Ciriminna, R. and Palmisano, G., 2008. Flexible solar cells. *ChemSusChem*, *1*(11), pp.880-891.

[26] Tao, M., 2008. Inorganic photovoltaic solar cells: silicon and beyond. *The Electrochemical Society Interface*, *17*(4), pp.30-35.

[27] Mitzi, D.B., Gunawan, O., Todorov, T.K., Wang, K. and Guha, S., 2011. The path towards a high-performance solution-processed kesterite solar cell. *Solar Energy Materials and Solar Cells*, *95*(6), pp.1421-1436.

[28] Sharma, S., Jain, K.K. and Sharma, A., 2015. Solar cells: in research and applications—a review. *Materials Sciences and Applications*, *6*(12), p.1145.

Chapter 2

Synopsis

Currently, non-renewable energy sources, which release dangerous greenhouse gases, account for the majority of the energy produced worldwide. The sun is also recognized as the most plentiful and pure form of renewable energy. The most obvious answer to the current energy crisis is to use solar cell technologies to harvest energy from the sun. Due to its inherent high efficiency of over 25% at converting solar energy into electricity, silicon solar cell technology has a large market share; however, the technology has not completely replaced fossil fuels as a source of energy. This chapter provides a detailed literature review of the progress made in improving first, second, and third generation solar cells.

In Chapter 2, a thorough review of the literature on specific features, such as the advantages and prospects of the first generations of mono- and polycrystalline silicon solar cells, is provided. Chapter 2 also includes a discussion of the second generation of solar cells, such as amorphous silicon and thin-film solar cells. This chapter delves into the third generation of solar cells as well as the advancement of photovoltaic materials such as polymers, perovskites, quantum dots, and dye-synthesized materials.

The chapter concludes with a review of traditional extraction methods as well as the most recent findings in the extraction of silica from agricultural wastes, specifically sugarcane bagasse, using inorganic acids to produce nano-silicon. Electrochemical, ball milling, and sol-gel processes are the three key processes discussed in detail. The most cost-effective source of silica from potential raw materials for nanosilicon preparation has been identified as sugarcane bagasse. Furthermore, in order to reduce reliance on petroleum and polymers, a book chapter considers the use of sugarcane bagasse ash as a substitute material for the development of fillers for rubber and other large-scale commodity polymers.

2 Brief history of solar energy materials (Historical background of first, second and third generation solar cells)

2.1 Historical background of first, second and third generation solar cells

The researcher's contributions to sustainability and quality of life have led to the desire to develop, manufacture, and find new technologies based on renewable energy resources. Solar energy has proven to be sustainable and has attracted great attention, with the sun considered the most abundant source of clean, renewable energy. This makes solar cell technology economically viable and sustainable and allows for potential reductions in greenhouse gases, thus making it an ideal source of energy while avoiding shortcomings associated with energy and the environment [1–4].

Figure 2.1 presents the predicted and potential role of various sources in the future, with the stages of eco-friendly and renewable energy sources. The energy sources presented in Figure 2.1 show water, biomass, wind, solar, and geothermal energy. All these energy sources are environmentally friendly and sustainable. Of the aforementioned clean energy sources, solar technology promises to be the most prolific and fast-growing sustainable renewable energy source. [5].

The anticipation is solely based on the fact that the amount of CO2 will consistently and relatively remain below 450 ppm/year. Figure 2.1 significantly indicates that by 2050, solar energy is predicted to play a big role among the renewable sources in contributing to this, a study done by Wang Y in 2017, reported in his book [5–7].

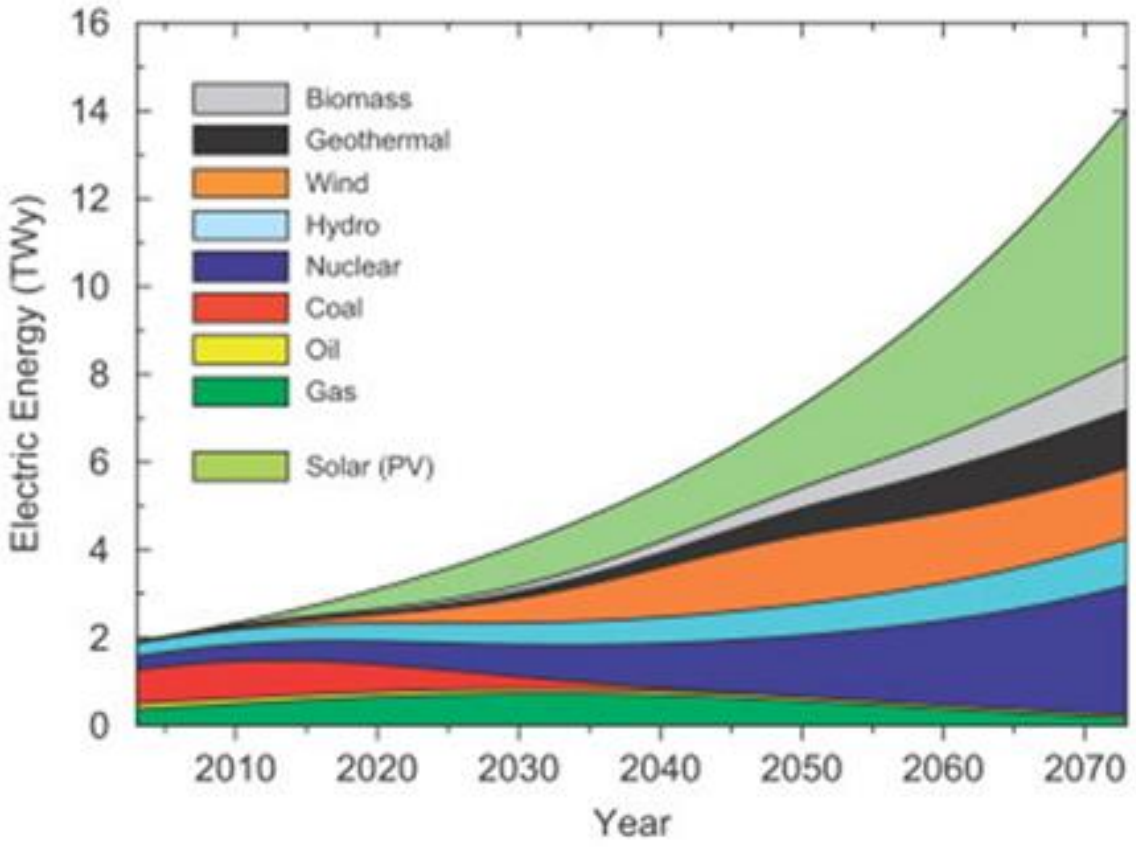

Figure 2.1. *Presents electrical energy production for the next 6 decades (with consideration that the emission of CO2 will be held under 450 ppmv). Re-used with permission [5], Copyright © 2008 Elsevier.*

Photovoltaics have the ability to generate electrical energy at a lower cost and they are eco-friendly. Thin film solar cells are favorable candidates in the field of photovoltaics because of their minimum material usage and rising efficiencies. The three most commonly known thin film technologies that are extensively studied and still under intensive investigation include α-silicon (α-Si), copper indium gallium selenide (CIGS), and star absorber materials, such as cadmium telluride (CdTe). The conventional inorganic silicon modules, interchangeably known as first generation solar cells, are the leading solar technology for most of residential and industrial markets. Presently, crystalline silicon wafers based on a high-quality float zone have realized a competitive advantage over traditional solar cells via the utilization of the carrier-selective layer approach [8].

The amorphous silicon incorporated into an intrinsic hydrogen layer placed on one or two sides of the float zone silicon wafer serves as a passivation layer for pre-induced carrier-selective contact. Moreover, the aforementioned architecture recorded a power conversion

efficiency of 26.6%, derived from the matrix of interdigitated back contact and heterojunction technologies, approaching the theoretical limit power conversion efficiency (PCE) of 29.1% for a silicon solar cell. Despite of its interesting characteristics and strong scalability for industrial and commercial use, the fabrication costs of this technology have halted, thereby making solar panels costly [8].

Thus, these drawbacks and limitations have led to the desire to research alternative materials such as (CIGS) and (CdTe), identified as second-generation thin film photovoltaics, to adequately compensate for the inability of silicon photovoltaics to provide feasible manufacturing and production and generate inexpensive energy. Although crystalline silicon solar cells currently possess greater than 55% of the market share, the module efficiencies of CIGS and CdTe technologies almost rival that of crystalline solar cells, with recorded efficiencies of 21.4% and 21.6%, respectively [8–11].

Parallel with the emerging materials utilized in thin film technology, most focus is on perovskite solar technology and organic solar cells, as well as dye-sensitized solar cells (DSSCs). These plastic single-junction-based devices exhibit efficiencies of 25.5% [12], 16–18.1% [12–16] and 13% [12,17], respectively. These are third generation solar cells also known as plastic solar cells. Similarly, exfoliated tungsten telluride (WTe) flake (CiGSe) based multilayer thin films have been reported with a PCE of 10.87%. Furthermore, the structural manipulations of the active materials for these cells have garnered immense momentum due to their ease of production, flexibility, and simple fabrication methodologies [17,18].

Several studies have reported on these low-cost, complexity-free, and easily manufactured organic solar cells, more especially the π–conjugated polymers. The comprehensive scientific contribution towards the area of application-specific properties of π–conjugated polymers (viz., design, modelling, and fabrication) in the quest to match the electrical conducting properties exhibited by chemically doped polyacetylene is noteworthy. The aforementioned optoelectronic properties have opened technological interest in various applications, such as nano-electronics, sensors, internet of things (IOT), energy storage photodetectors, memory devices, field effect transistors (FETs), nonlinear optical devices, electrochromic, light emitting diodes (LEDs), and photovoltaics [18–23].

The conjugated polymers have interesting features owing to the side-chains present in the polymeric materials, which result in significant thermal stability and solubility, and ultimately promote the fabrication of these nanostructure-based materials by deposition with simple techniques, such as spin coating—hence, their inexpensive and simple solution processability. Their single- and double-bond characteristics and their interesting and adequate π-excessive nature have opened a window of opportunity for newly classified advanced materials in the arena of photonics and electronics [23,24].

For this study, we propose to utilize novel polycrystalline silicon semiconductor thin film raw material extracted from sugarcane bagasse ash (SCBA) for solar applications. Currently SCBA is being used as the source of fuel in power-generation boilers to produce electricity. Recent studies have shown that SCBA is rich with mineral content including silicon, iron, and other minerals. The silicon is found mainly in the form of silicic acid and constitutes about 380 kg/ha of silicon composition. It is worth noting that pure silicon is further obtained from silica (SiO2) and it has been reported that the silica is biocompatible and eco-friendly [25,26].

The disposal of bagasse ash waste, therefore, poses a dumping challenge to the environment. Currently, there is very little published information available on the production of silicon nanoparticles from sugarcane bagasse ash for solar applications. Furthermore, quartz is at present the main source of nano silicon. It is obtained by sand mining, which has detrimental effects on the environment such as land degradation, erosion, fissures, and adverse effects on water supply and quality. Metallurgical-grade silicon (MG-Si) (600,000 tons/year) is produced through high-temperature carbothermal reduction of quartz, which requires an energy input of 50 kWh/kg [26,27].

Herein, the three generations of solar materials are presented, including important parameters affecting the overall power output of the solar devices. The future prospects and challenges faced with current solar technologies are also discussed in detail.

2.1.1. Overview of Solar Cell

2.1.1.1. Solar Cell Principle of Operation

Solar cells are mainly described based on their architecture; some consist mostly of metals (inorganic thin films), some nanomaterials (QD), some polymers (referred to as organic), etc. Traditionally, solar cells are electronic devices focused on converting sunlight into direct electrical energy because of the photoelectric effect from metals and inorganic semiconductors [28]. Figure 2.2 below shows a typical p-n junction silicon solar cell. The generation of electricity comes from the photons (light particles) when sunlight energy shines on the cell. Electrons (−) are ejected from doped Si (n-type) and move across to the positive (+) doped Si (p-type) material as illustrated in Figure 2.2 below.

2.1.2. Electronic Structure and Doping Mechanisms in Crystalline Silicon

2.1.2.1. Electronic Structure

For the originality of electrical conductivity and advanced optical properties, namely low band-gaps in inorganics, it is critical to assimilate the reactivity of these materials, whose electronic configuration is exhibited by doping agents in comparison with undoped inorganic materials. It is well known that the electronic structure of silicon is $[Ne]\ 3S^2 3P^2$, whereby valence electrons avail themselves to form four-bonds with neighboring (adjacent) atoms [29].

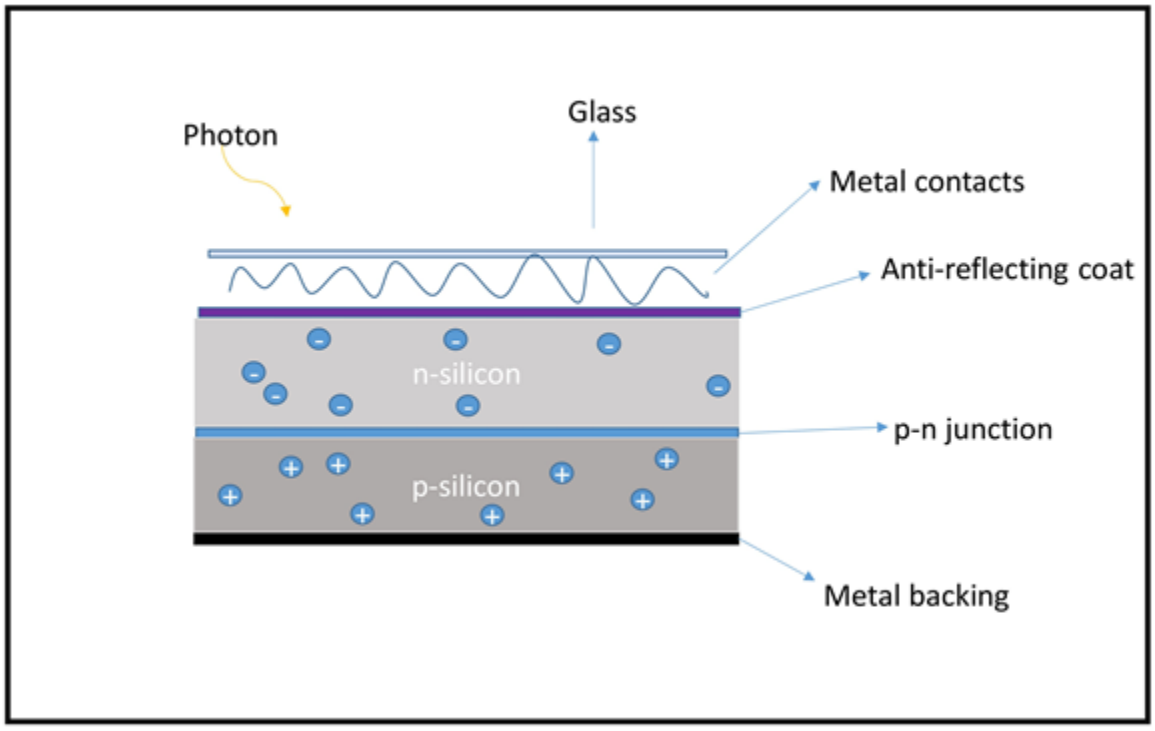

Figure 2.2. *Schematic structure of typical a silicon solar cell [28].*

2.1.2.2. Doping Mechanisms of Silicon Materials

The tailoring of materials is performed to attain electrical properties and semiconductor characteristics via doping. This process involves the introduction of foreign materials and/impurities into the bare material, known as the intrinsic semiconductor, to successfully modulate its optical, electrical, and structural properties, ultimately labelled as the extrinsic semiconductor material. As a result of doping, chemical changes are induced within the silicon material, resulting in the generation of charges which migrate within the silicon matrix.

There are various ways and routes to carry out doping including redox, in situ, chemical (gaseous and solution), induced-radiation doping, and charge injection. Additionally, these can be further distinguished by the type of electron transfer, such as doping via reducing agent (n-type) or oxidizing agent (p-type) [29–31].

2.1.2.2. P-type Doping

Traditionally, silicon semiconductor doping involves the introduction of foreign materials such as boron and phosphorus to the silicon matrix. The foreign molecules and atoms are referred to as p- and n-type dopants, respectively, due to their electronic nature. Parallel to the concept of an inorganic semiconductor, charge creation emerges from the valence shell during the p-type doping process, as silicon is 1 e- more and thus creates positive charges interchangeably referred to as holes, leaving the whole matrix with a positive charge. This process utilizes oxidizing agents such as boron [8,31].

2.1.2.3. N-type Doping

This process involves the generation of electrons via reducing agents such as phosphorus. In this case, referred to as n-type doping, the silicon matrix is altered as the reducing agent donates electrons, as illustrated in Figure 2.2, and the matrix generates a negative charge on the surface. N-type doping requires materials with an extra electron compared with the parent structure, silicon, as opposed to their counterpart p-type doping [31,32].

2.1.3. Important Parameters in a Solar Device

2.1.3.1. Principle of Charge Separation within a Solar Device

The concept of heterojunction cells relies on the efficient dissociation of an exciton, and the donor and acceptor material's proximity factor play a crucial role. The material thickness facilitates the optimum exciton diffusion length, usually a few tenths of a nanometer. Typically, the thickness of the active layer for organic semiconductors is in the range 80–200 nm. Recently, bulk heterojunctions have been deposited via co-sublimation of small molecules and/or the spin coating technique, using mixtures of polymers [33].

The shortcomings faced in heterojunction structures derive from the fact that hole and electron transportation to the electrodes is required to promote the separation of charge carriers to reach their corresponding electrodes (cathode and anode). For instance, if the individual layer and a given bilayer structure are larger than that of the exciton diffusion length, it is most likely the excitons will recombine as shown in Figure 2.3, and result in the loss photon indicated by the exciton with the star. Although if the excitons generated are

near the interface, there is likelihood that they can be separated into free charge carriers and thus diffuse or drift towards their corresponding electrodes, as shown in Figure 2.3 [33–35].

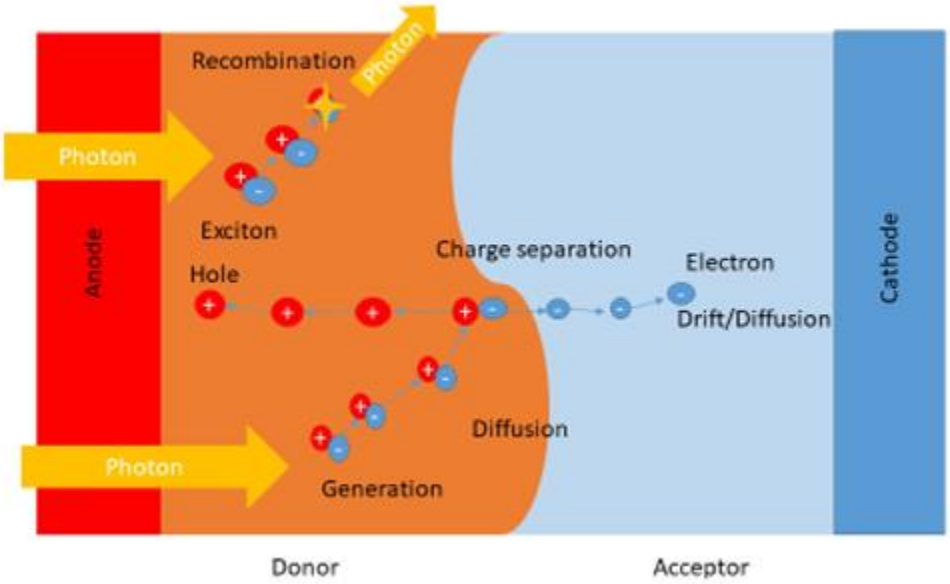

Figure 2.3. *Illustrate the principle of charge separation within a solar cell [33].*

It is imperative to know the solar cell performance, as shown in Figure 2.4, which can be carried out by determining various factors including the fill factor, efficiency, short-circuit current density, and open-circuit voltage [36]. As a result of irradiation, the open-circuit voltage (VOC) is cross-examined as the difference in the cell's potential at the terminals when there is zero current flow through the terminals. Interestingly, the short-circuit current density (Jsc) is produced from the cell upon irradiation at zero potential.

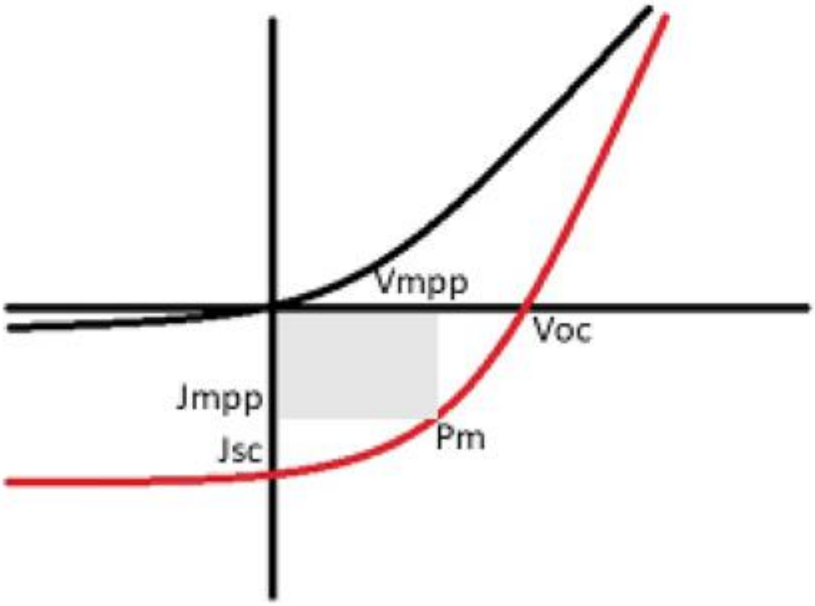

Figure 2.4. *Represents a schematic current–voltage curve from a solar cell device black (dark) and red (under illumination) [36–38].*

In addition, the fill factor (FF) is known to be the ratio between the cell's maximum power, shown in Equation (2.1) where Vmpp and Jmpp denote voltage at the maximum power point and current at the maximum power point, respectively.

$$FF = \frac{V_{mpp}J_{mp}}{V_{oc}J_{sc}} \quad (2.1)$$

Ultimately the power conversion efficiency (PCE) is determined to be the ratio of the cell's overall output power to incident radiant power.

$$PCE = \frac{V_{oc}J_{sc}FF}{P_{in}} \times 100\% \quad (2.2)$$

Innovative designs have made radical developments over the years, whereby thin film solar cell technology results in alternate material device structures. The rising efficiencies of thin film solar cells, in particular perovskite with 23% of the market share, have received significant attention in the photovoltaic market, mostly in the integrated photovoltaic (BIV) field. As shown in Figure 2.5, plastic solar cells (perovskite) have been rising in efficiency for over two decades, giving them potential as thin film PVs [39].

Thin film solar cells are favourable candidates in the field of photovoltaics because of their minimum material usage and rising efficiencies. The three most known thin film technologies extensively studied and still under intensive investigations include α-silicon (α-Si), copper indium gallium selenide (CIGS), and star absorber materials such as cadmium telluride (CdTe). Photovoltaics can generate electrical energy at a lower cost and they are environmentally friendly. Despite of the aforementioned property (the power conversion from these devices with an enormous amount of the sun's energy), these photovoltaic devices still produce about 30% or less of electricity from approximately 80–90% of the sun's energy absorbed [39,40].

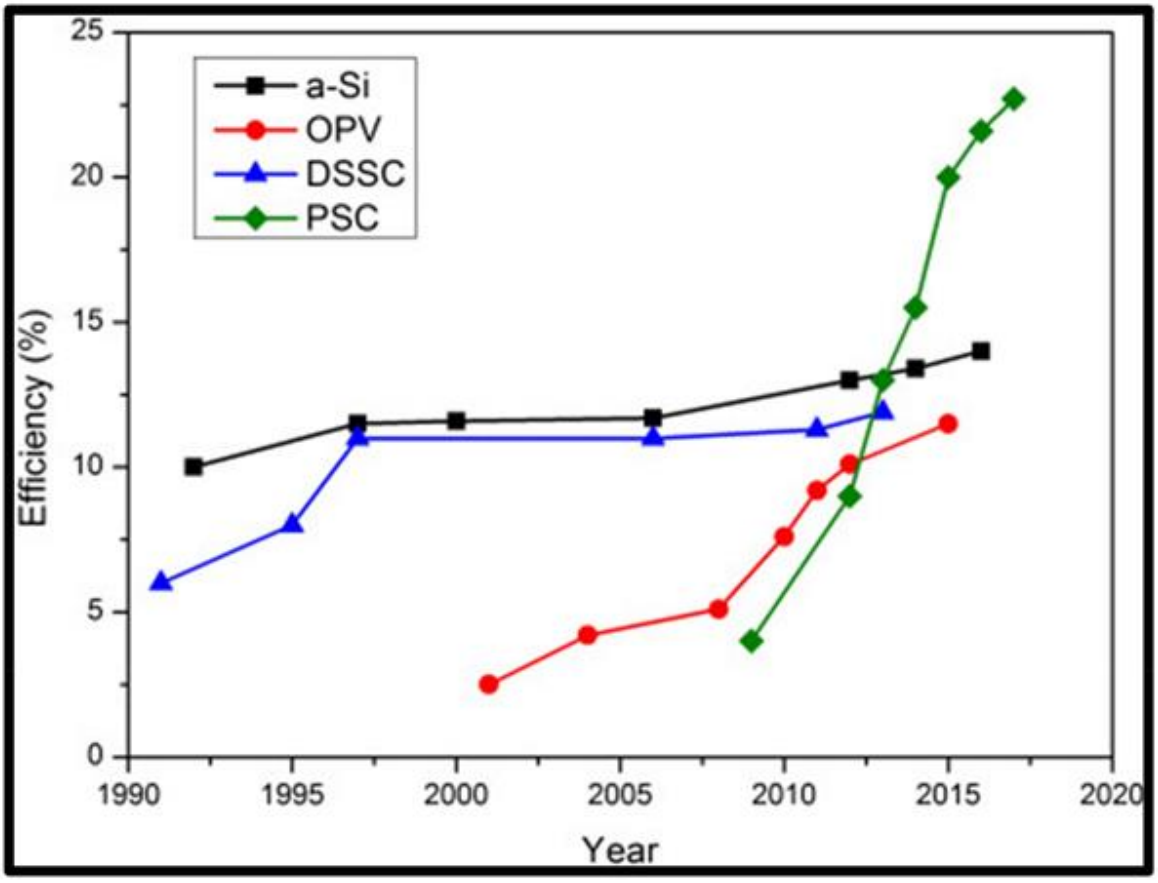

Figure 2.5. *Progress of perovskite solar cell efficiencies compared with other thin film PV technology, reused with permission from [39], Copyright © 2018 Elsevier.*

2.1.4. The First Generation Solar Cells

2.1.4.1. Crystalline Semiconductors

Crystalline materials are a solid material in which the structure's dimensional patterns are consistently continuous throughout to the edges of the whole sample and remain unbroken. They are divided into different forms, i.e., monocrystalline, polycrystalline, etc. Monocrystalline simply means a single crystal with a grain-boundary-free uniform crystal lattice, while polycrystalline materials are essential in photovoltaics with majority-carrier bulk diffusion length.

Polycrystalline semiconductors are low-cost materials relative to single-crystalline semiconductors. The first-generation solar cells were built on silicon wafers. These are the most successful technology to date with high power efficacy. However, limitations result from their inhomogeneous nature and the reduced carrier bulk diffusion length of the material. This is a result of grain boundaries and dislocations as well as several other physical and chemical shortcomings with which we are faced with these materials. A grain boundary denotes a region in the material where adjacent atoms are disordered, consequently resulting in incomplete atomic bonding. These structural defects induce the trapping of electrons [41].

However, many attempts have been made to reduce the degree of grain boundaries formed in polycrystalline materials. Although polycrystalline semiconductors still lag in efficiency compared with monocrystalline solar cells, their tenable band gaps make them ideal materials, and this property can prove to be significant to the power conversion efficiency as well as to mitigate costs (modules) by utilization of low material costs [42].

2.1.4.2. Nanomaterials

Nanoparticles are defined as the simplest form of structures with sizes in the nanometer range. In principle any collection of atoms bonded together with a structural radius less than 100 nm is essentially considered a nanoparticle. They differ from their bulk counterparts and isolated molecules owing to their chemical, electronic, and optical properties. The electronic properties of the materials are largely dependent on their dimensions and change dramatically as the density of states and the spatial length scale of the electronic motion are

reduced with decreasing size. Therefore, size-induced changes in the electronic structure affect the optical properties of nanoparticles [43].

Inorganic semiconductors have revolutionized electronic devices owing to their excellent high-field-effect mobilities and long -erm stability far exceeding that of known organic materials. Thus, they are conventional and the most commercialized types of electronic devices. Their main limitations are the material choice and fabrication strategies for the use of inorganic semiconductors, given that most polymer substrates are vulnerable to high operating temperatures required for traditional deposition methodologies, i.e., crystallization and doping. Researchers have reported on bottom-up approaches for inorganic semiconductors to produce zinc oxide (ZnO) nanowires. In addition, the dimensionality of these nanomaterials range from 1D and 2D with flexibility in portable electronics, as they possess outstanding optical, electrical, and mechanical properties [43].

2.1.4.3. Conducting Polymers

The conducting polymers possess excellent ionic and electronic conductivity, optical transparency coupled with mechanical flexibility, rendering them the best lightweight flexible substrates. The transparent conductive oxide components normally used are indium tin oxide (ITO) and fluorine-doped tin oxide (FTO). As a result of material shortages, brittleness, and costs, conducting polymers are a potential alternative for TCO due to their excellent, simple nano/microscale self-assembly, abundancy, and mechanical flexibility [44,45].

The commonly studied conducting polymers include polypyrrole (Ppy), polythiophene (PT), polyaniline (PANI), poly(3,4-ethylenedioxythiophene) (PEDOT), and their derivatives. The materials mentioned above have promising applications in photovoltaics, thin-film transistors, supercapacitors, gas sensors, LEDs, and wearable electronics. Furthermore, their charge transport mechanisms are not well understood yet; it has been reported that intra chain charge transport enhancement exists because of new electronegative groups in conjugated backbones and acceptor dimerization, promoting the carrier mobility and stability of semiconducting polymers [44,45].

2.1.4.4. Single and Poly-Crystalline

Mono-crystalline silicon solar devices are composed of single crystals of silicon. Henceforth, the Si material is made with macro ingots, which results in Si crystallites (monocrystalline Si) from the manufacturing process known as Czochralski [46–48].

The power efficiency is in the range 17–18% for the mono-crystalline silicon-based devices reported in [48]. However, due to the expensive and complicated process of forming single crystals, researchers have opted to modify the manufacturing processes. Molten silicon in a mold matrix of graphite produced polycrystalline silicon material. The as-prepared polycrystalline Si became the most popular solar cell worldwide since 2008, due to its economical properties, and constituted about 48% of solar cell production [49].

Although the solidification process of molten silicon produces a variety of crystal structures, and has proved to be cheaper to fabricate than monocrystalline silicon, it suffers very low efficiencies which lie between 12–14% [50].

2.1.5. Second Generation Devices (Thin Film Solar Cells)

In the quest to come up with alternative materials with superior electrical and optical properties, nanomaterials have been at centre-stage for several applications in electronics, sensors, energy, etc. The ability to fine-tune their properties on the atomic and molecular level has caught the attention of many researchers worldwide. However, thin films have proved to be more viable and cost-effective.

2.1.5.1. Amorphous Silicon (α-Si)

The second generation α-Si, CIGS, and CdTe thin films, have been at centre-stage as far as thin film solar cells evolution is concerned with Si still the star material in solar technology. The desired features of α-Si, such as its direct band gap, promote a fair fraction of sunlight to be absorbed into a thin layer of a few micrometers [51].

The amorphous Si is a material with low quality crystallinity, suffering from short order loose bonds temporarily resulting in minor carrier diffusion lengths with unfaceted electrical behaviour. Further studies were conducted which attempted to improve on the

aforementioned; hydrogen passivation (α-Si: H) proved to be a procedure for reducing loose bond densities by several orders of magnitude, thus improving the minority carrier length property [51].

The functionalization with H2 led to the light degradation known as Staebler–Wronski, whereby the efficiency of producing maximum electricity decreases. The optical band gap of α-Si: H of ≈ 1.7 eV can be fine-tuned to be more than 2 eV where maximum absorption starts. Moreover, it offers advantages such as shorter payback time (energy) and cost effective fabrication [8,51].

2.1.5.2. CdTe Thin Film

Since the 1950s, a great deal of attention has been placed on the development and increasing the efficiency of CdTe-based solar cells. Single-junction devices with an optimal band gap of 1.49 eV and a possible efficiency greater than 20% were desired for the CdTe solar cells to realize commercialization [52,53].

Furthermore, researchers reported on the first solar device with a significant conversion efficiency of 21.0% in 2014 [54]. Since then, CdTe thin film solar devices have realized a significant increase in efficiency to 22% [55]. However, this efficiency was not stable due to structural defects arising from grain boundaries and intra-grain dislocations. Another shortcoming was associated with a reduced lifespan for the minority carriers identified as one of the recombination factors, where it was presumably evident that the carriers recombine [56].

2.1.5.3. GIGS and CZTS Thin Films

Several decades ago, researchers extensively studied copper indium gallium selenide

(GIGS) as one of the candidates for thin film absorber material. The scarcity of raw materials and the toxicity of these materials led to a breakthrough in alternative materials, namely copper zinc tin sulfur (CZTS). This material is an analogue of GIGS, preferably when Sn (IV), S (VI), and Zn (II) replace indium (III), Ga (III), and Se (Vi), respectively [57].

The opto-electronic as well as the structural properties of both the aforementioned thin films can be further improved by the displacement of their constituent element with readily available and earth-abundant compositions and toxin-free elements such as Sn, Sb, S4, and CuS [58]. For chemical treatment with hydrazine via non-vacuum particle solution, researchers have reported the highest efficiency of 12.7%, whereby the theoretical efficiency value was 32.4%. [59,60].

However, CZTS cells are prone to undesirably low voltages induced in the bulk material at the charge extraction interfaces as result of recombination defects. In spite of this, crucial breakthroughs in the development of CZTS-based solar cells rely on finding an alternative back contact with lower optical loss and maintaining low series resistance in rendering a high performance for the full device [61].

2.1.5.4. Tin Antimony Sulfide

In the quest to produce an environmentally friendly and earth-abundant binary compound, antimony sulfide (Sb_2S_3) has emerged as a potential candidate thin film material compared to toxic Cd or Pb. The material possesses a desired band gap of approximately 1.7 eV with a strong light extinction coefficient of 1.8 × 105 cm−1 at 450 nm [62,63].

The abovementioned properties make antimony sulfide a suitable and ideal absorber material for thin film solar devices. Furthermore, the super efficiency reported for antimony sulfide-sensitized solar cells has reached about 7.5% using a highly mesoporous device structure [64]. Several methods were utilized to fabricate the Sb_2S_3 layer, including spin coating [65], chemical bath deposition (CBD) [66,67] and successive layer adsorption [68]. The hole transport materials (HTMs) enhanced the photo carrier extraction for the as fabricated solar cells [69].

Hence, the crystal quality of Sb_2S_3 determined the choice of HTMs, while some can poison the device stability in the long run, such as CuSCN, spiro-OMeTAD, or poly (3-hexylthiophene) (P3HT). The crystallinity of the absorber layer is crucial in this instance to avoid the utilization of HTMs. Further studies have revealed that the modification of planar

solar cells based on TiO_2/Sb_2S_3/P3HT planar solar cells has recorded 4.06% efficiency with the CBD method [70].

Therefore, the search to find the desired crystal quality of Sb_2S_3 and minimize decomposition continued; and the rapid thermal evaporation (RTE) method was adopted. Henceforth, an efficiency of 5.6% was achieved with the aforementioned method. Other methods were employed too, wherein, for traditional chalcogenide solar cells, annealing in selenium atmosphere was the preferred method to combat defect passivation and realize the improved crystallinity of Sb_2S_3 film. Consequently, sulfurization and selenization approaches were utilized to quench the oxides and passivate structural defects induced on the materials [71].

2.1.6. Third Generation

These materials show far more promising breakthroughs in solar technology. Their application is yet to gain momentum as research is still ongoing for third generation materials in photovoltaic devices.

2.1.6.1. Quantum Dots (Nanocrystal Based)

Nanotechnology has been the topic of interest in the science community for about a decade; various nanomaterials have been developed for several applications in electronics, sensors, the biomedical field, etc. Quantum dots (QDs) are nanoparticles of inorganic semiconductor materials. They usually have dimensions ranging from 1 nm to 10 nm which corresponds to 10–100 atoms. Their energy levels are quantized due to the confinement of electrons. The motion of electrons in the conduction band, valence band holes, and/exciton(s) is confined in all three spatial directions. Moreover, a variety of QDs have been traditionally produced from atoms in groups II-VI, III-V, and/IV-VI [72].

Quantum dot (QD) based photovoltaics absorb light from solution-processed nanocrystals and have versatile size-tunable band-gaps for fabrication in a wide range of substrates. These are a group of nanomaterials with good opto-electronic properties which are size dependent. Therefore, the band gap of colloidal metal chalcogenide nanocrystals is invariably dependent on the size of the quantum dots. Consequently, this promotes efficient collection of near-infrared photons and the generation of multi-junction solar cells [73].

The quantum dot photovoltaics significantly benefit for their simple room temperature processing, fabrication, and air-durability operation. However, the present challenges faced within this field are the fundamental understanding of QD surface chemistry as well as their inherent disorder in quantum dot films due to mid-gap states which limit open-circuit voltages [74].

Although they have not yet realized large-scale industrial application, these technologies offer desired device properties, earth-abundance composition reliance, and simple processing techniques. Ideal QD solar cells have been fabricated using PbS and/or PbSe. Notably, they have the potential for novel applications in solar PV [75,76].

Another study reported on ligand free, methyl ammonium lead iodide (MAPbI3) QD solar cells with PCE above 9%. These materials were synthesized in situ within a porous silica (SiO2) matrix with a narrow nanopore size distribution. The synthesis parameter control translated to fine control over QD size with a spectral position on their electronic bandgap, preventing disorder that could affect the performance of the as-built devices [77].

In the classical sense of the word, a nanometer-sized semiconducting crystal confined in all three spatial dimensions is referred to as a quantum dot. The prevalent features of QDs include the generation of multi-excitons known as MEG and their tunability in optical and electronic states through reductions in size and quantum confinement effects. The MEG character in QDs allows the devices to rival that of a single junction Shockley–Queisser (S-Q) limit with 33% PCE. The three commonly used QDs extensively studied for the past 3 decades include CdTe, CdS/Se, and PbS/Se, and these are well represented in the light display market. With the resurgence of halide perovskite QDs, there is a potential new methodology for solar harvesting technology [78].

The practical conditions for perovskite QDs (PQD) are similar to that of traditional QDs, whereby organic capping ligands are utilized for growth control (steric hindrance) and new surface states. However, the nature of the surface leads to structural defects, and affects morphology and material stability. Colloidal QDs are ideal candidates for large-area device fabrication via printing techniques better suited than their counterpart organic and perovskite

bulk counterparts. The highest PCE recorded for CsPbI3 QD-based solar cells was 16% better than that of PbS QDs, indicating a greater window of opportunity for next-generation QD photovoltaics [79,80].

2.1.6.2. Polymer Based Devices

Recently organic solar cells have attracted researchers as potential candidates for low-cost energy conversion devices. For a single-junction configuration, these cells recorded a power conversion efficiency of 9.2% [81], which increased to over 12% [82] for a tandem structure. Another study focused on fullerene-derivative bulk hetero-junction (architecture) solar cells. The optimal thickness of 100 nm for this technology was noted from the most prominent features such as optical interference and recombination losses [81,82].

Additionally, organic materials generally have high absorption coefficient, although a considerable amount of light is lost due to transmission in semi-transparent and reflective electrodes on organic solar cells. Nevertheless, the efficacy of organic-based solar cells can be significantly improved to over 10% by understanding and mitigating such losses [83].

2.1.6.2.1. p-Conjugated Polymers as Hole-Transporting Layers (HTLS)

Since a breakthrough in 1958, solar cells have rapidly received a great deal of attention due to their material abundancy, inexpensiveness, flexibility, and ease of production. The processability of these materials has led to novel designs and device optimization as well as innovative nano-engineered architectures and single-junctions which relatively enhance the power conversion efficiencies to just over 17%, and approaching 18% [84,85].

M. H. Gharahcheshmeh et al., reported on the use of texture and nanostructure to enhance the electrical conductivity of semicrystalline conjugated polymers via water assisted (W-A) oxidative chemical vapor deposition (oCVD). The results revealed the charge transport between chains within the crystallite π–π stacking distance and interchain charge transfer integral. Interestingly, the use of W-A combined with a volatile oxidant, antimony pentachloride, recorded an electrical conductivity between 7520 ± 240 S cm−1, for PEDOT thin films [44,85].

The control on synthesis parameters for π–π stacking distance reduced from 3.50 Å down to 3.43 Å and recorded an electrical conductivity improvement of ≈1140 %. In addition, the highest electrical conductivity is also associated with a minimum Urbach energy of 205 meV, indicative of high morphological order. Another feature was the figure of merit (FoM) for transparent conductors, which reached an optimal maximum value of 94, 1.9× and 6.7× higher than oCVD PEDOT grown without W-A and usage of vanadium oxytrichloride and iron chloride agents, respectively. This procedure is cost-effective due to W-A oCVD being a single step all dry processes, involving direct growth of mechanical flexibility, conformal coverage, and rough structured surfaces with minimal to no complexity or costly transfer steps [44,85].

2.1.6.3. Dye Sensitized Based Solar Cells

Further studies were done especially on dye-sensitized solar cells (DSSCs) as emerging photovoltaic technologies. This technology has main components which work in synergy for the optimum performance of the cell, namely the redox electrolyte and photo-anode counter electrode. Several of the single and polycrystalline semiconductor materials used in the photo-electrodes include Si, InP, and GaAs [86].

DSSCs have good tunable optical properties (i.e., color and transparency), and are easy to fabricate as well as having low-cost manufacturing processes, and are lastly earth abundant compositions with application-specific properties for photovoltaics. Their best recorded efficiency was only about 10% under irradiated sunlight. The main shortcoming of this technology is the choice of electrolyte which results in photo-degradation and destabilization of the cell, and thus a reduced lifespan [86].

Recent studies have reported on their improved power conversion efficiency of 14.3%. The stability of DSSCs has been relatively improved with time. Furthermore, regarding light absorption and electron transport in particular it is imperative to find and develop photo-electrode materials for the betterment of DSSCs. Material suitability and applicability in solar applications have a huge effect on the power conversion efficiency. In addition, TiO_2 is an ideal semiconductor photo-electrode material popular for DSSCs [87,88].

TiO_2 nanomaterial exhibits superior textural properties such as high surface area (a large number of contact sides to promote the adsorption of dye molecules), and optimum electron transfer. It has been reported elsewhere that commercial TiO_2, exhibits a band gap of 3.0–3.2 eV [89]

2.1.6.4. Perovskite Materials

Extensive research has continued over the years and a breakthrough has been made with recent polycrystalline films consisting of an organic cation (A), inorganic cation (B), and a halide (X) with the formula ABX_3. The hybrid organic-inorganic material is commonly known as a perovskite material—henceforth, perovskite-based solar cells [90].

The desirable properties of perovskite materials include their long carrier diffusion length, band gap tenability, low recombination losses, and abundant material availability (low cost). These exceptional properties see PCEs reaching 25.5% efficiency, while enjoying low fabrication costs and facile synthesis as certified by the National Renewable Energy Laboratory (NREL). It is worth noting that the aforementioned are not available for traditional silicon-based solar cells [91]. However, the parasitic absorption in the back reflector and hole-conducting layer results in photocurrent loss for the perovskite absorption spectrum. In the quest to discover and develop perovskite technology, researchers reported on quasi-2D perovskite thin films, $(C_6H_5CH_2NH_3)_2(FA)_8Pb_{29}I_{28}$, where FA is formamidinium (FA), lead (Pb), and iodine (I), with excellent moisture resistance and a relative humidity of 80%, reaching a PCE of 17.40%. The moisture resistance is attributed to the ammonium salts. The recent discovery showed that 2D perovskite is versatile and can attain long-term stability as well as high efficiencies for PSCs [92,93].

The development of third generation perovskite solar cells has attained efficiencies of just over 20%. The continuous ability to fine-tune the band gap using Cl instead of I exhibited 3.2 eV from 1.6 eV, and incorporating low-band-gap materials improves the efficiency. Polycrystalline films are formed from the perovskite salts by precipitation methods with varying polar solvents. In 2019, Noh et al., tested a perovskite solar cell and attained 23.3%

efficiency via an interface passivating method to minimize recombination at the interface [94].

Additionally, perovskite solar cells possess a significantly low fill factor of 0.73, which results from the non-uniform absorber (i.e., pinholes), and carrier shunt mechanisms caused by carrier-selective contacts (resistive losses associated with non-ideal carrier-selective contacts). Most importantly, severe environmental stability issues limit the industrial application of these materials. It is worthwhile to appreciate the possible market entry-point in which perovskite serves as a top cell in Si/perovskite tandem cells with a fundamentally large band gap [95].

2.1.7. Outlook

Greener technology involves a moderate methodology with non-hazardous chemicals and the utilization of organic acids and bases, resulting in significant time and energy savings while also allowing the synthesis of high-value compounds for specified applications. Green procedures set out to create no harmful by-products and allow tailoring for more precise control of particle shape, size, and appearance in the nano-realm. Bionanoparticle production is an environmentally friendly, low-cost, long-term approach for extracting high-value nano-silicon directly from naturally occurring agricultural wastes such as sugarcane bagasse, where Si is found in the form of SiO_2 [96,97].

2.1.7.1. Future Prospects and Challenges

Figure 2.6 below presents scheme(s) for a conventional (a) and inverted (b) solar cell device structure. It is possible to observe that the two proposed structures consist of several layers including transparent conductive oxide (TCO), a hole-transporting layer (HTL), an absorber layer, an electron transporting layer (ETL), and a metal. It is imperative to emphasize that these layers serve different functions synergistically to produce current from charge transportation induced by incident light [98].

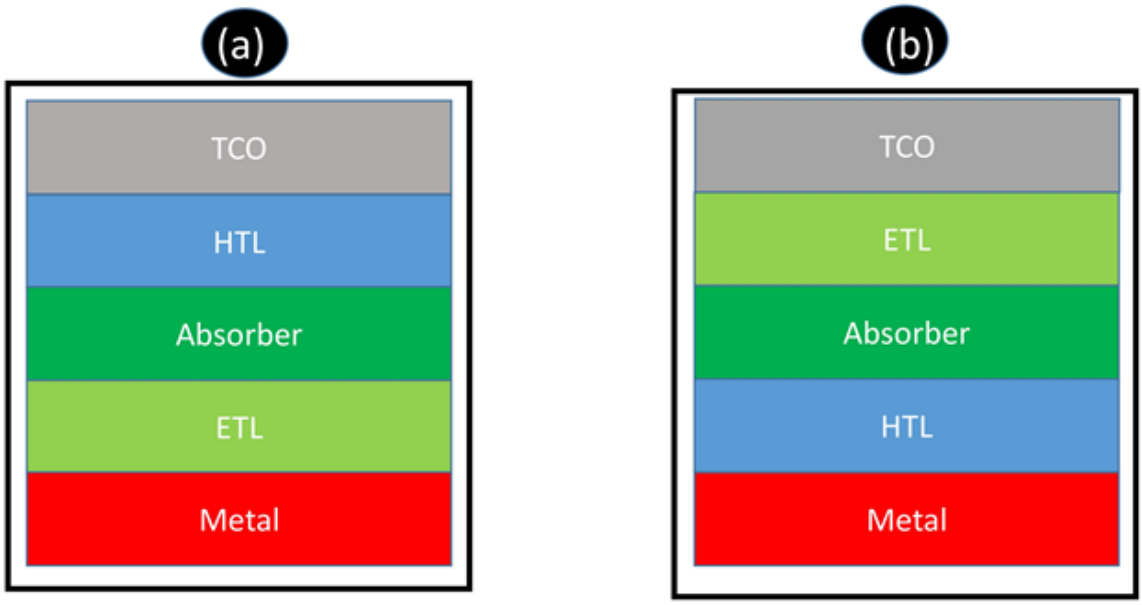

Figure 2.6. *Schematic representation a (a) typical solar cell and (b) inverted solar cell architecture.*

Transparent conducting oxide(s) are conventionally chosen as an anti-reflective coater (ARC), as well as the conducting anodic electrode on the front side of the cell. Normally, TCO layers with a thickness in the range 70 to 150 nm in silicon-based solar cells are desired to promote adequate transmission of light to the absorbing material and minimize optical losses. Researchers reported more than 90% minimal sheet resistance and smooth surface morphologies when the TCO layer, mostly indium tin oxide (ITO) is between 80 to 180 nm [96–98].

Metallization, has found to be effective at the rear/back side of the cell, namely gold (Au), aluminum (Al), and silver (Ag). Interestingly, Gwamuri et al. [98] successfully reported that an ITO thickness of about 50 nm produces transmittance of approximately 80% with higher sheet resistance data, which is not desired for solar technology. Thus, the threshold minimum of 70 nm must be corroborated in order to find synergism between smooth morphologies, sheet resistivity, and transmittance. Recommendations:

- Use alternative sources of solar materials, such biomass, to minimize costs.

- Use green technology, such as biomass(eco-friendly), a renewable source for solar materials. â Use hybrid organic-silicon heterojunction solar cells.

- Employ solar-grade silicon from silica (metallothermic reduction as compared to carbothermal reduction process). â Enormous scientific research efforts in the past were devoted to the development and optimization of the following;

- ETL, HTL, perovskite composition, thickness, process, and device structures.

- The state-of-the-art perovskite and non-toxic solar cells will lead to the development and discovery of new Pb-free perovskite light absorber materials which are environmentally friendly and critical in the field of PVs. The new research area will be imperative in realizing stable and eco-friendly perovskite PVs for real-world applications.

2.2 General overview of Extraction and Synthesis of Silicon Nanoparticles (SiNPs) from Sugarcane Bagasse Ash

2.2.1 Background

Valorization of sugarcane bagasse has been studied extensively over the years, with its niche applications in the sugar industry and bioenergy production. Silicon dioxide (SiO2), often known as silica, is a useful inorganic multifunctional chemical substance that is one of the basic materials. Silica can be found in nature as quartz, sand, or flint. Gel and amorphous forms are also possible, with both crystalline and amorphous forms found in the earth's crust [82,83]. In their study, El Sayed and El-Sammi reported numerous silica content in different sources: Sorghum (88.75%), wheat (90.56%), corn (64.32%), bamboo (57.40%), bagasse (73%.00%), lantana (23%.38), sunflower (25.32%), rice husk (93.00%), rice straw (82.00%), and bread fruit tree (81.80%) [83].

The silica comes from the soil in the form of silicic acid, which the sugarcane plant absorbs and collects around the cellulose micro-compartments. The quantity of silicon in the soil influences silica concentration. Sugarcane roots play a key role in absorbing silicic acid from

the soil and delivering it to the shoots, where it is stored as amorphous silica. Amorphous silica predominates in sugarcane bagasse ash with other metallic contaminants [82,83].

In this study, the use of bases such as NaOH, KOH and acids like HF, H_2SO_4, HNO_3, and HCl for the pre-treatment of the ash, and yield silica with desirable properties. The sugarcane bagasse ash is rich with silica of about 73%, and it is economically feasible due to the conversion of raw material to the production of silica gels and powders [84,85]. The sugarcane bagasse has been investigated as the potential raw material and source of sugar, juice, and fuel in the ethanol industry (shown in Figure 1) and valuable material in the cementious industry [86].

Many industrial processes (shown in Figure 2.7) in the transformation of sugarcane into sugar and ethanol, namely, the burning process of the biomass for energy production, result in ashes with high impurity content, such as iron and aluminium oxides, hindering the process of obtaining silica with satisfactory purity values [6]. Thus, the resulting ashes require additional purification processes HCl acid leaching allied or not to a sol–gel method [86,87].

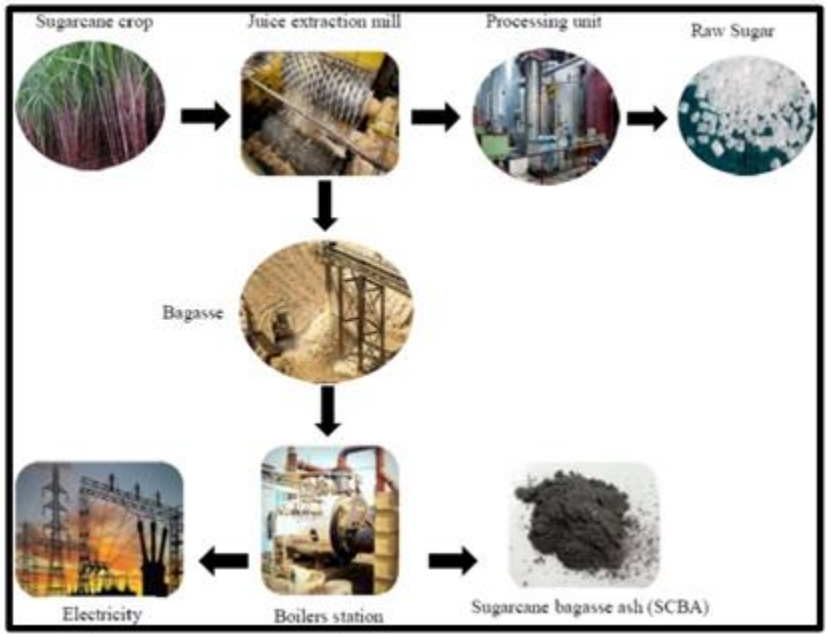

Figure 2.7. *Flow diagram of sugarcane bagasse ash [86,87].*

The silica nanocomposites (soluble silicates) are widely used in the glass, ceramic, and cement industries as a major component and in cosmetic, pharmaceutical, and detergent industries as bonding and adhesive agents. Notably, silica has been used as a major precursor in a variety of applications as inorganic and organometallic materials, which have desirable applications in synthetic chemistry as a catalyst, coating for electronic optical materials, and thin films [87].

Sugarcane Bagasse in South Africa

The sugarcane, shown in Figure 2.8, is an economical and strategic crop for the Mpumalanga and Kwazulu Natal, where the production is located, it is comprised of a substantial percentage of field crop gross farming income across the two provinces. To date, about 22,949 registered sugarcane growers annually produce an average of 20 million tons of sugarcane from 14 million supply areas, ballooning from southern Kwazulu-Natal to the Mpumalanga Lowveld [88].

Figure 2.8. *Images of a typical sugarcane plantation, stalks, and bagasse from the South African sugar industry [8].*

Presently, the growers are represented by the Southern African Cane Growers Association (SACGA) and the South African Farmers Development Association (SAFDA). Thus, there are approximately 21,581 small-scale growers, of whom about 12,019 delivered cane in the 2018/2019 season, with the production at 9.33% of the total crop. This is composed of 116 consolidated units, including co-operatives, trusts, and projects, with the make-up of 7536 individual beneficiaries. There are 1368 large-scale growers, including 345 black emerging farmers, and they produce 81.17% of total sugarcane. Milling companies with their own sugar estates produce 9.17% of the crop [89].

Advanced studies have been ongoing to investigate the various ways for the production of silica from sugarcane bagasse using simple processing routes. The traditional routes moderately utilized for agricultural wastes to silica include synthetic routes, such as acid treatment, calcination, partial burning, leaching, enzymatic treatment, pyrolysis, hydrolysis, and sol–gel. Traditionally, silica is produced by reaction of sodium carbonate powder and quartz sand at higher temperatures to form sodium silicate, which will then react with sulfuric acid to precipitate silica [90].

This method is considered hazardous to the ecosystem since most of its by-products (sodium sulphate, carbon dioxide, and lots of wastewater) are detrimental to the environment. In this review, the production of silicon nanoparticles from nano-silica is explained in detail, emphasizing the importance of turning waste into wealth. Interestingly, biomass is in abundance and serves as the future source of renewable energy reservoirs [91].

2.2.2. Extraction of Silica

The extraction of silica from various agro-wastes has been acknowledged by many researchers across the globe. The agricultural wastes have been identified as the potential raw material for the preparation of silicon composites. The sugarcane bagasse ash is an abundant by-product of agro-food waste materials. These waste materials pose a threat to the environment and thus require proper utilization to get valuable products. It is thus the cheapest source of silica production, and the chemical compositions of a typical sugarcane bagasse ash with geographical locations are shown in Table 1. Moreover, the benefits include: Easy to handle and affordable. It is noteworthy to realize the potential reasons to have several methods to produce silica from various agro-wastes. These include, low

material consumption, thus reduced costs, the high silica content in the agro-wastes, relative silica quality, nature of the material (amorphous), energy content, and eventually, low energy consumption [92,93].

Table 2.1. *Elemental composition (%) of sugarcane bagasse ash from various countries: Analysis and authors.*

SiO_2	Fe_2O_3	Al_2O_3	CaO	MgO	SO_3/SO_4	K_2O	Loss of Ignition (LOI)	Country	Authors
62.1	5.42	5.54	1.0	1.12	-	2.22	-	Uganda	(Basika, et al. 2015). [94]
84.0	1.7	1.1	0.5	0.6	-	0.5	3.1	South Africa	(Aboyade et al. 2011) [95]
72.8	5.5	6.4	3.8	2.3	-	2.7	3.7	Columbia	(Torres Agredo et al. 2014) [96]
96.2	1.7	0.2	0.1	0.1	0.1	0.3	1.04	Brazil	(Sales and Lima 2010) [97]
31.41	6.02	7.57	16.06	1.07	0.78	1.58	32.2	Brazil	(Castaldelli et al. 2013) [98]
67.82	2.56	6.33	1.54	2.03	-	2.87	2.31	Thirukovikur	(Hariharan et al. 2014) [99]
87.59	0.67	0.57	2.59	1.65	0.003	3.64	NA	India	(Modani and Vyawahare 2013) [100]
62.43	6.98	4.28	11.8	2.51	1.48	3.53	4.73	India	(Kawade, Rathi, and Girge 2013) [101]

66.89	29.18	29.18	1.92	0.83	0.56	NA	0.72	India	(Hussein et al. 2014) [102]
41.15	2.70	7.00	3.20	0.12	0.03	8.75	17.7	Nigeria	(Otoko 2014) [103]
77.25	4.21	6.37	4.05	2.61	0.11	2.34	1.40	Sudan	(Hussein et al. 2014) [104]
72.85	6.96	1.08	9.97	6.49	NA	6.71	4.23	Nigeria	(Abdulkadir, Oyejobi, and Lawal 2014) [105]
44.70	2.90	2.40	14.9	3.50	NA	4.40	16.7	Iran	(Abbasi and Zargar 2013) [106]

The table above shows the chemical make-up in the extracted silica from sugarcane bagasse ash from various countries, and it is quite evident that it is composed mostly of SiO_2. In South Africa, the bagasse constitutes approximately 84% of SiO_2, the third-highest after India and Brazil with 87.59% and 96.2%, respectively. This makes sugarcane bagasse an ideal source of SiO_2 to investigate and explore for further studies [104,106,106].

The calculation below was carried out to find the percentage yield from the chemical treatment reported in [107]. The results from XRF, XRD, and SEM showed the metal oxides present and key findings on silica, which were calculated using the approximation calculation method [107].

100 g of SBA introduces approximately 76.34 of SiO_2 ... ... (2.3)

Therefore, unknown (X) amount of SCBA will introduce 73.21 g of SiO_2 ... ... (2.4)

The aforementioned implies, = $\frac{100\ x\ 73}{76.34} = \frac{7300}{76.34} = 95.625\ g\ of\ SCBA$ ... ... (2.5)

For, Al_2O_3 since 100 g SCBA introduces 6.7 g of Al_2O_3, then: 95.625 g of SCBA will introduce $=\frac{95.625\ x\ 6.7}{100} = \frac{640.688}{100} = 6.407\ g\ of\ Al_2O_3$ ... ... (2.6)

Fe_2O_3: since 100 g SCBA introduces 6.3 g of Fe_2O_3, then: 95 625 g of SCBA will introduce $\frac{95.625\ x\ 6.3}{100} = \frac{602.438}{100} = 6.024\ g\ of\ Fe_2O_3$ ... ... (2.7)

CaO: Since 100 g SCBA introduces 2.8 g CaO, then: 95.625 g of SCBA will introduce $=\frac{95.625\ x\ 2.8}{100} = \frac{267.75}{100} = 2.678\ g\ of\ CaO$ ... ... (2.8)

MgO: Since 100 g SCBA introduces 3.2 g MgO, then: 95.625 g of SCBA will introduce = $\frac{95.625\ x\ 3.2}{100} = \frac{306}{100} = 3.06\ g\ of\ Mg$ ... ... (2.9)

P_2O_5: Since 100 g SCBA introduces 4.0 g P_2O_5, then: 95.625 g of SCBA will introduce = $\frac{95.625\ x\ 4.0}{100} = \frac{382.5}{100} = 3.825\ g\ of\ P_2O_5$ ... ... (2.10)

Na_2O: Since 100 g SCBA introduces 1.1 g Na_2O, then: 95.625 g of SCBA will introduce = $\frac{95.625\ x\ 1.1}{100} = \frac{105.188}{100} = 1.052\ g\ of\ Na_2O$ ... ... (2.11)

K_2O: Since 100 g SCBA introduces 2.4 g K_2O, then: 95.625 g of SCBA will introduce = $\frac{95.625\ x\ 2.4}{100} = \frac{229.5}{100} = 2.295\ g\ of\ K_2O$ ... ... (2.12)

LOI: Since 100 g SCBA introduces 0.9 g LOI, then: 95.625 g of SCBA will introduce = $\frac{95.625\ x\ 0.9}{100} = \frac{86.063}{100} = 0.861\ g\ of\ LOI$ ... ... (2.13)

2.2.2.1. Electrochemical Process

The electrochemical procedure is considered one of the most versatile techniques to synthesize silicon nanoparticles (SiNPs). The procedure involves the filling of a Teflon cell with a mixture of aqueous hydrofluoric acid (HF) and ethanol, subsequently followed by etching of a silicon wafer carried out under steady current supply, as shown in Figure 2.9 [108]. The reaction mechanism of diluting HF for silicon wafer etching is presented below:

$$SiO_2 + 4HF \rightarrow SiF_4 + 2H_2O \ldots \ldots \ldots \ldots \ldots \ldots \ldots \ldots \ldots \ldots \ldots \ldots \ldots \ldots \ldots \ldots \ldots \ldots \ldots \ldots \ldots \ldots \ldots \ldots \ldots . (2.14)$$

$$SiF_4(g) + 4Na(l) \rightarrow Si(s, powder) + 4NaF(s) \ldots \ldots \ldots \ldots \ldots \ldots \ldots \ldots \ldots \ldots \ldots \ldots \ldots \ldots \ldots (2.15)$$

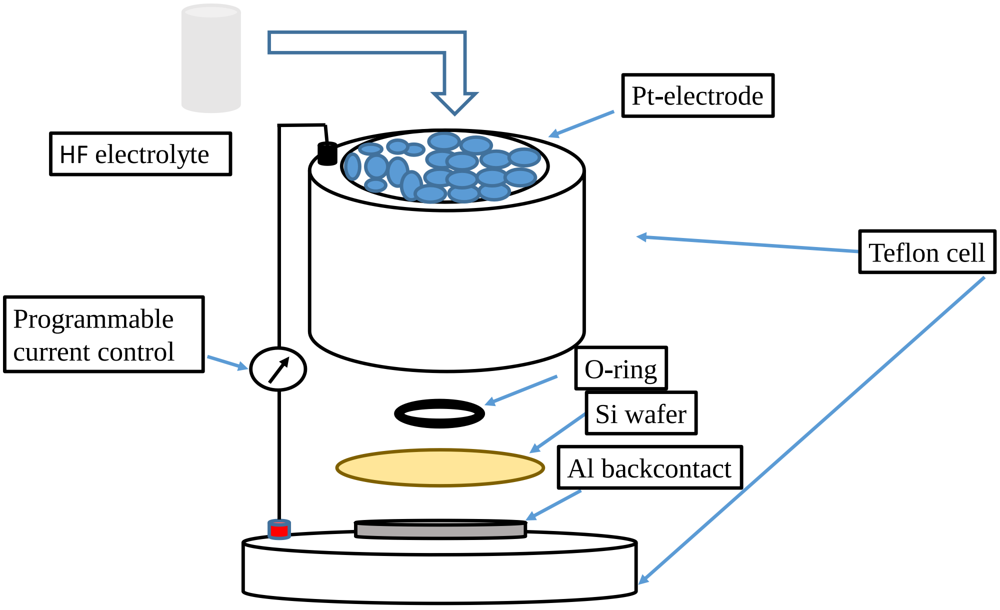

Figure 2.9. *Electrochemical etching set-up.*

The fundamental approach is the perspective of producing porous silicon (PSi), traditionally known as silicon nanocrystal thin film, which surpassed photo luminescent SiNPs developed from vanostatic adonization.

Triumphs and Challenges

The distortion or break-up treatment is performed on an etched PSi layer for sonication procedure in order to obtain the desired quantum-confined colloidal silicon nanoparticles (SiNPs). Furthermore, it is not easy to manipulate and alter the properties of PSi thin-film and surface morphology due to the irreversible effect caused by the electrolyte composition, silicon dopant type, dopant concentration, and etching time. However, ethanol can alter and prevent the bubble break-up and reduce the hydrophobicity, which ultimately leads to an

effective pore formation, an advantageous feature, and consequently, uniformity retained as a result of hydrogen-terminated silicon nanocrystals [109–111].

2.2.2.2. Ball Milling Process

Ball milling is a popular method because of its simplicity and requiring relatively inexpensive equipment to operate and can be deployed on a wide range of other materials. Nano-crystalline materials can be successfully produced using the aforementioned process. Lam et al., 2000, synthesized ultra-fine SiNPs with 5 nm using solid graphite (C) in concurrent with silicon dioxide SiO_2 in a planetary ball miller shown in Figure 2.10 for about 7–10 days on a larger scale. The mixture was loaded on a stainless-steel vial together with stainless-steel balls (7.5 mm diameter), and the molar ratio employed was 1:1 graphite-SiO_2 as shown in the reaction mechanism below [111].

$$SiO_2 + C\ (graphite) \rightarrow Si\ + \uparrow (CO_2)_x \ldots\ldots\ldots\ldots\ldots\ldots\ldots\ldots\ldots\ldots\ldots\ldots\ldots\ldots\ldots\ldots\ldots\ldots\ldots (2.16)$$

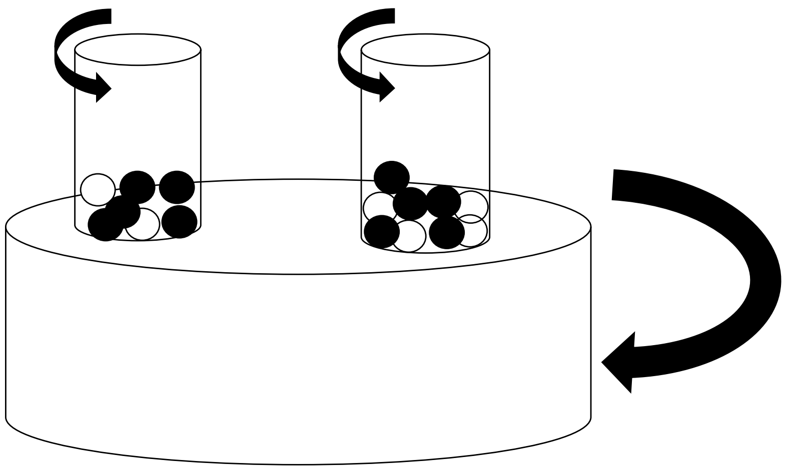

Figure 2.10. *Planetary ball mill for the preparation of SiNPs.*

The content was then sealed with a Viton O-ring. However, the vial was first purged with argon to remove other gases, with the remaining argon set to atmospheric pressure. After a period of 7–10 days, respectively, the powders (milled) were then annealed in a hydraulic press for 48 h at 150 °C under a loading of 30 kgf/mm^2. In addition, the annealed powders

were then put back into a vial and further milled for another 2 more hours to break up the pressed tablet into powder form [111].

The resulted NPs were reported to have been covered with an amorphous SiO_2 layer of 1 nm in thickness and produced a multi-peak PL spectrum because of a wide range of particle sizes present.

Triumphs and Challenges

The physical methods usually can achieve size controllability of the as-synthesized SiNPs. The major drawback is that the productivity is not scalable and the chemistry of Si QDs to be stabilized is not well established [107]. Furthermore, the presence of aggregates presents a complex and coarse shape apart from the size distribution. Thus, it limits the utilization of ball milling synthetic route despite of its convenience and inexpensiveness [111].

2.2.2.3. Sol–Gel Process

The sol–gel procedure is a wet chemical approach traditionally known as chemical solution deposition. It involves, several steps, namely, hydrolysis and polycondensation, gelation, aging, densification, and crystallization. The processing of inorganic ceramic and glass materials was first conducted as early as the mid-1800s by Ebelman and Graham's studies on silica gels [112]. The process mainly involves alkaline extraction, followed by acid precipitation.

Sugarcane bagasse is cleaned and made moisture-free by drying. Additionally, studies have reported that acid pre-treatment is one of the effective ways to remove of ionic impurities from sugarcane bagasse [113].

Therefore, 1 M HCl is used for pre-treatment shown in Figure 2.11, in a water bath and heated at 75 °C. The sample is subsequently filtered numerous times to discard metallic ions and further dried in an oven. The as-obtained sugarcane bagasse ash is then immersed in 1 M $NaOH$ and refluxed for an hour at 90 °C to produce sodium silicates solution from the sugarcane bagasse, as shown in the following equation [113,114].

$$SiO_2\,(s)\ + 2NaOH_{(aq)} \rightarrow Na_2SiO_{3(aq)}\ +\ H_2O_{(aq)} \ldots\ldots\ldots\ldots\ldots\ldots\ldots\ldots\ldots\ldots\ldots\ldots\ldots (2.17)$$

$$Na_2SiO_{3(aq)} + 2HCl_{(aq)} \rightarrow SiO_{2(gel)} + 2NaCl_{(aq)} + H_2O(l) \ldots\ldots\ldots\ldots\ldots\ldots\ldots\ldots\ldots (2.18)$$

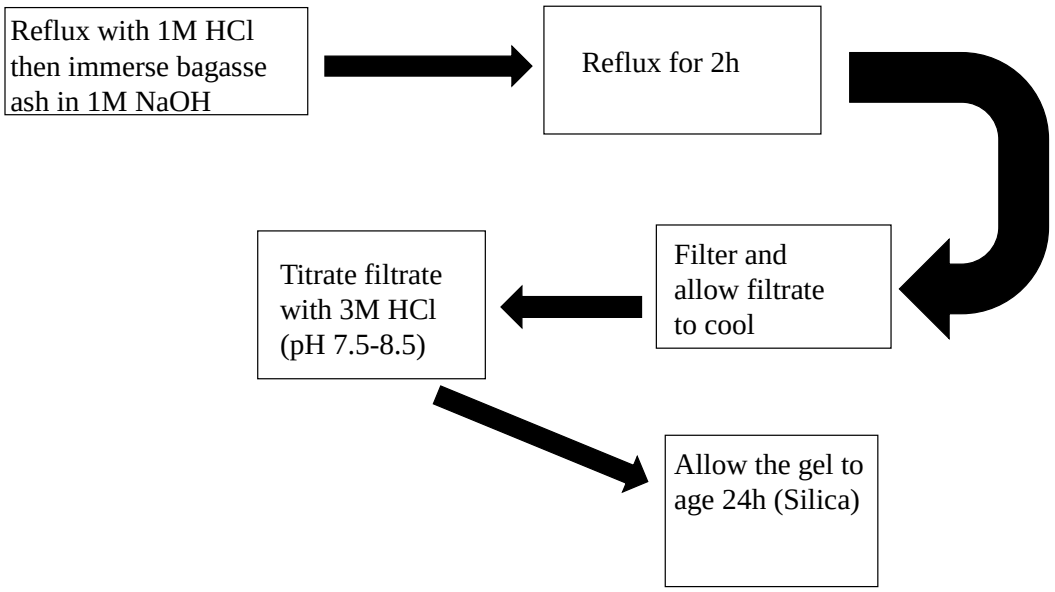

Figure 2.11. *Sol gel method for silica preparation.*

The key findings of the investigation were the observations made during the hydrolysis of tetraethyl orthosilicate (TEOS), $Si(OC_2H_5)$, under acidic media yielded SiO_2 in the form of a "glass-like" material [115]. Roy and co-workers did another breakthrough study where they highlighted the potential for achieving desired and efficiently high levels of homogeneity in colloidal gels. They used the sol–gel method in the 1950s and 1960s to synthesize a large number of unique ceramic oxides of novel chemical make-up, such as Al, Si, Ti, Zr, and others, which could not be achieved by other ceramic methods [115].

The high purity silica xerogels were prepared from bagasse ash to form sodium silicate by the sol–gel method. Subsequently, the mixture was treated with acid for gelating formation,

whereby condensation reaction, the siloxane linkage between surface silanol groups as shown in the following reaction mechanism [116];

$$Si(OH)_4 + HO - Si(OH)_3 \rightarrow (OH)_3Si - O - Si(OH)_3 + H_2O \ldots\ldots\ldots\ldots\ldots\ldots\ldots (2.19)$$

The precipitation procedure with the pH was maintained at > 7 [115]. The sodium silicate solution with the hydrochloric acid process can be shown as:

$$Na_2O.xSiO_2 + 2HCl \rightarrow xSiO_2 \downarrow + 2NaCl + H_2O \ldots\ldots\ldots\ldots\ldots\ldots\ldots\ldots\ldots\ldots\ldots\ldots (2.20)$$

Moreover, purification with demineralized water was found to be successful for the purity as high as 99 wt%. The structural properties indicated that the as-prepared silica xerogels were amorphous in nature [117].

Triumphs and Challenges

The chemical methods, however, showed that there is room to manipulate the SiNPs by fine-tuning the synthesis and achieve the desired properties via surface modification and controllable particle size distribution of Si Quantum Dots. However, the question of purity always arises from residual side products. The high yield and desirable uniform properties have attracted researchers worldwide to produce Si QDs using electrochemical techniques under certain conditions from porous silicon. The shape and size distribution, as well as particle size control are still a major challenge for this technique [118,119].

Several methods have been utilized by many researchers to study the production of nanoparticles from various feedstock. Basically, the sol–gel method is most preferred for this current study as it allows for altering of the materials from the nano-level to achieve desirable properties. Silicon nanoparticles possess high physical characteristics, outstanding opto-electronic properties (i.e., photoluminescence), active surface state, and biocompatibility, making them an ideal material and attractive to be utilized in solar cell fabrication [120,121].

2.2.3. Reduction methods of Silica into Silicon Nanoparticles

Below is the discussion of two methods used to reduce silica to silicon, including carbothermic and magnesiothermic reduction.

2.2.3.1. Carbothermic Reduction of Silica to Silicon

Carbothermic reduction is traditionally an industrial procedure used to manufacture-grade silicon dioxide in an electric arc furnace according to the simplified reaction Equation (19) below. The method involves high temperatures (2000 °C) and high-energy consumption, shown in Figure 2.12. The flow chart displays the processes involved to get high purity silica from precursor materials to silicon, using the synthetic reduction routes. Some other methods involve tetrafluoride shown in (20) similar to (c) and (b) decomposition of silane (22), however, they might not be economically viable [122–124].

$$SiO_2(s) + 2C \rightarrow Si(s) + 2CO(g) \quad \ldots\ldots (2.21)$$

$$SiF_4(g) + 4Na(l) \rightarrow Si(s, powder) + 4NaF(s) \quad \ldots\ldots (2.22)$$

$$SiH_4(g) \rightarrow Si(s, powder) + 2H_2(s) \quad \ldots\ldots (2.23)$$

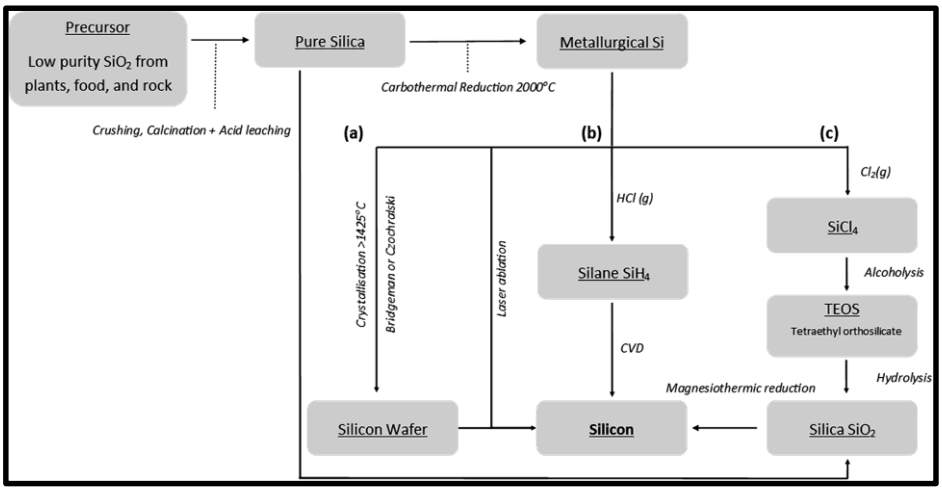

Figure 2.12. *Flow chart of existing bulk silicon synthesis routes, including magnesium reduction [125].*

The electric arc furnace requires about 1900 °C to melt sand, which translates to 50 kWh of energy for a kilogram of sand. In addition, for 60,000 tons of metallurgical-grade silicon expected to be produced annually, the required energy could be 30 TWh. Therefore, it is notably evident that the aforementioned process is energy-intensive, making it quite expensive as well as environmentally unsustainable.

Hence, it is worth investigating other alternative sources for silicon, agricultural wastes (sugarcane bagasse). The carbothermic procedure involves waste product on waste, which is advantageous for this route, synthesized activated carbon from waste material. Recently, studies have reported the use of the microwave process for carbothermic reduction of silica to silicon [124,125].

2.2.3.2. Magnesiothermic Reduction of Silica to Silicon

The metallothermic reduction of silica via magnesiothermic reduction procedure leads to the formation of silicon using very low temperatures and reaction time. The procedure is not energy-intensive and thus inexpensive. The progress of the reaction depends on the experimental conditions, with temperatures below the melting point of magnesium of 650 °C, moreover, in a solid-state reaction (2) dominates [126,127].

$$SiO_2 + 2Mg \rightarrow Si + 2MgO \quad \ldots\ldots (224)$$

$$SiO_2 + 4Mg \rightarrow Mg_2Si + 2MgO \quad \ldots\ldots (2.25)$$

$$2Mg + Si \rightarrow Mg_2Si \quad \ldots\ldots (2.26)$$

$$SiO_2 + 2MgO \rightarrow Mg_2SiO_4 \quad \ldots\ldots (2.27)$$

The magnesiothermic reduction has shown the potential to produce silicon from silica in the temperature range of 500 and 950 °C, which allows template-assisted design of silicon structures. Furthermore, the method has demonstrated the ability to preserve structural and intricate features in the as-synthesized silicon as small as 15 nm. The production of pure silicon requires one last step, where nitric acid (HNO_3) and hydrochloric acid (HCl) are

added to remove any unreacted silica and excess magnesium present in the sample, essentially, other studies report the use of two acids aqua regia than single acid addition, consequently, leaving silicon replica behind with improved and higher surface area than the starting template [128].

2.2.4. Purification of Silicon

Production of silicon from several agricultural wastes is not usually obtained directly without passing through the refining process. Thus, purification of silicon is an essential part, especially in industrial solar-grade (SoG)-silicon. Due to the shortage of semiconductor-grade, which is expensive, it has been a great challenge for its production [129,130].

This later led to the new ways of upgrading the metallurgical-grade silicon at a lower cost though at the expense of loss of some of silicon. The upgraded metallurgical-grade silicon (UMG-Si) generally contains impurities, which affects the photovoltaic performance, namely, short-circuit current (JSC), open-circuit voltage (VOC), fill factor (FF), and power conversion efficiency in silicon-based solar cells [131–134].

Furthermore, the phosphorus diffusion gettering process has been widely utilized to improve the performance of Si solar cells. Moreover, the enhanced performance in the photovoltaic technology has been mainly due to improving the electrical properties of UMG-Si wafers and solar cells. The minority-carrier recombination lifetime and photovoltaic performance degradation of p-type silicon solar cells, as well as the effects of metallic contaminant type and concentration thereof (Al, Cu, Ni, and Fe), have been reported [135].

Therefore, the stable SoG-Si has led to the quest to find suitable purification methods and to reduce the production cost minimally without affecting the desired properties of the built solar cells. It is worth noting that these several purification methods are usually the simple preparation of SoG-Si from lower grades, mostly the MG-Si. Consequently, it has been shown that heat treatment could be used to essentially modify the morphology of purified silicon.

Presently, the solvent refining process has been proved to be an important purification method that is beneficiation to the cost due to its high purification efficiency and low

processing temperature. It usually involves alloying silicon with another element to enable the solvation and solidification with recrystallization of silicon from the solvent at a much lower temperature than the melting point of silicon, subsequently followed by separation of the crystallized silicon [136,137]. Several other refining methods include directional solidification, fractional melting, leaching, slag treatment/gas blowing, electron beam melting, etc. [137].

2.3 Sugarcane bagasse ash: An agricultural residue with potential rubber filler properties

2.3.1. Background

Sugarcane commonly known as "*saccharum officinarum L*" is a commercially grown crop in harvesting season under climate conditions of slightly sunny and colder. And, it is produced annually in most parts worldwide, with 100 million tonnes produced by both Brazil and India. South Africa produces about 19.3 million tonnes of sugarcane annually followed by Nigeria and Uganda with two of largest producers of sugar cane on African soil [138–140].

Sugar cane in South Africa is grown in the Kwa-Zulu Natal Province and Mpumalanga Province as shown in Figure 2.13. Sugar cane production in the Kwa-Zulu Natal Province is composed of gross farming located across the two provinces whereby about 22,949 registered sugarcane growers produce annually 20 million tons of sugarcane from approximately 14 million supply sections, extending from southern Kwazulu-Natal to Mpumalanga Lowveld as shown in Figure 2.13 [141].

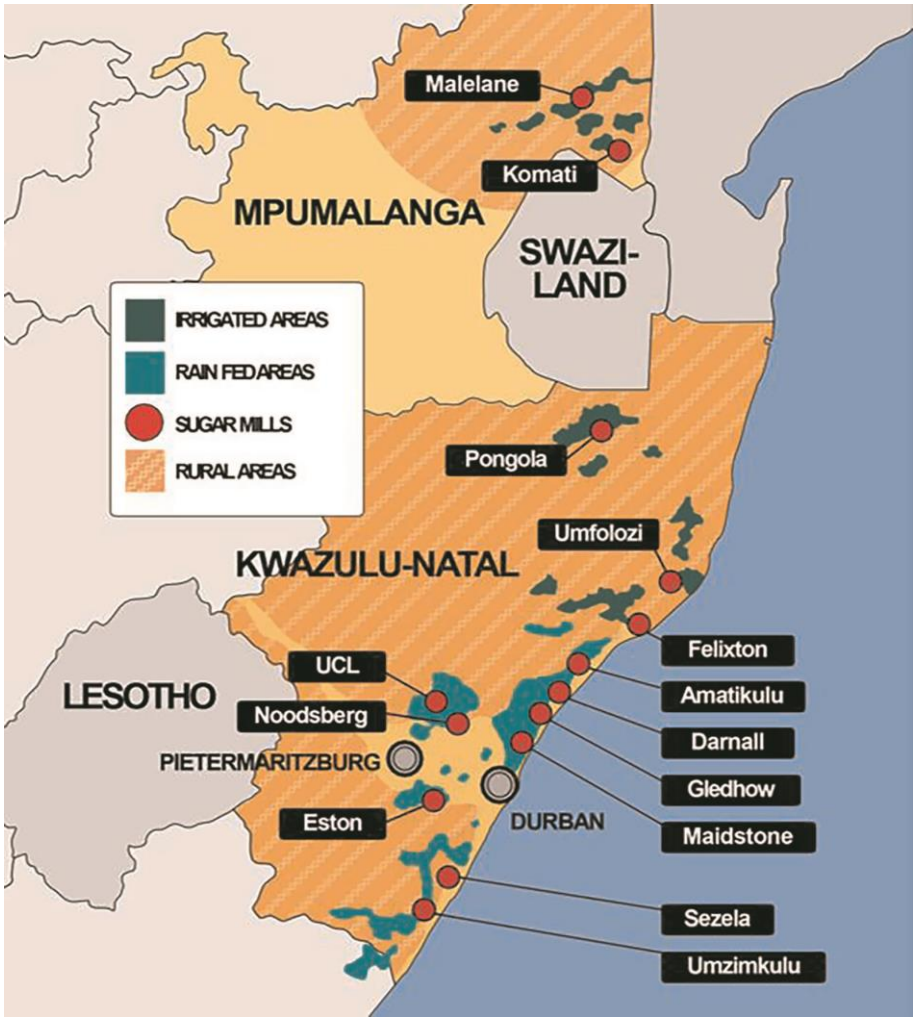

Figure 2.13. *Represents sugarcane plantations regions in the Mpumalanga and KwaZulu-Natal provinces of South Africa [141].*

Sugarcane primarily it is the source of sugar and juice, and can be used as a raw material in various industries for production of sugar, jiggery and syrups. In spite of that these industrial processes generate considerable quantities of residual bagasse, which is often used to produce heat energy via combustion. Interestingly, about 25–30 wt residual lignocellulose bagasse (RSB) is produced per kg of sugarcane processed in sugar mills [142–145]. The crop accumulates to approximately 380 kg/pa of silicon in a 12-month-old-crop. In addition, silicon in this state is a solid waste as silica (SiO_2). It has been reported that natural silica is safe to handle, cheap and simple work-up extraction from various sources. The fate of bagasse ash poses a challenge to the environment [146].

Nowadays, research has swiftly shifted focus to the industrial agricultural wastes to address the ever-growing concerns for the inadequate disposal of residues produced from agro-

wastes. Consequently, led to the development of hybrid composites via reinforcements in polymer science. The use of substitute materials such as sugarcane bagasse as a filler in rubber and cementious application, has become a global concern to look at ways to minimize the disposal of wastes especially those which are nonbiodegradable and pose a threat to the eco-system. Therefore, recycling and re-use of these residues released as wastes from industries has been efficient route to minimize the disposal of wastes which are not environmentally friendly and pose a threat to the quality of life (micro-organisms) [147].

Notably the re use of recycled fillers as reinforcements from renewable sources has received an increased attention with the aim of synthesizing alternate materials in addressing shortcomings related to the fairly and low sustainable of conventionally reinforced polymer composites. Carbonaceous nanomaterials from various sources such as wood, jute, cotton and bagasse have been introduced into a polymer matrix as reinforcements which have recently gained momentum in polymeric composites, this is due to their production means being inexpensive, fast and do-able [148].

Additionally, sugarcane bagasse their composites possess good chemical, physical and mechanical properties and is considered a low-cost and low-density material which possesses potential application-specific mechanical strength and stiffness values [149]. Thus, researchers reported on the mechanical properties of the composites (elasticity and elongation at break) whereby they measured using the average of the three properties in Table 2.2. In relation to the stress–strain, the mechanical properties in terms of tensile strength, the values measured from sugarcane bagasse ash SCBA with optimized silane treatment were found to be the most desired and excellent.

Table 2.2. *Mechanical properties of the composites with and with no silane coupling agent.*

Property	Pure gum	25 per hundred rubber (phr) pristine	25 per hundred rubber (phr) in situ silane treatment	25 per hundred rubber (phr) with optimized silane treatment
Stress	4.02	4.23	4.96	11.47

(MPa)				
Modulus (E)(MPa)	0.32	0.37	1.03	0.62
Strain (%)	974	625	442	857.4

For modified application of silane coupling agent, Bis[3-(triethoxysilyl)propyl] Tetrasulfide (TESPT), in the SCBA-Natural Rubber interaction, SCBA particles were homogenously dispersed in the NR matrix, from the method reported in [150, 151]. The samples with a significant amount (phr) of SCBA were studied to understand and aim for greater interfacial adhesion within the treatments. Hence, the composites displayed improved mechanical response, the bold in the table imply to the best results observed in the samples. Moreover, the use of SCBA can be a feasible substitute material as filler in Natural Rubber (NR) due to excellent mechanical properties [152].

Interestingly, sugarcane bagasse has been used as reinforcing phase in cementitious and polymer composites. And, it comprises of waste generated from industrial production of sugar, fuel and other beverages derived from sugarcane. Sugarcane bagasse ash is mostly composed of silica in various forms structurally including crystalline, vitreous and amorphous. The amorphous silica from SCBA has been utilized as a filler in polymer composites. Wimolmala and Sombatsompop reported for the first time the utilization of SCBA with a particle size in the range 45–145 μm as a filler in a rubber matrix with a concentration of 15 phr (per hundred rubber). Although, they incorporated high content of N-cyclihexyl-2-benzothiazole sulphonamide (CBS), which, in spite of improving the crosslinks sections and the mechanical resistance of the composites, significantly minimized their life time. Traditionally, the alkaline treatment is utilized followed by a strong acid for neutralization to produce silica gel, as illustrated below [153–155]:

$$SiO_{2(s)} + 2NaOH_{(aq)} \rightarrow Na_2SiO_{3(aq)} + H_2O_{(aq)} \ldots\ldots\ldots\ldots\ldots\ldots\ldots\ldots\ldots\ldots\ldots\ldots (2.28)$$

$$Na_2SiO_{3(aq)} + 2HCl_{(aq)} \rightarrow SiO_{2(gel)} + 2NaCl_{(aq)} + H_2O_{(l)} \ldots\ldots\ldots\ldots\ldots\ldots\ldots (2.29)$$

Other studies have reported the use of sugarcane fibres as reinforcing filler, which implies the environmentally-friendly application of this natural resource. In this current study, the structural and morphological properties of sugarcane bagasse ash were studied as well as thermal properties potential for reinforcements in rubber materials. The use of citric acid (an organic acid) during treatment step to remove any inorganic impurities from the ash proved to be useful tool in realizing green methodology for the use of sugarcane bagasse ash [156].

Nanomaterials have allowed researchers to effectively manipulate and exploit materials at the nanometer scale to produce new functionalities. And, to fine-tune their properties from an atomic level, to get desired properties to suit particular applications. In essence, rubber materials are desired to be inexpensive, due to the biomaterials (filler/polymer matrix) and their fabrication methods as well as their resources which is of paramount importance as compared to conventional silica from non-natural resources. In this work surface treatment was performed using citric acid potentially to improve the interfacial adhesion of waste and its higher interactions with elastomeric matrix. The structural, morphological and thermal properties of SCBA potential for filler matrix interaction were analyzed.

2.3.2. Results and discussion

2.3.2.1. Powder X-ray diffraction and FTIR analysis

The X-ray diffraction pattern of untreated (i) and treated (ii) Sugarcane bagasse ash (SCBA) is presented in Figure 2.14a. The x-ray diffraction pattern reveals diffraction peaks associated with the presence of quartz silica @ 2θ = 27 (JCP phase from ICDD: 01–083-0539), and broad peak corresponding to the amorphous nature of silica in the bagasse sample @ 2θ = 12 and between 2θ = 22 and 28. The attributed traces of silica in the form of quartz in the bagasse ash was reported to be as a result of accumulation of minerals from the soil. The obtained bagasse proves to be heavily impure as shown in Figure 2.14a (i) for untreated bagasse ash. The acid treated bagasse, Figure 2.14a (ii) ash show crystalline peaks attributed to silica as well as smooth peaks as compared to the untreated bagasse ash [157].

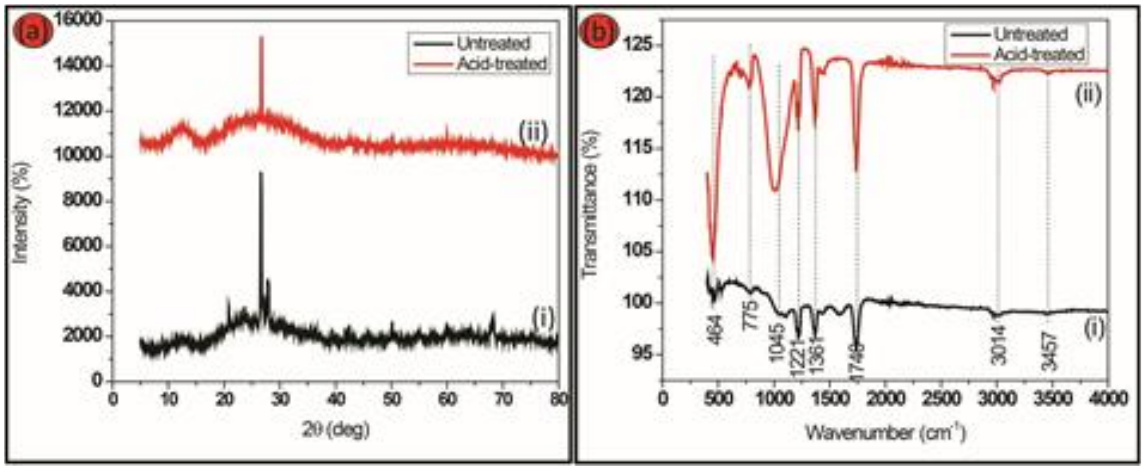

Figure 2.14. *Presents XRD spectra of (a) untreated bagasse ash (i) and treated bagasse ash with citric acid (ii), and FTIR spectra of (b) untreated bagasse ash (i) and treated bagasse ash with citric acid (ii).*

Figure 2.14b, presents FTIR spectra of untreated (i) and acid-treated (ii) bagasse ash. The key functional groups existing in the bagasse ash were identified and characteristics peaks for SCBA with absorption bands between 1046 and 1221 cm^{1} corresponds to asymmetric vibration of the Si-O-Si bonds. The peaks at 464 and 775 cm^{-1}, correspond to Si-OH present on the surface of the particles. The peaks at 1361 and 1740 cm^{-1} are associated with organic matter in the material and C=O, respectively. The peaks at 3014 and 3457 cm^{-1} are as a result of organic matter in the ash C-O and OH group, respectively.

SCBA material it is possible to observe the pronounced peaks and intense peaks for the acid leached sample in Figure 2.14b (ii). It is noteworthy to realize the evolution and disappearance of functional groups and the appearance of key functional groups. This confirms successful incorporation of new functionalities on the acid leached sample (ii) Figure 2.14b. Moreover, the highly narrow and pronounced band at around 1046 cm^{-1} which is associated with crystalline silica, is in agreement with the results obtained from XRD diffractograms(s) [157, 158].

2.3.2.2. SEM–EDX analysis

The surface morphologies for the untreated and treated ash were cross examined using Scanning Electron Microscopy (SEM), presented in Figure 2.15A untreated bagasse and (c) for acid-treated bagasse ash. The SEM images, it is possible to observe the agglomerates of irregular morphology and sizes as well as spherical-rice like particles present in the samples.

Although, organic acid leaching process was effective on the surface morphology as observed in (d) with rice-like shape observed, the morphological differences confirm the surface characteristics analysis (FTIR) discussed earlier, where the pre-treatment.

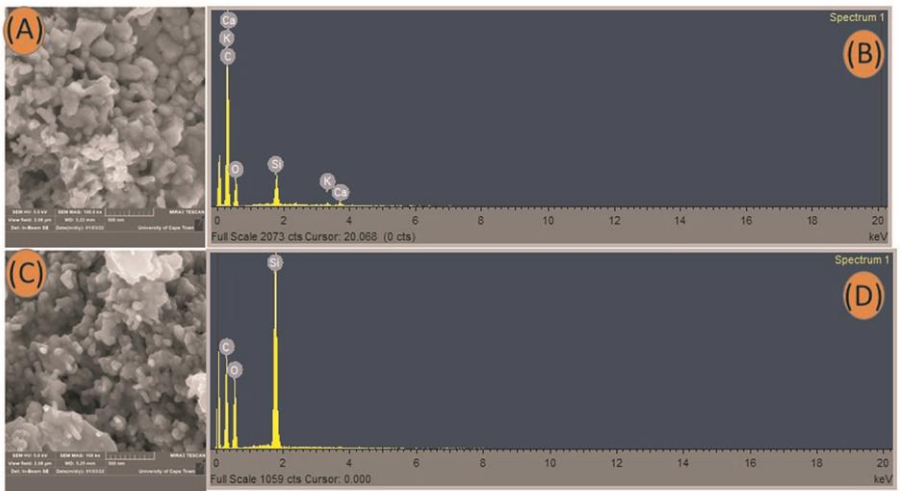

Figure 2.15. *SEM images of (A) untreated bagasse ash, corresponding EDX spectrum (B) and image of (C) treated bagasse ash with citric acid and corresponding EDX spectrum (D).*

with citric acid significantly improved the formation of silica for the acid-leached sample [158, 159].

The EDX results exhibit that the chemical composition of SCBA untreated and treated with citric acid obtained by SEM–EDX shown in Figure 2.15B and d, respectively, that acid treatment is an effective tool to mitigate impurities from the increment of Si matter in the samples for acid-leached. In addition, the acid-treated bagasse ash reveal closely packed particles due to the increased formation of hemicellulose removal bonds. The acid leaching treatment results in the degradation of cellulose and hemicellulose inspired bonds, thus the resulting cellulose chains generate new hydrogen bonds to replace the removed ones. In essence, improves filler polymer interaction [160].

Table 2.3 shows that citric acid is a useful organic acid for the pre-treatment process. The increased morphology of silica in the powders of the ash is as result of the selective removal of the synthesis residues using citric acid, thereby reducing metallic impurities present as compared to the morphology from the untreated ash.

The samples show that pre-treatment of the ash results in significant reduction in carbon content as shown in Table 2.3 below, and silicon increased from 1.78% to 5.27%.

Table 2.3. *Elemental composition of pristine scba and treated scba.*

Element	Untreated SCBA (%)	Acid-treated SCBA (%)
C	74.92	69.36
O	22.45	25.37
Si	1.78	5.27
K	0.26	—
Ca	0.59	—

2.4. Conclusion

Crystalline silicon solar cells have been used for many decades. Although this technology is at its maturity stage, it is still not financially feasible for developing countries due to the high cost of raw materials and the large surface area required. Solar cell research based on heterojunctions (donor–acceptor) with staggered electronic band alignment, named the type-II configuration, has the potential to address efficiency limitations in already existing technologies. In spite of this, it is in still in its mature research stage and its application might be attained in the near future. Thin film technology is presently producing suitable candidates for application-specific properties where there are non-permanent structures, such as there being no flat roof in buildings, and this is a niche market for these solar cells. Interestingly, the efficiency of thin film solar cells has improved over the years when raw materials are utilized. Silicon remains the most commercialized, and hybrid architecture allows for the maximum potential of utilizing this star material as well as looking for alternative sources to eventually minimize the fabrication costs of these devices.

The review provides information about the importance of conventional procedures to produce nano-silicon from sugarcane bagasse. The electrochemical process can produce highly porous quantum-confined colloidal silicon nanoparticles. The disadvantage arises from the overall material properties because it is not easy to manipulate due to the irreversible effect caused by electrolyte composition, the ball milling procedure is popular for its relatively simplistic (ease of operation) and inexpensive approach to producing sizeable silicon nanoparticles, however, the major limitation is the inability of scalability and the chemistry of Si quantum dots (stability). Another conventional method discussed is the sol–gel procedure with the ability to fine-tune the material property via surface chemistry (modification) and controllable particle size distribution, although the purity factor has always been the major drawback for this method arising from residual by-products. Interestingly, a window of opportunity for improvement still exists for the three discussed procedures for the production of highly pure silicon nanoparticles from sugarcane bagasse ash, which will serve as an important synthetic route in lowering the manufacturing costs and providing low-cost polycrystalline silicon semiconductors for application in thin-film solar technology.

Based on the findings, we concluded that acid-leaching significantly improved the chemical, physical and thermal properties of bagasse ash. The ash is mostly carbonaceous material. And, the major component of SCBA is silica from the elemental composition studies. The SCBA contains both amorphous and crystalline silica. The reduction of inorganic impurities makes the bagasse residue potential to serve as a filler in polymer composites, and presents a promising and feasible alternative substitute material for the rubber industry. The advantage of this finding is that the use of organic acid proved essentially and equally compatible for the current study as eco-friendly and green method for acid-leaching process.

Furthermore, the filler material will enhance the thermal and mechanical properties of the polymer matrix. These new route to recycle the agricultural residue from the sugarcane industry is pre-conceived as eco-friendly and cost-effective due to the readily available of the plant in tropical countries, and could be used as reinforcing filler in polymer matrix interaction. Therefore, presents a niche application in south Africa as it has never been done before.

2.5. References.

[1] Ali, N., Hussain, A., Ahmed, R., Wang, M.K., Zhao, C., Haq, B.U. and Fu, Y.Q., 2016. Advances in nanostructured thin film materials for solar cell applications. *Renewable and Sustainable Energy Reviews*, *59*, pp.726-737.

[2] Asim, N., Sopian, K., Ahmadi, S., Saeedfar, K., Alghoul, M.A., Saadatian, O. and Zaidi, S.H., 2012. A review on the role of materials science in solar cells. *Renewable and sustainable energy reviews*, *16*(8), pp.5834-5847.

[3] Dhakal, T.P., Peng, C.Y., Tobias, R.R., Dasharathy, R. and Westgate, C.R., 2014. Characterization of a CZTS thin film solar cell grown by sputtering method. *Solar Energy*, *100*, pp.23-30.

[4] An, W.J., 2012. *Aerosol Processes Enabling Solar Energy Applications*. Washington University in St. Louis.

[5] Wang, Y., 2017. *Sub 2 nm particle characterization in systems with aerosol formation and growth*. Washington University in St. Louis.

[6] Ahmed, K., Ewees, A.A., El Aziz, M.A., Hassanien, A.E., Gaber, T., Tsai, P.W. and Pan, J.S., 2016, October. A hybrid krill-ANFIS model for wind speed forecasting. In *International Conference on Advanced Intelligent Systems and Informatics* (pp. 365-372). Springer, Cham.

[7] Goldschmidt, J.C. and Fischer, S., 2015. Upconversion for photovoltaics–a review of materials, devices and concepts for performance enhancement. *Advanced Optical Materials*, *3*(4), pp.510-535.

[8] Scrosati, B. and Garche, J., 2010. Lithium batteries: Status, prospects and future. *Journal of power sources*, *195*(9), pp.2419-2430.

[9] Aberle, A.G., 2009. Thin-film solar cells. *Thin solid films*, *517*(17), pp.4706-4710.

[10] Green, M.A., Emery, K., Hishikawa, Y., Warta, W. and Dunlop, E.D., 2015. Solar cell efficiency tables (Version 45). *Progress in photovoltaics: research and applications*, *23*(1), pp.1-9.

[11] Lee, T.D. and Ebong, A.U., 2017. A review of thin film solar cell technologies and challenges. *Renewable and Sustainable Energy Reviews*, *70*, pp.1286-1297.

[12] P.J Reddy., 2010. Science and Technology of Photovoltaics, 2nd edition, CRC Press, Leiden.

[13]Wolden, C.A., Kurtin, J., Baxter, J.B., Repins, I., Shaheen, S.E., Torvik, J.T., Rockett, A.A., Fthenakis, V.M. and Aydil, E.S., 2011. Photovoltaic manufacturing: Present status, future prospects, and research needs. *Journal of Vacuum Science & Technology A: Vacuum, Surfaces, and Films*, *29*(3), p.030801.

[14] Guo, Q., Ford, G.M., Yang, W.C., Walker, B.C., Stach, E.A., Hillhouse, H.W. and Agrawal, R., 2010. Fabrication of 7.2% efficient CZTSSe solar cells using CZTS nanocrystals. *Journal of the American Chemical Society*, *132*(49), pp.17384-17386.

[15] Luque, A. and Hegedus, S. eds., 2011. *Handbook of photovoltaic science and engineering*. John Wiley & Sons.

[16] Catchpole, K.R., McCann, M.J., Weber, K.J. and Blakers, A.W., 2001. A review of thin-film crystalline silicon for solar cell applications. Part 2: Foreign substrates. *Solar Energy Materials and Solar Cells*, *68*(2), pp.173-215.

[17] Shah, A., Torres, P., Tscharner, R., Wyrsch, N. and Keppner, H., 1999. Photovoltaic technology: the case for thin-film solar cells. *science*, *285*(5428), pp.692-698.

[18] Mathew, S., Yella, A., Gao, P., Humphry-Baker, R., Curchod, B.F., Ashari-Astani, N., Tavernelli, I., Rothlisberger, U., Nazeeruddin, M.K. and Grätzel, M., 2014. Dye-sensitized solar cells with 13% efficiency achieved through the molecular engineering of porphyrin sensitizers. *Nature chemistry*, *6*(3), p.242.

[19] Mathew, S., Yella, A., Gao, P., Humphry-Baker, R., Curchod, B.F., Ashari-Astani, N., Tavernelli, I., Rothlisberger, U., Nazeeruddin, M.K. and Grätzel, M., 2014. Dye-sensitized solar cells with 13% efficiency achieved through the molecular engineering of porphyrin sensitizers. *Nature chemistry*, *6*(3), p.242.

[20] Noh, J.H., Im, S.H., Heo, J.H., Mandal, T.N. and Seok, S.I., 2013. Chemical management for colorful, efficient, and stable inorganic–organic hybrid nanostructured solar cells. *Nano letters*, *13*(4), pp.1764-1769.

[21] Pandey, A.K., Tyagi, V.V., Jeyraj, A., Selvaraj, L., Rahim, N.A. and Tyagi, S.K., 2016. Recent advances in solar photovoltaic systems for emerging trends and advanced applications. *Renewable and Sustainable Energy Reviews*, *53*, pp.859-884.

[22] Shin, B., Gunawan, O., Zhu, Y., Bojarczuk, N.A., Chey, S.J. and Guha, S., 2013. Thin film solar cell with 8.4% power conversion efficiency using an earth-abundant Cu2ZnSnS4 absorber. *Progress in Photovoltaics: Research and Applications*, *21*(1), pp.72-76.

[23] Song, S., 2013. Device Modeling and Characterization for CIGS Solar Cells.

[24] Wu, X., 2004. High-efficiency polycrystalline CdTe thin-film solar cells. *Solar energy*, *77*(6), pp.803-814.

[25] Jehl, Z., Erfurth, F., Naghavi, N., Lombez, L., Gerard, I., Bouttemy, M., Tran-Van, P., Etcheberry, A., Voorwinden, G., Dimmler, B. and Wischmann, W., 2011. Thinning of CIGS solar cells: part II: cell characterizations. *Thin solid films*, *519*(21), pp.7212-7215.

[26] Ramanathan, K., Noufi, R., To, B., Young, D.L., Bhattacharya, R., Contreras, M.A., Dhere, R.G. and Teeter, G., 2006, May. Processing and properties of sub-micron CIGS solar cells. In *2006 IEEE 4th World Conference on Photovoltaic Energy Conference* (Vol. 1, pp. 380-383). IEEE.

[27] Lundberg, O., Bodegård, M., Malmström, J. and Stolt, L., 2003. Influence of the Cu (In, Ga) Se2 thickness and Ga grading on solar cell performance. *Progress in Photovoltaics: Research and Applications*, *11*(2), pp.77-88.

[28]Kanevce, A., 2007. *Anticipated performance of Cu (In, Ga) Se2 solar cells in the thin-film limit* (Doctoral dissertation, Colorado State University).

[29] Srinivas, B., Balaji, S., NagendraBabu, M. and Reddy, Y.S. (2015) Review on Present and Advance Materials for SolarCells. *International Journal of Engineering Research-Online*, **3**, 178-182.

[30] Wurfel, P. and Wurfel, U. (2009) Physics of Solar Cells: From Basic Principles to Advanced Concepts. John Wiley &Sons, Hoboken.

[31] Dmitrijev, S. (2006) Principles of Semiconductor Devices. Oxford University Press,Oxford.

[32] Bertolli, M. (2008) Solar Cell Materials. Course: Solid State II. Department of Physics, University of Tennessee,Knoxville.

[33] Saga, T. (2010) Advances in Crystalline Silicon Solar Cell Technology for Industrial Mass Production. *NPG Asia Materials*, **2**, 96-102. http://dx.doi.org/10.1038/asiamat.2010.82

[34] Jayakumar, P. (2009) Solar Energy Resource Assessment Handbook. Renewable Energy Corporation Network for theAsia Pacific.

[35] Zywitzki, O., Modes, T., Morgner, H., Metzner, C., Siepchen, B., Späth, B., Drost, C., Krishnakumar, V. and Frauenstein, S., 2013. Effect of chlorine activation treatment on electron beam induced current signal distribution of cadmium telluride thin film solar cells. *Journal of Applied Physics*, *114*(16), p.163518.

[36] Poplawsky, J.D., Paudel, N.R., Li, C., Parish, C.M., Leonard, D., Yan, Y. and Pennycook, S.J., 2014. Direct imaging of Cl-and Cu-induced short-circuit efficiency changes in CdTe solar cells. *Advanced Energy Materials*, *4*(15), p.1400454.

[37] Ellingson, R.J., Beard, M.C., Johnson, J.C., Yu, P., Micic, O.I., Nozik, A.J., Shabaev, A. and Efros, A.L., 2005. Highly efficient multiple exciton generation in colloidal PbSe and PbS quantum dots. *Nano letters*, *5*(5), pp.865-871.

[38] Chuang, C.H.M., Brown, P.R., Bulović, V. and Bawendi, M.G., 2014. Improved performance and stability in quantum dot solar cells through band alignment engineering. *Nature materials*, *13*(8), p.796.

[39] Gloeckler, M., Sankin, I. and Zhao, Z., 2013. CdTe solar cells at the threshold to 20% efficiency. *IEEE Journal of Photovoltaics*, *3*(4), pp.1389-1393.

[40] Green, M.A., Emery, K., Hishikawa, Y., Warta, W. and Dunlop, E.D., 2015. Solar cell efficiency tables (Version 45). *Progress in photovoltaics: research and applications*, *23*(1), pp.1-9.

[41] Ali, N., Hussain, A., Ahmed, R., Wang, M.K., Zhao, C., Haq, B.U. and Fu, Y.Q., 2016. Advances in nanostructured thin film materials for solar cell applications. *Renewable and Sustainable Energy Reviews*, *59*, pp.726-737.

[42] Fthenakis, V.M. and Kim, H.C., 2007. CdTe photovoltaics: Life cycle environmental profile and comparisons. *Thin Solid Films*, *515*(15), pp.5961-5963.

[43] Huang, L., Zhao, Y. and Cai, D., 2009. Homojunction and heterojunction based on CdTe polycrystalline thin films. *Materials Letters*, *63*(24-25), pp.2082-2084.

[44] Dale, P.J., Peter, L.M., Loken, A. and Scragg, J., 2009. Towards sustainable photovoltaic solar energy conversion: studies of new absorber materials. *ECS Transactions*, *19*(3), pp.179-187.

[45] Chen, S., Gong, X.G., Walsh, A. and Wei, S.H., 2009. Crystal and electronic band structure of Cu 2 ZnSn X 4 (X= S and Se) photovoltaic absorbers: First-principles insights. *Applied Physics Letters*, *94*(4), p.041903.

[46] Bhosale, S.M., Suryawanshi, M.P., Gaikwad, M.A., Bhosale, P.N., Kim, J.H. and Moholkar, A.V., 2014. Influence of growth temperatures on the properties of photoactive CZTS thin films using a spray pyrolysis technique. *Materials Letters*, *129*, pp.153-155.

[47] Nitsche, R., Sargent, D.F. and Wild, P., 1967. Crystal growth of quaternary 122464 chalcogenides by iodine vapor transport. *Journal of Crystal Growth*, *1*(1), pp.52-53.

[48] Zhang, S., 2010. *Organic nanostructured thin film devices and coatings for clean energy*. CRC press.

[49] Abdelkader, D., Rabeh, M.B., Khemiri, N. and Kanzari, M., 2014. Investigation on optical properties of SnxSbySz sulfosalts thin films. *Materials Science in Semiconductor Processing*, *21*, pp.14-19.

[50] Versavel, M.Y. and Haber, J.A., 2007. Structural and optical properties of amorphous and crystalline antimony sulfide thin-films. *Thin Solid Films*, *515*(18), pp.7171-7176.

[51] Choi, Y.C., Lee, D.U., Noh, J.H., Kim, E.K. and Seok, S.I., 2014. Highly improved Sb2S3 sensitized-inorganic–organic heterojunction solar cells and quantification of traps by deep-level transient spectroscopy. *Advanced Functional Materials*, *24*(23), pp.3587-3592.

[52] Choi, Y.C. and Seok, S.I., 2015. Efficient Sb2S3-Sensitized Solar Cells Via Single-Step Deposition of Sb2S3 Using S/Sb-Ratio-Controlled SbCl3-Thiourea Complex Solution. *Advanced Functional Materials*, *25*(19), pp.2892-2898.

[53] Ito, S., Tsujimoto, K., Nguyen, D.C., Manabe, K. and Nishino, H., 2013. Doping effects in Sb2S3 absorber for full-inorganic printed solar cells with 5.7% conversion efficiency. *International Journal of Hydrogen Energy*, *38*(36), pp.16749-16754.

[54] Gödel, K.C., Choi, Y.C., Roose, B., Sadhanala, A., Snaith, H.J., Seok, S.I., Steiner, U. and Pathak, S.K., 2015. Efficient room temperature aqueous Sb 2 S 3 synthesis for inorganic–organic sensitized solar cells with 5.1% efficiencies. *Chemical Communications*, *51*(41), pp.8640-8643.

[55] Huerta-Flores, A.M., García-Gómez, N.A., De la Parra-Arciniega, S.M. and Sánchez, E.M., 2016. Fabrication and characterization of a nanostructured TiO2/In2S3-Sb2S3/CuSCN extremely thin absorber (eta) solar cell. *Semiconductor Science and Technology*, *31*(8), p.085011.

[56] Li, J.B., Chawla, V. and Clemens, B.M., 2012. Investigating the role of grain boundaries in CZTS and CZTSSe thin film solar cells with scanning probe microscopy. *Advanced Materials*, *24*(6), pp.720-723.

[57] Shaikh, J.S., Shaikh, N.S., Mali, S.S., Patil, J.V., Pawar, K.K., Kanjanaboos, P., Hong, C.K., Kim, J.H. and Patil, P.S., 2018. Nanoarchitectures in dye-sensitized solar cells: metal oxides, oxide perovskites and carbon-based materials. *Nanoscale*, *10*(11), pp.4987-5034.

[58] Carlson, D.E. and Wronski, C.R., 1976. Amorphous silicon solar cell. *Applied Physics Letters*, *28*(11), pp.671-673.

[59] Lan, X., Masala, S. and Sargent, E.H., 2014. Charge-extraction strategies for colloidal quantum dot photovoltaics. *Nature materials*, *13*(3), pp.233-240.

[60] Lan, X., Bai, J., Masala, S., Thon, S.M., Ren, Y., Kramer, I.J., Hoogland, S., Simchi, A., Koleilat, G.I., Paz-Soldan, D. and Ning, Z., 2013. Self-Assembled, Nanowire Network Electrodes for Depleted Bulk Heterojunction Solar Cells. *Advanced Materials*, *25*(12), pp.1769-1773.

[61] Semonin, O.E., Luther, J.M. and Beard, M.C., 2012. Quantum dots for next-generation photovoltaics. *Materials today*, *15*(11), pp.508-515.

[62] Tang, J. and Sargent, E.H., 2011. Infrared colloidal quantum dots for photovoltaics: fundamentals and recent progress. *Advanced materials*, *23*(1), pp.12-29.

[63]Brown, P.R., Kim, D., Lunt, R.R., Zhao, N., Bawendi, M.G., Grossman, J.C. and Bulovic, V., 2014. Energy level modification in lead sulfide quantum dot thin films through ligand exchange. *ACS nano*, *8*(6), pp.5863-5872.

[64] Ip, A.H., Thon, S.M., Hoogland, S., Voznyy, O., Zhitomirsky, D., Debnath, R., Levina, L., Rollny, L.R., Carey, G.H., Fischer, A. and Kemp, K.W., 2012. Hybrid passivated colloidal quantum dot solids. *Nature nanotechnology*, *7*(9), p.577.

[65]Jasieniak, J., Califano, M. and Watkins, S.E., 2011. Size-dependent valence and conduction band-edge energies of semiconductor nanocrystals. *ACS nano, 5*(7), pp.5888-5902.

[66] He, Z., Zhong, C., Su, S., Xu, M., Wu, H. and Cao, Y., 2012. Enhanced power-conversion efficiency in polymer solar cells using an inverted device structure. *Nature photonics*, *6*(9), p.591.

[67] Boudouris, B.W., 2013. Engineering optoelectronically active macromolecules for polymer-based photovoltaic and thermoelectric devices. *Current Opinion in Chemical Engineering*, *2*(3), pp.294-301.

[68] Gilot, J., Barbu, I., Wienk, M.M. and Janssen, R.A., 2007. The use of ZnO as optical spacer in polymer solar cells: theoretical and experimental study. *Applied Physics Letters*, *91*(11), p.113520.

[69] Tang, Z., Tress, W. and Inganäs, O., 2014. Light trapping in thin film organic solar cells. *Materials today*, *17*(8), pp.389-396.

[70] Wang, Y., Hu, J., Wu, Y., Xu, J., Lu, J., Zhao, H. and Qian, B., 2014. Radiation damage effects on double-junction GaInP2/GaAs solar cells. *Nuclear Instruments and Methods in Physics Research Section B: Beam Interactions with Materials and Atoms*, *330*, pp.76-81.

[71] Wang, W., Winkler, M.T., Gunawan, O., Gokmen, T., Todorov, T.K., Zhu, Y. and Mitzi, D.B., 2014. Device characteristics of CZTSSe thin-film solar cells with 12.6% efficiency. *Advanced Energy Materials*, *4*(7), p.1301465.

[72] Zimmermann, E., Pfadler, T., Kalb, J., Dorman, J.A., Sommer, D., Hahn, G., Weickert, J. and Schmidt-Mende, L., 2015. Toward high-efficiency solution-processed planar heterojunction Sb2S3 solar cells. *Advanced Science*, *2*(5), p.1500059.

[73] Ke, W., Fang, G., Liu, Q., Xiong, L., Qin, P., Tao, H., Wang, J., Lei, H., Li, B., Wan, J. and Yang, G., 2015. Low-temperature solution-processed tin oxide as an alternative electron transporting layer for efficient perovskite solar cells. *Journal of the American Chemical Society*, *137*(21), pp.6730-6733.

[74] Ma, X., Zhong, J., Li, M., Chen, J., Zhang, Y., Wu, S., Gao, X., Lu, X., Liu, J.M. and Liu, H., 2016. Hybrid solar cells using solution-processed TiO2/Sb2S3 bilayer as electron transport layer. *Solar Energy*, *133*, pp.103-110.

[75] Kim, D.H., Lee, S.J., Park, M.S., Kang, J.K., Heo, J.H., Im, S.H. and Sung, S.J., 2014. Highly reproducible planar Sb 2 S 3-sensitized solar cells based on atomic layer deposition. *Nanoscale*, *6*(23), pp.14549-14554.

[76] Green, M.A., Ho-Baillie, A. and Snaith, H.J., 2014. The emergence of perovskite solar cells. *Nature photonics*, *8*(7), p.506.

[77] Snaith, H.J., 2013. Perovskites: the emergence of a new era for low-cost, high-efficiency solar cells. *The journal of physical chemistry letters*, *4*(21), pp.3623-3630.

[78] Xing, G., Mathews, N., Lim, S.S., Yantara, N., Liu, X., Sabba, D., Grätzel, M., Mhaisalkar, S. and Sum, T.C., 2014. Low-temperature solution-processed wavelength-tunable perovskites for lasing. *Nature materials*, *13*(5), p.476.

[79] Stranks, S.D., Eperon, G.E., Grancini, G., Menelaou, C., Alcocer, M.J., Leijtens, T., Herz, L.M., Petrozza, A. and Snaith, H.J., 2013. Electron-hole diffusion lengths exceeding 1 micrometer in an organometaltrihalide perovskite absorber. *Science*, *342*(6156), pp.341-344.

[80] Xing, G., Mathews, N., Sun, S., Lim, S.S., Lam, Y.M., Grätzel, M., Mhaisalkar, S. and Sum, T.C., 2013. Long-range balanced electron-and hole-transport lengths in organic-inorganic CH3NH3PbI3. *Science*, *342*(6156), pp.344-347.

[81] Ball, J.M., Lee, M.M., Hey, A. and Snaith, H.J., 2013. Low-temperature processed meso-superstructured to thin-film perovskite solar cells. *Energy & Environmental Science*, *6*(6), pp.1739-1743.

[82] Mohd, N.K., Wee, N.N.A.N. and Azmi, A.A., 2017, September. Green synthesis of silica nanoparticles using sugarcane bagasse. In *AIP conference proceedings* (Vol. 1885, No. 1, p. 020123). AIP Publishing LLC.

[83] Faizul, C.P., Chik, A., Bari, M. and Noorina, H.J., 2014. Extraction of silica from palm ash using organic acid leaching treatment. In *Key Engineering Materials* (Vol. 594, pp. 329-333). Trans Tech Publications Ltd.

[84] Das, D., Yang, Y., O'Brien, J.S., Breznan, D., Nimesh, S., Bernatchez, S., Hill, M., Sayari, A., Vincent, R. and Kumarathasan, P., 2014. Synthesis and Physicochemical Characterization of Mesoporous Nanoparticles. *Journal of Nanomaterials*, *2014*.

[85] Faizul, C.P., Abdullah, C. and Fazlul, M., 2013. Extraction of silica from palm ashvia citric acid leaching treatment.

[86] Yadav, A.L., Sairam, V., Muruganandam, L. and Srinivasan, K., 2020. An overview of the influences of mechanical and chemical processing on sugarcane bagasse ash characterisation as a supplementary cementitious material. *Journal of Cleaner Production*, *245*, p.118854.

[87] Yadav, A.L., Sairam, V., Muruganandam, L. and Srinivasan, K., 2020. An overview of the influences of mechanical and chemical processing on sugarcane bagasse ash characterisation as a supplementary cementitious material. *Journal of Cleaner Production*, *245*, p.118854.

[88] Dlamini, M., Nicholson, R.J. and Kadwa, M., 2019. Potential economic benefit of additional transformation initiatives to small scale growers in the South African sugar industry-2018/19. In *Proceedings of the Annual Congress-South African Sugar Technologists' Association* (No. 92, pp. 22-24). South African Sugar Technologists' Association.

[89] Singels, A., McFarlane, S.A., Basdew, I., Keeping, M.G., Nicholson, R., Pilusa, T., Sithole, P. and Titshall, L.W., 2019. Review of South African sugarcane production in the 2018/19 season: too much of a good thing? In *Proceedings of the Annual Congress-South African Sugar Technologists' Association* (No. 92, pp. 1-16). South African Sugar Technologists' Association.

[90] Ma, X., Zhou, B., Gao, W., Qu, Y., Wang, L., Wang, Z. and Zhu, Y., 2012. A recyclable method for production of pure silica from rice hull ash. *Powder Technology*, *217*, pp.497-501.

[91] Farirai, F., Ozonoh, M., Aniokete, T.C., Eterigho-Ikelegbe, O., Mupa, M., Zeyi, B. and Daramola, M.O., 2021. Methods of extracting silica and silicon from agricultural waste ashes and application of the produced silicon in solar cells: a mini-review. *International Journal of Sustainable Engineering*, *14*(1), pp.57-78.

[92] Zhang, L., Xu, C.C. and Champagne, P., 2010. Overview of recent advances in thermo-chemical conversion of biomass. *Energy conversion and management*, *51*(5), pp.969-982.

[93] Zhang, L., Xu, C.C. and Champagne, P., 2010. Energy recovery from secondary pulp/paper-mill sludge and sewage sludge with supercritical water treatment. *Bioresource technology*, *101*(8), pp.2713-2721.

[94] Basika, E., Kigozi, J. and Kiggundu, N., 2015. Investigation of Sugar Cane Bagasse Ash as a Binding Material for the Construction Industry. *Journal of Global Ecology and Environment*, *2*(4), pp.205-208.

[95] Aboyade, A.O., Hugo, T.J., Carrier, M., Meyer, E.L., Stahl, R., Knoetze, J.H. and Görgens, J.F., 2011. Non-isothermal kinetic analysis of the devolatilization of corn cobs and sugar cane bagasse in an inert atmosphere. *Thermochimica Acta*, *517*(1-2), pp.81-89.

[96] Torres Agredo, J., Mejía de Gutiérrez, R., Escandón Giraldo, C.E. and González Salcedo, L.O., 2014. Characterization of sugar cane bagasse ash as supplementary material for Portland cement. *Ingeniería e Investigación*, *34*(1), pp.5-10.

[97] Sales, A. and Lima, S.A., 2010. Use of Brazilian sugarcane bagasse ash in concrete as sand replacement. *Waste management*, *30*(6), pp.1114-1122.

[98] Castaldelli, V.N., Akasaki, J.L., Melges, J.L., Tashima, M.M., Soriano, L., Borrachero, M.V., Monzó, J. and Payá, J., 2013. Use of slag/sugar cane bagasse ash (SCBA) blends in the production of alkali-activated materials. *Materials*, *6*(8), pp.3108-3127.

[99] Hariharan, B., Arbeláez, P., Girshick, R. and Malik, J., 2014, September. Simultaneous detection and segmentation. In *European conference on computer vision* (pp. 297-312). Springer, Cham.

[100] Modani, P.O. and Vyawahare, M.R., 2013. Utilization of bagasse ash as a partial replacement of fine aggregate in concrete. *Procedia Engineering*, *51*, pp.25-29.

[101] Kawade, U.R., Rathi, V.R. and Girge, V.D., 2013. Effect of use of Bagasse Ash on Strength of Concrete. *International Journal of Innovative Research in Science, Engineering and Technology*, *2*(7), pp.2997-3000.

[102] El Hussein, M., Hirst, S., Salyers, V. and Osuji, J., 2014. Using grounded theory as a method of inquiry: Advantages and disadvantages. *Qualitative Report*, *19*(27).

[103] Otoko, G.R. and Honest, B.K., 2014. Stabilization of Nigerian deltaic laterites with saw dust ash. *Int. J. Sci. Res. Manag*, *2*(8), pp.1287-1292.

[104] Abdulkadir, T.S., Oyejobi, D.O. and Lawal, A.A., 2014. Evaluation of sugarcane bagasse ash as a replacement for cement in concrete works. *Acta Technica Corviniensis-Bulletin of Engineering*, *7*(3), p.71.

[105] Abbasi, A. and Zargar, A., 2013. Using baggase ash in concrete as pozzolan. *Middle East Journal of Scientific Research*, *13*(6), pp.716-719.

[106] Ahire, J.H., Wang, Q., Coxon, P.R., Malhotra, G., Brydson, R., Chen, R. and Chao, Y., 2012. Highly luminescent and nontoxic amine-capped nanoparticles from porous silicon:

synthesis and their use in biomedical imaging. *ACS applied materials & interfaces*, *4*(6), pp.3285-3292.

[107] Bley, R.A. and Kauzlarich, S.M., 1996. A low-temperature solution phase route for the synthesis of silicon nanoclusters. *Journal of the American Chemical Society*, *118*(49), pp.12461-12462.

[108] Plettl, A., Enderle, F., Saitner, M., Manzke, A., Pfahler, C., Wiedemann, S. and Ziemann, P., 2009. Non-Close-Packed Crystals from Self-Assembled Polystyrene Spheres by Isotropic Plasma Etching: Adding Flexibility to Colloid Lithography. *Advanced Functional Materials*, *19*(20), pp.3279-3284.

[109] Lam, C., Zhang, Y.F., Tang, Y.H., Lee, C.S., Bello, I. and Lee, S.T., 2000. Large-scale synthesis of ultrafine Si nanoparticles by ball milling. *Journal of crystal growth*, *220*(4), pp.466-470.

[110] Gorji, B., Ghasri, M.A., Fazaeli, R. and Niksirat, N., 2012. Synthesis and characterizations of silica nanoparticles by a new sol-gel method. *Journal of Applied Chemical Research*, *6*(3), pp.22-26.

[111] Hench, L.L. and West, J.K., 1990. The sol-gel process. *Chemical reviews*, *90*(1), pp.33-72.

[112] Mohd, N.K., Wee, N.N.A.N. and Azmi, A.A., 2017, September. Green synthesis of silica nanoparticles using sugarcane bagasse. In *AIP conference proceedings* (Vol. 1885, No. 1, p. 020123). AIP Publishing LLC.

[113] Singh, S.P. and Endley, N., 2020. Fabrication of nano-silica from agricultural residue and their application. In *Nanomaterials for Agriculture and Forestry Applications* (pp. 107-134). Elsevier.

[114] Thuc, C.N.H. and Thuc, H.H., 2013. Synthesis of silica nanoparticles from Vietnamese rice husk by sol–gel method. *Nanoscale research letters*, *8*(1), pp.1-10.

[115] Haile Asmelash, A., 2019. *Synthesis and Characterization of Nanosilica-zinc Coatings with Silane Coupling Agents on Glass Substrates* (Doctoral dissertation, ASTU)

[116] Aramaki, S. and Roy, R., 1959. Revised equilibrium diagram for the system Al_2O_3-SiO_2. *Nature*, *184*(4686), pp.631-632.

[117] Kalapathy, U., Proctor, A. and Shultz, J., 2000. Production and properties of flexible sodium silicate films from rice hull ash silica. *Bioresource technology*, *72*(2), pp.99-106.

[118] Iler, K.R., 1979. The chemistry of silica. *Solubility, polymerization, colloid and surface properties and biochemistry of silica*.

[119] Kalapathy, U., Proctor, A. and Shultz, J., 2000. Silica xerogels from rice hull ash: structure, density and mechanical strength as affected by gelation pH and silica concentration. *Journal of Chemical Technology & Biotechnology*, *75*(6), pp.464-468.

[120] Realmuto, L., Hunting, K.L. and Parkin, R., 2013. State Health Agency Workforce Shortages and Implications for Public Health: A Case Study of Restaurant Inspections in Louisian. *Journal of environmental health*, *76*(5), pp.32-37.

[121] Zou, J., Sanelle, P., Pettigrew, K.A. and Kauzlarich, S.M., 2006. Size and spectroscopy of silicon nanoparticles prepared via reduction of SiCl 4. *Journal of Cluster Science*, *17*(4), pp.565-578.

[122] Brus, L., 1994. Luminescence of silicon materials: chains, sheets, nanocrystals, nanowires, microcrystals, and porous silicon. *The Journal of Physical Chemistry*, *98*(14), pp.3575-3581.

[123] Koch, E.C. and Clement, D., 2007. Special materials in pyrotechnics: VI. Silicon–an old fuel with new perspectives. *Propellants, Explosives, Pyrotechnics: An International Journal Dealing with Scientific and Technological Aspects of Energetic Materials*, *32*(3), pp.205-212.

[124] Nakajima, K. and Usami, N. eds., 2009. *Crystal growth of Si for solar cells* (Vol. 97). Berlin, Heidelberg: Springer.

[125] Yermekova, Z., Mansurov, Z. and Mukasyan, A.S., 2010. Combustion synthesis of silicon nanopowders. *International Journal of Self-Propagating High-Temperature Synthesis*, *19*(2), pp.94-101.

[126] Entwistle, J., Rennie, A. and Patwardhan, S., 2018. A review of magnesiothermic reduction of silica to porous silicon for lithium-ion battery applications and beyond. *Journal of Materials Chemistry A*, *6*(38), pp.18344-18356.

[127] Gao, P., Huang, X., Zhao, Y., Hu, X., Cen, D., Gao, G., Bao, Z., Mei, Y., Di, Z. and Wu, G., 2018. Formation of Si hollow structures as promising anode materials through reduction of silica in AlCl3–NaCl molten salt. *ACS nano*, *12*(11), pp.11481-11490.

[128] Jing, C.A.I., Luo, X.T., Lu, C.H., Haarberg, G.M., Laurent, A., Kongstein, O.E. and Wang, S.L., 2012. Purification of metallurgical grade silicon by electrorefining in molten salts. *Transactions of Nonferrous Metals Society of China*, *22*(12), pp.3103-3107.

[129] Coletti, G., Bronsveld, P.C., Hahn, G., Warta, W., Macdonald, D., Ceccaroli, B., Wambach, K., Le Quang, N. and Fernandez, J.M., 2011. Impact of metal contamination in silicon solar cells. *Advanced Functional Materials*, *21*(5), pp.879-890.

[130] Lee, I.J., Paik, U. and Park, J.G., 2013. Effects of metallic contaminant type and concentration on photovoltaic performance degradation of p-type silicon solar cells. *Journal of the Korean Physical Society*, *63*(1), pp.47-52.

[131] Morita, K. and Yoshikawa, T., 2011. Thermodynamic evaluation of new metallurgical refining processes for SOG-silicon production. *Transactions of Nonferrous Metals Society of China*, *21*(3), pp.685-690.

[132] Delannoy, Y., 2012. Purification of silicon for photovoltaic applications. *Journal of Crystal Growth*, *360*, pp.61-67.

[133] Martorano, M.A., Neto, J.F., Oliveira, T.S. and Tsubaki, T.O., 2011. Refining of metallurgical silicon by directional solidification. *Materials Science and Engineering: B*, *176*(3), pp.217-226.

[134] Belomoin, G., Therrien, J., Smith, A., Rao, S., Twesten, R., Chaieb, S., Nayfeh, M.H., Wagner, L. and Mitas, L., 2002. Observation of a magic discrete family of ultrabright Si nanoparticles. *Applied Physics Letters*, *80*(5), pp.841-843.

[135] Won, C.W., Nersisyan, H.H. and Won, H.I., 2011. Solar-grade silicon powder prepared by combining combustion synthesis with hydrometallurgy. *Solar Energy Materials and Solar Cells*, *95*(2), pp.745-750.

[136] Su, H.J., Zhang, J., Lin, L.I.U. and Fu, H.Z., 2012. Preparation, microstructure and dislocation of solar-grade multicrystalline silicon by directional solidification from metallurgical-grade silicon. *Transactions of Nonferrous Metals Society of China*, *22*(10), pp.2548-2553.

[137] Yasuda, K., Saegusa, K. and Okabe, T.H., 2011. Production of solar-grade silicon by halidothermic reduction of silicon tetrachloride. *Metallurgical and Materials Transactions B*, *42*(1), pp.37-49.

[138] Abdyukhanov, I.M., Abdyukhanov, M.A., Kuz'min, Y.A. and Merkushkin, V.M., 2000. Production of metallurgical silicon of enhanced quality for land-based solar cells. *Metal science and heat treatment*, *42*(6), pp.246-249.

[139] He, Z.W., Liu, X.Q., Su, Q. and Wang, Y.Y., 2006. Improvement of electrical properties of low dielectric constant nanoporous silica films prepared using sol–gel method with catalyst HF. *Applied Physics A*, *82*(2), pp.349-355.

[140] Su, Y. and Huang, J., 2012. Two consensus problems for discrete-time multi-agent systems with switching network topology. *Automatica*, *48*(9), pp.1988-1997.

[141] Xu WP, Zhang YY, Wang Q, Li ZJ, Nie YH. Thermoelectric effects in triple quantum dots coupled to a normal and a superconducting leads. Physics Letters A. 2016 Feb 22;380(7-8):958-64.

[142] Al-Hamamre Z, Saidan M, Hararah M, Rawajfeh K, Alkhasawneh HE, Al-Shannag M. Wastes and biomass materials as sustainable-renewable energy resources for Jordan. Renewable and Sustainable Energy Reviews. 2017 Jan 1;67:295-314.

[143] Santos F, Rabelo S, De Matos M, Eichler P, editors. Sugarcane biorefinery, technology and perspectives. Academic Press; 2019 Nov 21.

[144] Singels A, McFarlane SA, Basdew I, Keeping MG, Nicholson R, Pilusa T, Sithole P, Titshall LW. Review of South African sugarcane production in the 2018/19 season: too much of a good thing?. InProceedings of the Annual Congress-South African Sugar Technologists' Association 2019 (No. 92, pp. 1-16). South African Sugar Technologists' Association.

[145] Birru E, Erlich C, Martin A. Energy performance comparisons and enhancements in the sugar cane industry. Biomass Conversion and Biorefinery. 2019 Jun;9(2):267-82.

[146] Rabelo SC, Carrere H, Maciel Filho R, Costa AC. Production of bioethanol, methane and heat from sugarcane bagasse in a biorefinery concept. Bioresource technology. 2011 Sep 1;102(17):7887-95.

[147] Canilha L, Chandel AK, Suzane dos Santos Milessi T, Antunes FA, Luiz da Costa Freitas W, das Graças Almeida Felipe M, da Silva SS. Bioconversion of sugarcane biomass into ethanol: an overview about composition, pretreatment methods, detoxification of hydrolysates, enzymatic saccharification, and ethanol fermentation. Journal of Biomedicine and Biotechnology. 2012 Oct;2012.

[148] Nikodinovic-Runic J, Guzik M, Kenny ST, Babu R, Werker A, Connor KE. Carbon-rich wastes as feedstocks for biodegradable polymer (polyhydroxyalkanoate) production using bacteria. Advances in applied microbiology. 2013 Jan 1;84:139-200.

[149] Norsuraya S, Fazlena H, Norhasyimi R. Sugarcane bagasse as a renewable source of silica to synthesize Santa Barbara Amorphous-15 (SBA-15). Procedia engineering. 2016 Jan 1;148:839-46.

[150] Ortiz de Zárate D, García-Meca C, Pinilla-Cienfuegos E, Ayúcar JA, Griol A, Bellières L, Hontañón E, Kruis FE, Martí J. Green and sustainable manufacture of ultrapure engineered nanomaterials. Nanomaterials. 2020 Mar;10(3):466.

[151] Faruk O, Bledzki AK, Fink HP, Sain M. Biocomposites reinforced with natural fibers: 2000–2010. Progress in polymer science. 2012 Nov 1;37(11):1552-96.

[152] Mittal G, Rhee KY, Mišković-Stanković V, Hui D. Reinforcements in multi-scale polymer composites: Processing, properties, and applications. Composites Part B: Engineering. 2018 Apr 1;138:122-39.

[153] Seroka NS, Taziwa RT, Khotseng L. Extraction and Synthesis of Silicon Nanoparticles (SiNPs) from Sugarcane Bagasse Ash: A Mini-Review. *Applied Sciences*. 2022 Feb 23;12(5):2310.

[154] Barrera Torres G, Dognani G, da Silva Agostini DL, dos Santos RJ, Camargo Cabrera F, Gutierrez Aguilar CM, de Paiva FF, Rainho Teixeira S, Job AE. Potential eco-friendly application of sugarcane bagasse ash in the rubber industry. Waste and Biomass Valorization. 2021 Aug;12(8):4599-613.

[155] Kaewsakul W. Silica-reinforced natural rubber for low rolling resistance, energy-saving tires: aspects of mixing, formulation and compatibilization.

[156] Katare VD, Madurwar MV. Experimental characterization of sugarcane biomass ash–A review. Construction and Building Materials. 2017 Oct 15;152:1-5.

[157] Abraham E, Deepa B, Pothan LA, John M, Narine SS, Thomas S, Anandjiwala R. Physicomechanical properties of nanocomposites based on cellulose nanofibre and natural rubber latex. Cellulose. 2013 Feb;20(1):417-27.

[158] Mohd NK, Wee NN, Azmi AA. Green synthesis of silica nanoparticles using sugarcane bagasse. InAIP conference proceedings 2017 Sep 26 (Vol. 1885, No. 1, p. 020123). AIP Publishing LLC.

[159] de Paiva FF, de Maria VP, Torres GB, Dognani G, dos Santos RJ, Cabrera FC, Job AE. Sugarcane bagasse fiber as semi-reinforcement filler in natural rubber composite sandals. Journal of Material Cycles and Waste Management. 2019 Mar;21(2):326-35.

[160] de Lima VM, Barros LC, de Melo Neto AA. Characterization of sugarcane bagasse ash (SBA) and its evaluation for use in alkali-activated slag mixtures. Cerâmica. 2021 Feb 10;67:123-30.

Chapter 3: Preparation of Silica, Silicon nanoparticles, Silicon thin films to match the visible region of the solar spectrum, potential for application thin film for solar cells

Synopsis

Nanomaterials exhibit phenomenal properties that require sophisticated analytical instruments to fully understand their behaviour at the electronic and molecular level. It is critical to use various characterization techniques to better understand their structural, size distribution, morphology, functionalities, and crystalline properties. The characterization techniques include microscopy (High-resolution Transmission Electron Microscopy (TEM) and Scanning Electron Microscopy-Energy dispersive x-ray spectroscopy (SEM)), Fourier-Transform Infrared Spectroscopy (FTIR), Atomic Force Microscopy (AFM), Raman spectroscopy, X-ray Diffraction (XRD) spectroscopy, and electrical characterization by Oscilla AM1.5. Optical studies were exploited using UV-Vis. And thermal stability was evaluated using Thermogravimetric analysis (TGA). The yield of major elements was cross-examined using X-ray fluorescence spectroscopy (XRF). The surface properties were analysed via Brunauer-Emmett-Telle (BET).

3.1. Background

It is worth noting that research is underway, to find new research methods with the aim of manufacturing and purifying silicon or emerging materials which can be used as a substrate for energy conversion, more especially reduction of the costs to produce photovoltaics devices. Interestingly, an increase in demand for power generation of solar cells makes solar grade silicon a candidate for huge placement in the energy market [1-3].

Therefore, this presented new ideas to seek cheap and readily available sources of silicon. Industrial wastes, particularly sugarcane bagasse, are considered one of the promising resources of silica. It essentially contains other minerals including amorphous silica, aluminium, iron, etc, which can be readily purified by dissolving in alkaline solution. In addition, there are several reserves large enough across the globe, to get the silica in a

reduced cost. Silica is a mineral found in various forms from agricultural waste including sugarcane waste, wheat straw, rice husk, corn cab ash, coconut husk grasses and cow dang ash [4-5].

3.2 Methodology and Materials

Sugarcane bagasse was collected from Illovo Sugar Mill company, Kwazulu Natal, burnt to ashes and ground to fine powder prior to use. The chemicals utilized in the preparation were citric acid ≥99.5%, L-cysteine hydrochloride ≥98% and Tetrapropylammonium hydroxide 1.0 M in H_2O purchased from Sigma Aldrich. Sugarcane was procured from Sugar Illovo South Africa Company. The synthesis was done using deionized water from the Milli-Q water purification system (Millipore, Bedford, MA, USA).

3.3 Synthetic route for the preparation of Biosilica from sugarcane bagasse

3.3.1 Preparation of Sugarcane bagasse ash (SCBA)

In a typical preparation procedure sugarcane ash was soaked for a period of 24 hours in double deionized water to remove any dust particles. The soaked sugarcane was then oven dried for a period of 6 hours. The soaked, dried sugarcane was then burnt in open air to obtain a black ash sugarcane bagasse ash (SCBA)

3.3.2 Leaching using citric acid

10.0g of sugarcane bagasse ash, was added to 500 ml beaker of 5% citric acid solution. The black solution of sugarcane bagasse ash and % 5 citric acid solution was then transferred into a 500 ml volumetric flash. The resulting solution in the 500 ml volumetric flask was first stirred at 450 rpm, which was subsequently refluxed for 24 hours. The resulting pale yellow-green solution was then filtered using Buchner funnel 70mm filter paper. The trapped precipitate was then washed with double deionized water until the pH of the decant was 3-5 until the pH of the supernatant reached 6.5. The resulting black sugar cane bagasse

supernatant was then dried in an oven 40 °C overnight and ground to a fine powder and stored in sample vials. Subsequently labeled SCBA-ca leached.

3.3.3 Leaching using citric acid L-cysteine hydrochloride

The same process was repeated using 5% L-cysteine hydrochloride (L cys):
10.0g of sugarcane bagasse ash, was added to 500 ml beaker of 5% L-cysteine hydrochloride solution. The black solution of sugarcane bagasse ash and % 5 L-cysteine hydrochloride solution was then transferred into a 500 ml volumetric flash. The resulting solution in the 500 ml volumetric flask was first stirred at 450 rpm, which was subsequently refluxed for 24 hours. The resulting colorless-foam solution was then filtered using Buchner funnel 70mm filter paper. The trapped precipitate was then washed with double deionized water until the pH of the decant was 3-5 until the pH of the supernatant reached 6.5. The resulting black sugar cane bagasse supernatant was then dried in an oven 40 °C overnight and ground to a fine powder and stored in sample vials. Subsequently labeled SCBA-L cys leached.

3.4. Extraction of Silica

Sugarcane bagasse as received was soaked in deionized water, dried in the sun then underwent incomplete combustion to obtain black soot then stored in sample vial as shown in figure 3.1. The ash was then immersed in two organic acids 5% prepared solution(s) and refluxed for leaching treatment.

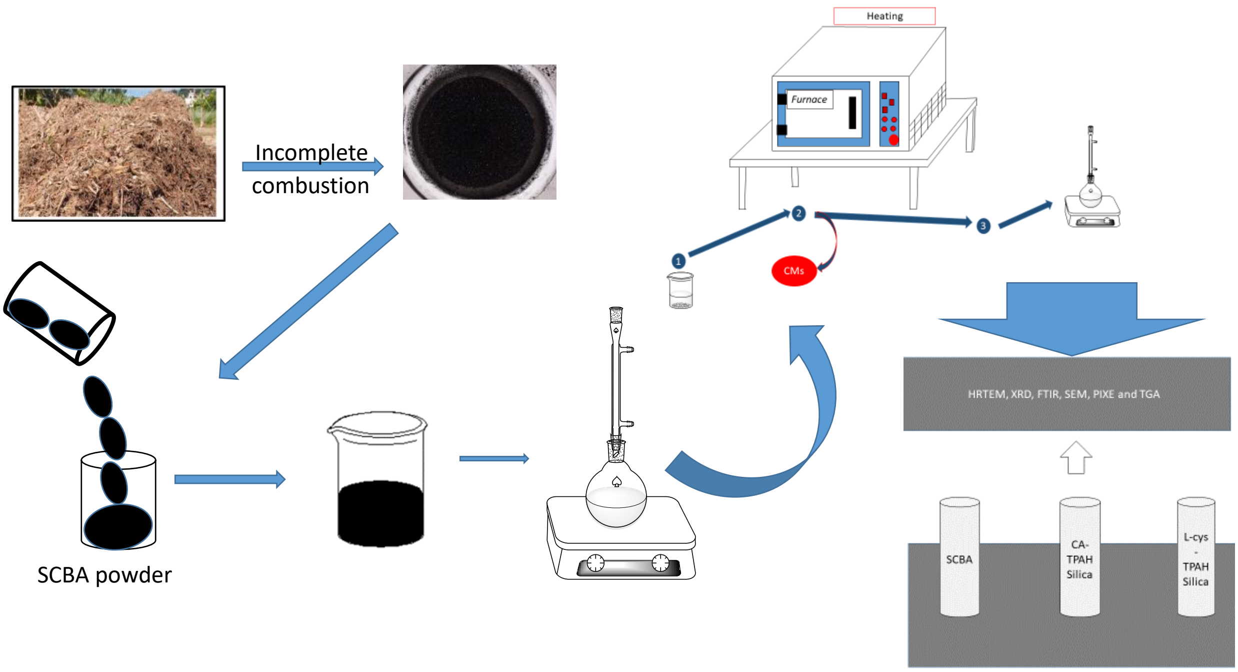

***Figure 3.1**: Schematic illustration for the production of silica from sugarcane bagasse ash.*

The leached sample is further exposed to pyrolysis in a muffle furnace and reacted with Tetrapropyl Ammonium hydroxide for silica extraction subsequently burnt in air to burn away carbon, nitrogen and hydrogen from the multi-crystalline product to obtain bio-silica. The as-produced solid powder is then analyzed for its structural, morphological, thermal and textural properties.

3.4.1. SCBA-CA leached.

In a typical procedure the 2.0032 g SCBA-CA was placed in a ceramic crucible, which was heated at 700 °C for 4 hours (residence time) in a muffle furnace at 10 ^{0}C/min heating rate (gradient time) to burn away carbonaceous material and form crystalline silica. This resulted in formation of an orange-brown product(s). Then 2 ml of Tetrapropyl ammonium hydroxide was added to the orange-brown product shown in equation 3.1, whilst stirring at 350 rpm for 1 hour. The solution was then heated at 200 °C in air for the first 2 hours and then further heated at 600 °C for 1 to burn away the excess carbon, nitrogen, and hydrogen, shown in equation 3.2. Heating resulted in the oxidation of C, H and N to form respective oxide. As result silica oxide(s) was formed as nano powders laballed CA-TPAH-silica.

$$SiO_2 + [N(C_3H_7)_4]OH \rightarrow [N(C_3H_7)_4]OH(SiO_2)_{48} \dots \dots \dots \dots (3.1)$$

$$[N(C_3H_7)_4]OH(SiO_2)_{48} + \Delta \rightarrow (SiO_2)_x(s) \downarrow + (CO)_x(g) \uparrow + (H)_x(g) \uparrow + (NO)_x(g) \quad (3.2)$$

3.4.2. SCBA-L cys leached.

About 2.0032 g SCBA-L cys was placed in a ceramic crucible, which was heated at 700 °C for 4 hours (residence time) in a muffle furnace at 10 ^{0}C/min heating rate (gradient time) to burn away carbonaceous material and form crystalline silica. This resulted in formation of a light orange-brown product(s). Then 2 ml of Tetrapropylammonium hydroxide (TPAH) was added to the orange-brown product whilst stirring at 350 rpm for 1 hour, shown in equation 1. The solution was then heated at 200 °C in air for the first 2 hours and then further heated at 600 °C for 1 to burn away the excess carbon, nitrogen, and hydrogen as shown in equation 2. Heating resulted in the oxidation of C, H and N to form respective oxide. As result silica oxide(s) was formed as nano powders laballed L cys-TPAH-Silica.

$$SiO_2 + [N(C_3H_7)_4]OH \rightarrow [N(C_3H_7)_4]OH(SiO_2)_{48} \ldots\ldots\ldots\ldots\ldots\ldots\ldots\ldots\ldots\ldots\ldots\ldots\ldots\ldots. (3.3)$$
$$[N(C_3H_7)_4]OH(SiO_2)_{48} + \Delta \rightarrow (SiO_2)_x(s) \downarrow + (CO)_x(g) \uparrow + (H)_x(g) \uparrow + (NO)_x(g) \quad (3.4)$$

3.5 Synthetic route the preparation of SCBA nano Silicon

The as-synthesized bio silica from sugarcane bagasse ash and Mg chips used for the magnesiothermic reduction was 2.5 g and 3.0 g, respectively. The mixture was subjected to pyrolysis at 700 ^{0}C for 4h in a tube furnace under nitrogen (N_2), as shown in figure 3.2 below. A portion of dark brown-greyish powder (as-reduced silica) was immersed in Aquaregia (1 HNO_3: 3 HCl) to remove excess Mg and unreacted silica, reported in previous studies by Bao et al [13]. The as-produced dark grey powder Silicon was further studied for physicochemical properties using Raman Spectroscopy for purity, Fourier Transform Infrared spectroscopy for evolution of surface chemistry and textural properties (specific surface area, pore volume and pore diameter

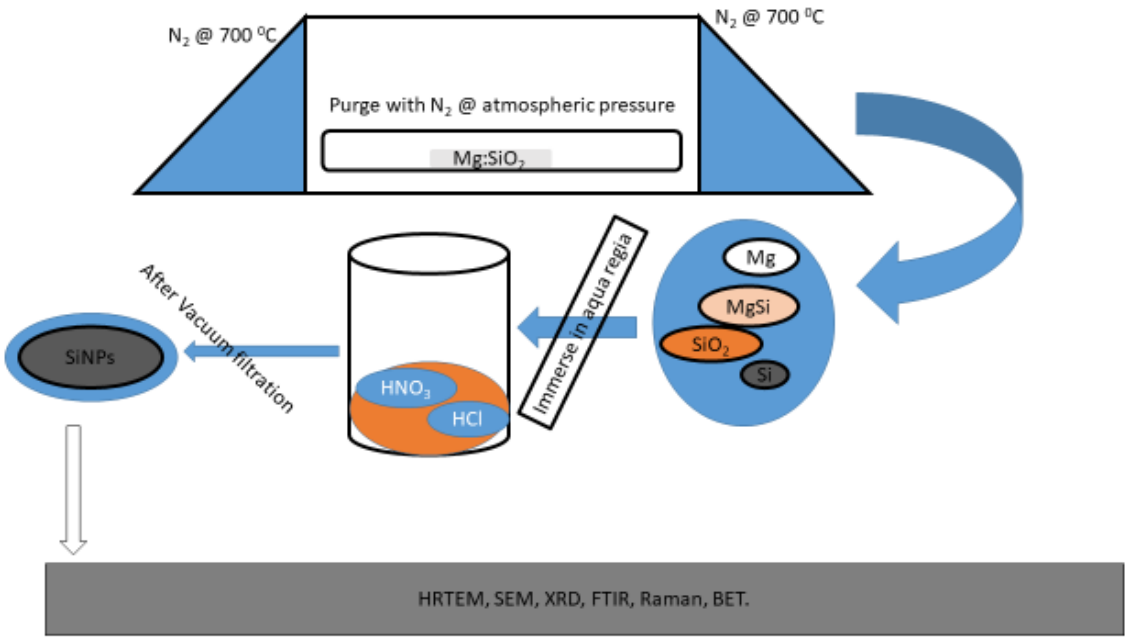

***Figure 3.2**: Magnesiothermic reduction of nano-silica into nano-silicon*

3.6 Characterisation techniques

A detailed study of the characteristics of the most promising and as-developed thin films will be performed. Their physical, chemical, electrical and optical properties of newly produced thin films will be characterized using the following equipment:

3.6.1. Fourier Transform Infrared (FTIR)

FTIR is a simple yet critical analytical instrument mainly used to monitor and confirm the successful introduction of new functionalities of material under study. The technique is capable of measuring absorption resulting from vibrational and rotational changes along the infrared region (IR), of the analyte. Furthermore, the analyte should be IR active, which is the ability of molecules with a dipole moment to absorb the infrared light [6].

The more the dipole moments the more pronounced peaks. And, the transmittance of SCBA, Silica and nano Silicon were performed using FTIR from 400 to 4000 cm^{-1}, PerkinElmer, Spectrum Two, Spectrophotometer [7]. Thus, further analysed for determination of functional groups.

3.6.2. Scanning Electron Microscopy (SEM)

Scanning electron microscopy analysis was performed using SEM (TESCAN, VEGA) to observe surface morphology of Silica, nano Silicon and polymer as-prepared thin films. The samples were prepared on an aluminium stub and carbon sputtered on a carbon coater before analysis. Consequently, the size and shape of the thin films were also examined. Both SEM and TEM, samples must be conductive.

Henceforth, the principle on SEM is based on the bombardment of electrons onto the sample and upon interaction, an image is formed. The type of sample under study determines which detector to be used for quality and high-resolution image. The technique is coupled with EDS (energy dispersive spectroscopy) for elemental composition [8].

3.6.3. High Resolution Transmission Electron Microscopy (HR-TEM)

The image formation in transmission electron microscopy (TEM) results from electron bombardment onto the sample, from filament as the source of hot electrons. The samples were prepared using ethanol, and sonicated for 5 mins, drop coated onto the copper grids coated with carbon/ gold so that the sample is conductive.

The material size determines workable conditions where the images formed can be fine focused and magnified to capture quality images on a camera [9]. The image analysis was performed using high-resolution TEM (JEOL, 2100).

3.6.4. Raman spectroscopy

The laser Raman spectroscopy (Brucker senterra Raman spectrometer) was used in this study to investigate the vibrational and rotational changes of Raman active molecules. The resulting spectra exhibit observable changes in ID/IG band for different nanomaterials. Here,

the laser utilized was set to 532 nm (Excitation wavelength). A laser beam of 532 nm was used to scan the sample to avoid photobleaching, for all nanocomposites under study. The laser Raman spectrometer utilized in this project was a Bruker Senterra fitted with a 50× objective lens for imaging. And, the spectral data were evaluated using OPUS 7.1 software.

3.6.5 Thermogravimetric analysis (TGA)

The thermal stability and behaviour of our samples were studied using TGA technique, PerkinElmer, Simultaneous Thermal Analyzer, STA 8000. The studies were conducted at room temperature from 30 ℃ to 800 ℃ at 10 ℃ /min and the cooling was done at 40 ℃ /min.

3.6.6 Ultraviolet Visible Spectroscopy (UV/Vis)

The optical properties of the as-synthesized materials were cross-examined using UV/Vis 920, Wirsam Scientific, Cape Town. The analysis was conducted at room temperature from 200 nm to 600 nm wavelengths.

3.6.7 X-ray Fluorescence Spectroscopy

Panalytical Axios wavelength-dispersive XRF spectrometer with sample changer (56 sample capacity) and a rhodium end-window X-ray tube A Claisse fluxer is available to aid in the preparation of fusion disks. There is a Claisse Fluxer available to help with fusion disk preparation. Powder briquettes are made using a hydraulic cold press and die.
A specially constructed hydraulic splitter, a Sturtevant laboratory jaw-crusher, and a Seibtechnik swing mill with carbon steel cassettes of various sizes are used for sample preparation. The major elements in the synthesized materials were examined using the above mentioned technique.

3.6.7 Brunauer–Emmett–Telle (BET)

The Brunauer-Emmett-Teller (BET) theory is a key analytical tool for the measurement of the specific surface area of materials. It seeks to explain the physical adsorption of gas molecules on a solid surface. The textural properties of the samples were analysed via ASAP 2020 V4.04 technique, analysis bath temperature was -195.685 ℃.

3.6.8 Atomic Force Microscopy (AFM)

Surface and object manipulation and nanoscale imaging are combined in a software and hardware configuration known as NanoMan VS. A sample can be probed using both immediate and pre-programmed commands in between image scans of the field of view. By controlling the force applied through the probe and the voltage on the tip and the sample, a variety of fundamental activities are made possible.

The samples were subjected to AFM to study the surface roughness in 2D and 3D. The film thickness was also evaluated.

3.6.9 Ossila

The films were prepared on ITO glass photovoltaic substrates. The substrates were sequentially sonicated in soap water for 10 minutes, then soaked in isopropanol for 10 minutes, and lastly soaked in acetone for 10 minutes before drying in an oven at $40°C$ for 20 minutes.

3.6.10 Oscilla

The photovoltaics properties were evaluated using solar simulator, Class AAA, 150 W, 50 x 50 mm, model no: SciSun-150, Sciencetech. The electrical properties were obtained from simulations conducted under light AM1.5.

1) Structural purity identification, and crystallographic analysis, atomic bonding (functionalisation) and strain was determined by X-Ray Diffraction (XRD), Raman

spectroscopy and Fourier Transform infra-red spectroscopy (FTIR). Structural and morphological analysis: Particle size will be determined using High Resolution Transmission Electron Microscopy (HRTEM), and Small-Angle X-ray Spectroscopy (SAXS). High Resolution Scanning Electron Microscopy (HRSEM) and Atomic Force Microscopy (AFM) will be used to image down to discern interfaces, surface topography, cross sections in thin film materials and surface film thickness.

2) The elemental composition of the new materials will be determined using EDS. The thermal properties will be done using Thermogravimetric (TGA) analysis while their oxidative properties were determined by XRF. Whilst surface areas, and porosity will be determined using Nitrogen-purged BET.

3) Opto-electronic studies: Analysis and evaluation of optical and electrical properties of the thin films will be studied using Ultraviolet Visible spectroscopy(UV-Vis).

The phase composition of silica samples was analysed using the X-ray diffractometer (XRD), German Diffractometer D2 PHASER Bruker X-Ray with Cu-Kα radiation. The measurement was carried out at ambient temperature. Fourier Transform Infrared (FTIR) spectroscopy was used to confirm the synthesis of silica and silicon in the range of 4000 to 400 cm^{-1} through appearance of functional groups. These experiments were performed using Perkin Elmer FTIR, Spectrum Two, Spectrophotometer. Transmission Electron Microscopy (TEM JEOL, JEM-2010, Japan) at an accelerating voltage of 200 kV was used to examine the particle size and distribution of the prepared materials. The TEM specimens were prepared by placing a few drops of silica, silicon (dispersed in ethanol) solutions on a copper grid. The UV-vis absorption data was obtained for thin films deposited onto a clean ITO

glass substrate. The absorption spectra were acquired at room temperature using UV-Vis spectrometer UV/Vis 920.

3.7 Thin film preparation

The thin films were prepared by NEE-4000 E-Beam, from Nano Master, Inc. It has 10 KV power supply to the e-gun. Most importantly, the main chamber can be kept at low 10^{-7} Torr range at all times and evaporation can start just a few minutes after loading the wafer. The second configuration features a single large chamber design that allows e-beam evaporation guns, magnetrons, and thermal evaporation mounted onto the baseplate. In this configuration coating of multiple wafers are possible using planetary substrate holder. Furthermore, individual e-beam evaporators can use a combinatorial evaporation system from NANO-MASTER that uses substrate masking and computer-controlled evaporation rates.

The ITO glass substrates were first washed in deionized water followed by isopropanol then in acetone for 15 minutes in a sonicator. The substrates were then dried in an oven at 40 ^{0}C for 30 minutes. The cleaned substrates are then loaded on a pre-cleaned e-beam sample holder. There were six pockets but only four pockets were used and loaded with our target(s) onto e-beam liners as shown in table 3.1 below.

Table 3.1 *: Fabrication of thin flims using e-beam PVD.*

Material	Liner	Pocket (#)	Pressure (initial) (Torr)	Pressure (working)	Substrate temperature (^{0}C)	Deposition rate (Å/s)	Thickness (Å)
Si	Ta	1	$1.3x10^{-6}$	2.4×10^{-6}	249	2.9	500.05
Bi	Al_2O_3	2	$6.1x10^{-7}$	1.6×10^{-6}	250	0.1-4	193
Si	Ta	1	$1.1x10^{-6}$	7.2×10^{-6}	246	1.17-1.16	500.07

B	C	3	$1.1x10^{-5}$	5.2×10^{-7}	248	0.3-0.8	57
Ag	Al_2O_3	4	$1.2x10^{-6}$	9.5×10^{-7}	250	0.5-1.26	500.17

The e-beam PVD technique was operated at room temperature with a cooling system at 19 ^{0}C. The power was 9.96 Kv. The filament was at 15.8 A. And, the emission was operated at 2%. The e-beam liners for silicon target was tangtulum coated, bismuth and silver was alumina coated and boron was graphite coated. These liners are crucial as they are subjected to very high temperatures, the choice of liners is inspired by the fact that upon elevated temperatures contamination is prevented when the right liners are used for different materials. The fabricated cells were further characterized by UV/Vis, Raman and AFM. And, electrical properties were characterized using Ossila testing station at AM1.5 under light simulation.

To create an n-type layer of silicon with bismuth, beam liner #1 was loaded with silicon target and deposited 50 nm, followed by 19.3 nm of bismuth target loaded in beam liner #2, as tabulated in table 1. Furthermore, a 50 nm silicon target was deposited and blended with boron located at beam liner #3 to form a p-type silicon with boron layer. Finally, a 50 nm back contact was deposited with silver target at beam liner #4 to complete the cell.

3.8. References

[1] Pires, J.C.S., Otubo, J., Braga, A.F.B. and Mei, P.R., 2005. The purification of metallurgical grade silicon by electron beam melting. *Journal of Materials Processing Technology*, *169*(1), pp.16-20.

[2] Degoulange, J., Périchaud, I., Trassy, C. and Martinuzzi, S., 2008. Multicrystalline silicon wafers prepared from upgraded metallurgical feedstock. *Solar Energy Materials and Solar Cells*, *92*(10), pp.1269-1273.

[3] Hopkins, R.H., Seidensticker, R.G., Davis, J.R., Rai-Choudhury, P., Blais, P.D. and McCormick, J.R., 1977. Crystal growth considerations in the use of “solar grade” silicon. *Journal of Crystal Growth*, *42*, pp.493-498.

[4] Hakamada, M., Fukunaka, Y., Oishi, T., Nishiyama, T. and Kusuda, H., 2010. Carbothermic reduction of amorphous silica refined from diatomaceous earth. *Metallurgical and Materials Transactions B*, *41*(2), pp.350-358.

[5] Gaoxiang, D.U., Guocheng, L.Ü. and Xuwen, H.E., 2013. Apparent dissolution kinetics of diatomite in alkaline solution. *Chinese Journal of Chemical Engineering*, *21*(7), pp.736-741.

[6] Amand, L. & Tullin, C.J. 1999, "The Theory Behind FTIR analysis", Dep.Of Energy Conversion, Chalmers University of Technology, Sweden, springer. Chapter 1, pp. 106-112.

[7] Stuart, B. 2005, "Infrared spectroscopy", Kirk-Othmer Encyclopedia of Chemical Technology, pp. 73-82.

[8] Goldstein, J.I., Newbury, D.E., Michael, J.R., Ritchie, N.W., Scott, J.H.J. & Joy, D.C. 2017, Scanning electron microscopy and X-ray microanalysis, Springer. Chapter 4, pp. 239-246.

[9] Reimer, L. 2013, Scanning electron microscopy: physics of image formation and microanalysis, Springer. Chapter 7, pp. 413-419.

Chapter 4: Preparation of nanosilica from sugarcane bagasse ash

Synopsis

Sugarcane bagasse ash was used as a source of silica in the thermochemical synthesis of silica nanoparticles. It was crucial to research how different purification techniques, such as chemical treatments, as well as operational and practical circumstances affect the structural, morphological, thermal, and textural characteristics of the produced nanoparticles. Different levels of silica purity, more than 79%, were possible with the leaching process that was explored. The significant potential for usage in a variety of technical disciplines, including optical, electronics, biotechnology, and, ideally, the source of nano-silicon via magnesiothermic reduction, is indicated by these application-specific features, such as large surface area and pore volume.

Abstract

Sugarcane bagasse South Africa is an agricultural waste that poses many environmental and human health problems. Sugarcane bagasse dumps attract many insects that harm the health of the population and cause many diseases. Sugarcane ash is a naturally renewable source of silica. This study presents for the first time the extraction of nanosilica from sugar cane bagasse ash using L-cysteine hydrochloride monohydrate acid and Tetrapropy lammonium Hydroxide. The structural, morphological, and chemical properties of the extracted silica nanoparticles was cross examined using XRD, FTIR, SEM-EDS, and TGA. SEM analysis presents agglomerates of irregular sizes. It is possible to observe the structure of nanosilica formed by the presence of agglomerates of irregular shapes, as well as the presence of some spherical particles distributed in the structure. XRD analysis has revealed 2θ angles at 20, 26, 36, 39, 50, and 59 which shows that each peak on the XRD pattern is indicative of certain crystalline cubic phases of nanosilica, similar to results reported in the literature by Jagadesh et al. in 2015. The crystallite size estimated by the Scherrer equation based on the aforementioned peaks for ca-silica and L-cys-silica for the extracted particles had an average diameter of 26 nm and 29 nm, respectively. Furthermore, BET showed a specific surface area of 21.6511 m^2/g and 116.005 m^2/g for ca-silica and L-cys silica, respectively. The Infrared (IR) spectra showed peaks at 461.231 cm^{-1}, 787.381 cm^{-1} and 1045.99 cm^{-1} which corresponds to the Si~O~Si bending vibration, the Si~O~Si stretch vibration, and the Si~O~Si stretching vibration, respectively. This confirms the successful extraction of nanosilica from sugar cane bagasse ash. TGA analysis has revealed that the as received

sugarcane bagasse has high loss on ignition (LOI) of 18%, corresponding to the presence of the unburnt or partial burnt particles, similar to results reported by Yadav et al. This study has shown that sugar cane bagasse ash is a natural resource of silica which should be harnessed for industrial purposes in South Africa.

4.1. Background

In nanotechnology, “green” synthesis has received a great deal of attention as a reliable, sustainable, and environmentally friendly protocol for synthesis for a wide range of nanomaterials for the development of solar cells. In essence, green synthesis is regarded as an important route to reduce the pernicious effects associated with the traditional methods of synthesis of nanoparticles for preparation of solar cell electrodes. It is well known that the four most important parameters for the synthesis of nanoparticles using the green protocol are the selection of an environmentally friendly solvent, a source of nanomaterials, a reducing agent, and a harmless material for stabilization [1,2,3].

Plants are known as natural chemical factories that are economical and have no conservation. Rodríguez-Félix, F. et al., reported on the biosynthesis of silver (Ag) using aqueous extract from waste such as safflower (Carthmus tinctorius L.), a well-known crop from the Northwest of Mexico. Parallel to environmental pollution reduction, industrial agro-waste and food research was further done on efficiency and environmentally friendly properties of phytochemicals from safflower by-product via the UPLC-DAD-MS method [4]. In addition, researchers reported on the development and quality of food packaging which stems from the composites of zein films with no-ultrafiltred and ultrafiltred betalains extract(s) from the beetroot (Beta vulgrains) bagasse that is feasible for food packaging. Bio-inspired methods are emerging as viable options for producing highly valued silver nanoparticles while promoting sustainability. The green synthesis of Ag from agri-food waste extracts and by-products are flexible to manage, cost-effective, and possess potential application in health for antimicrobial and anticancer activity [4,5,6,7].

The synthesis of nanomaterials from agricultural waste is considered green because agricultural waste is an environmental hazard if not handled properly. For instance, sugarcane bagasse dumps attract many insects that harm the health of the population and

cause many diseases. At the same time, sugarcane ash is a renewable source of silicon. Elemental analysis of sugar cane bagasse ash Fortunate et-al has revealed 71.49 wt% silica [8,9,10]. Another study reported on the sustainable and green synthesis of silver (Ag) nanoparticles with potential applications in medicine and the food industry as antibacterial agents.

Thus, it is quite evident that conventional methods utilize very harsh and strong chemicals such as HCl, HNO_3, H_2SO_4, NaOH and KOH. Mohd NK, et al., in 2017 reported the green synthesis of nanosilica from sugarcane bagasse using HCl and NaOH [1,11]. However, the fate of this hazardous chemical is of utmost importance, as it requires adequate care in disposal. Thus, several researchers have extensively explored other synthetic methods to get the raw materials of SiO_2, as they are affordable and suitable in various applications [12]. A few decades ago, studies demonstrated that silica can be feasibly extracted from various agricultural wastes, such as rice straw, rice husk, corn cub, sugarcane bagasse and palm ash. Interestingly, there is a dearth of scientific articles that report on the synthesis of silica from sugarcane bagasse [13,14,15,16].

In this research, sugarcane bagasse is chosen as a natural source of silica nanoparticles. The advantages of this method are that it is less toxic and requires minimal chemical consumption. Furthermore, in this method metallic impurities will be removed by organic acid (pretreatment process). The absence of metallic impurities will lead to the high purity of silica nanoparticles production at the end of this research study. Taking advantage of agricultural waste utilization as a source of silica, this project is not only economically feasible, but also may provide a significant impact to environmental control [17,18].

The confirmation of desired functional groups vibration is determined by Fourier Transform Infrared (FTIR) spectroscopy, while size determination and morphology has been conducted using a scanning electron microscope (SEM-EDS). The structural characteristics were confirmed by X-ray powder diffraction (XRD). The thermal behavior was studied using a Thermogravimetric (TGA) analyzer, and the surface area of silica nanoparticles was determined using a BET surface area analyzer. Reporting for the first time extraction of silica from bagasse ash, using L-cysteine hydrochloride monohydrate,qualifies, this work to be

considered novel, because there are only a few published analyses related to sugarcane bagasse ash being used as a source of silica using organic bases.

4.2 Characterization of the synthesized materials

4.2.1 Powder X-ray diffraction analysis

The XRD patterns presented in Figure 4.1 show the calcined bagasse (i) SCBA-CA leached 4.1 (ii) CA-TPAH silica, Figure 1 (iii) SCBA L-Cys leached and Figure 4.1 (iv) L-cys-TPAH silica., revealed diffraction peaks at 2 theta angles of 20, 26, 36, 39, 50, and 59 corresponding to the crystalline phases of silica. The diffraction peak at 2theta angle 26 reveals that the extracted and calcined sugar cane bagasse consists of silica nanoparticles with a 101 cubic phase crystalline structure. Similar observations have been observed by Katare, V.D. and Madurwar, M.V. (2017), who revealed crystalline peaks of silica at 2θ = 26 [19]. This observation confirms the successful extraction of silica nanoparticles from sugar cane bagasse from our samples [1,19,20,21].

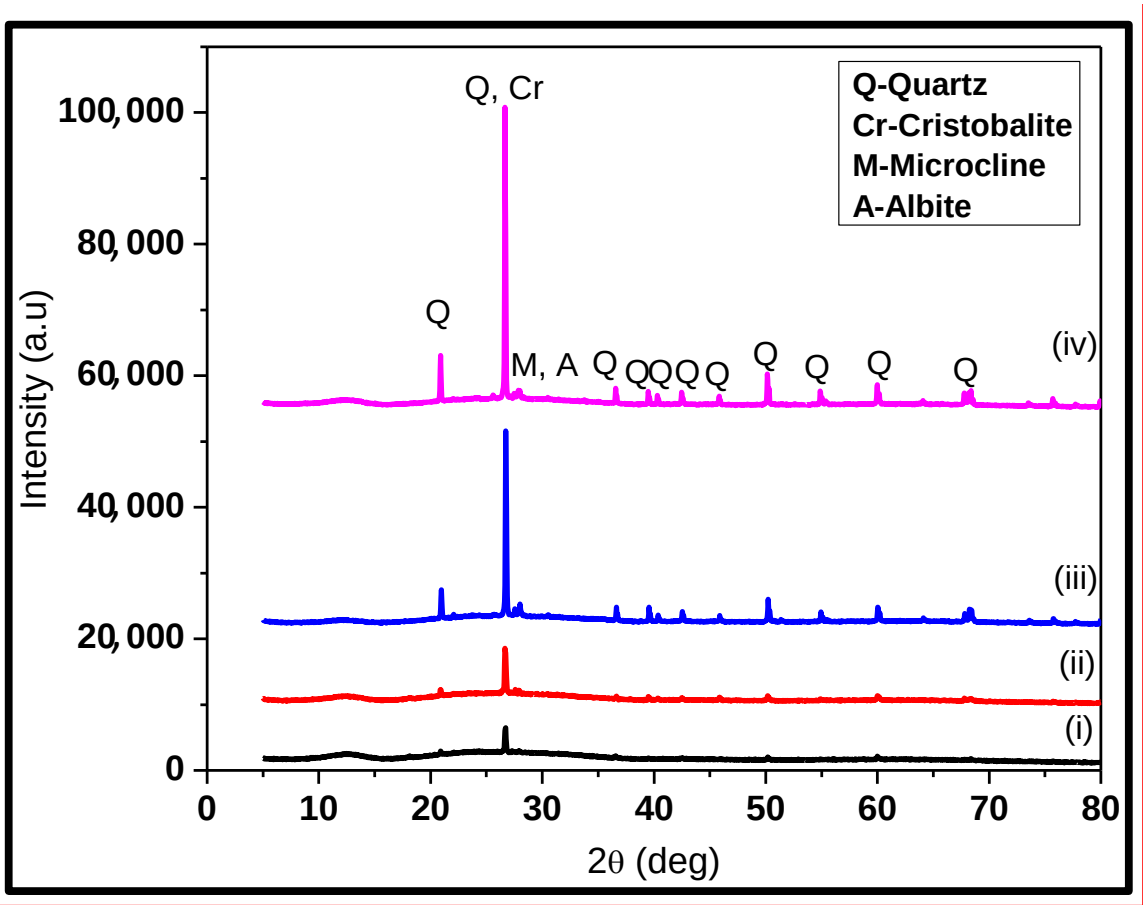

***Figure 4.1**: The XRD patterns for bagasse (i) SCBA CA leached (ii) CA-TPAH silica calcined bagasse (iii) SCBA L-Cys leached and (iv) L-cys-TPAH silica.*

Figure 4.1 shows the XRD spectra of samples treated with Figure 4.1 (i), Figure 4.1 (ii) citric acid and Figure 4.1 (iii), Figure 4.1 (iv) L-cysteine hydrochloride monohydrate. It is quite evident that the characteristic peak at 2θ = 26 of quartz is associated with crystalline silica, and is present in both samples. However, the low intense peak for quartz crystalline peak on Figure 4.1 (i) reveals the weak leaching efficiency of citric acid as compared to Figure 4.1 (iii) L-cysteine hydrochloride [19,20,21,22].

It is worth noting that the intense peak at 2θ = 26 is characteristic of Quartz silica (JCP phase from ICDD: 01-083-0539) [20]. Furthermore, the crystalline silica is slightly more intense in (iv) than in (ii) [22]. The synthesized silica presented other peaks characteristic of cristobalite, which forms at higher temperatures indicating varied phases of silica in the sample [20]. Additionally, microcline ($KAlSi_3O_8$) and albite ($NaAlSi_3O_8$) minerals were also identified for the as-prepared silica shown in the diffraction patterns of low and weak peaks

[21,22,23]. As mentioned earlier, the diffraction peaks at 2θ= 20, 26, 36, 39, 50, and 59 show that silica is highly crystalline mostly in a quartz form [24]. The average diameter sizes were determined to be approximately 26 nm and 29 nm using Scherrer's formula for silica acid-leached with CA and L-Cys, respectively. The crystallite size was estimated by Scherrer's formula as shown in Equation (5) below:

$$Dp = \frac{K\lambda}{\beta \cos\theta} \quad (4.1)$$

whereby Dp is the Average crystallite size (nm), and K is known as the Scherrer constant. The K values vary from 0.68 to 2.08, and preferably K = 0.94 is utilized for spherical crystallites with cubic symmetry and λ-X-ray wavelength. For mini XRD, $CuK\alpha$ the λ = 1.54178 Å is normally desired. Additionally, θ is the peak position and β is identified by FWHM (full Width at Half Maximum) of XRD peak determined from one half of 2θ.

4.2.2. FTIR analysis

FTIR spectral analysis identified key functional groups existing in the bagasse ash, the leached samples and the nano-silica, which was operated at room temperature with wavelength range of 400–4000 cm^{-1}. Figure 4.2, shows the FTIR analysis of the prepared Figure 4.2a (iii) silica, and exhibit bands at 461.231 cm^{-1}, 787.381 cm^{-1} and 1045.99 cm^{-1} correspond to the Si~O~Si bending vibration, Si~O~Si stretch vibration and Si~O~Si stretching vibration, respectively. Interestingly, the evolution and disappearance of functional groups and the appearance of more prominent groups reveal the incorporation of new functionalities on our samples. The carbonyl group band is present in both (a) (i), (b) (iv) leached samples and (a) (ii), (b) (v) calcined samples however not observed for the silica spectra of both samples in (a) iii and (b) vi, which confirms the successful formation of silica groups, predominant in the material [1,24,25,26,27]

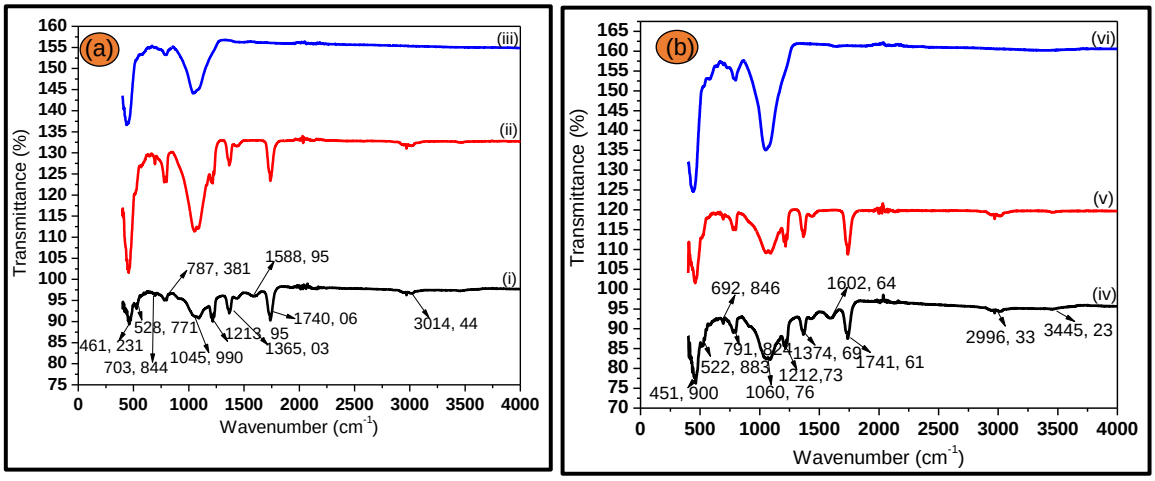

***Figure 4.2**: FTIR spectra of **(a)** SCBA (i) CA leached, (ii) calcined, (iii) silica and **(b)** SCBA (iv) acid-leached with L-Cysteine Hydrochloride, (v) calcined and (vi) Silica.FTIR spectra of (a) SCBA (i) CA leached, (ii) Calcined, (iii) Silica and (b) SCBA (iv) Acid-leached with L-Cysteine Hydrochloride, (v) Calcined and (vi) Silica.*

Similarly, the results obtained for as-produced (vi) silica in Figure 4.2 b showed identical behavior of new functionalities. The bands at 451. 900 cm^{-1}, 791.803 cm^{-1} and 1060.76 cm^{-1} are attributed to the Si~O~Si bending vibration, the Si~O~Si stretch vibration and the Si~O~Si stretching vibration [1,28].

Despite that, the silica in Figure 4.2 b (vi), showed a highly narrow and pronounced band at around 1060.76 cm^{-1} which is characteristic of crystalline silica, confirming the results obtained from XRD diffractogram(s). Additionally, the band at 3014.44 cm^{-1} corresponded to C–H stretch in (a) i and ii, respectively, whereas in (b) iv and v, the C–H band is at 2996.33 cm^{-1}. The weak absorption band for hydroxyl group (OH) exhibited weak is observed for treated bagasse with L-Cys in (b) iv, v at around 3445.23 cm^{-1} [26,27,28].

4.2.3. SEM-EDS analysis

The EDS results confirm that acid treatment is an efficient tool to minimize impurities from the increment (wt) of Si matter in the matrix, and thus the extraction of silica from sugar cane was successful. In addition, the results indicate that TPAH is a useful organic solvent for extraction of silica from sugar cane bagasse ash acid treated with L-cysteine hydrochloride monohydrate.

It can be observed that the morphology of powders from ash to silica and the selective removal of the synthesis residues using acid solution resulted in the formation of silica material with high composition, most importantly silica from ash-treated with L-cysteine hydrochloride monohydrate [29]. This may be due to the chloride present in the acid which was sufficient for the significant removal of metallic impurities as compared to the silica from ash treated with citric acid.

The surface morphologies of silica produced from SCBA were determined by SEM, and the SEM images are shown in Figure 4.3. The SEM images show that the samples in Figure 4.3a,b consist of agglomerates of irregular sizes, as well as the presence of some spherical particles distributed in the network of pores during silica synthesis, as there are irregular sizes of rice-like and spherical shape [27,28,29]. The morphological changes are in line with the surface characteristics analysis (FTIR), where the introduction of Tetrapropyl Ammonium Hydroxide on the calcined SCBA increased the formation of silica.

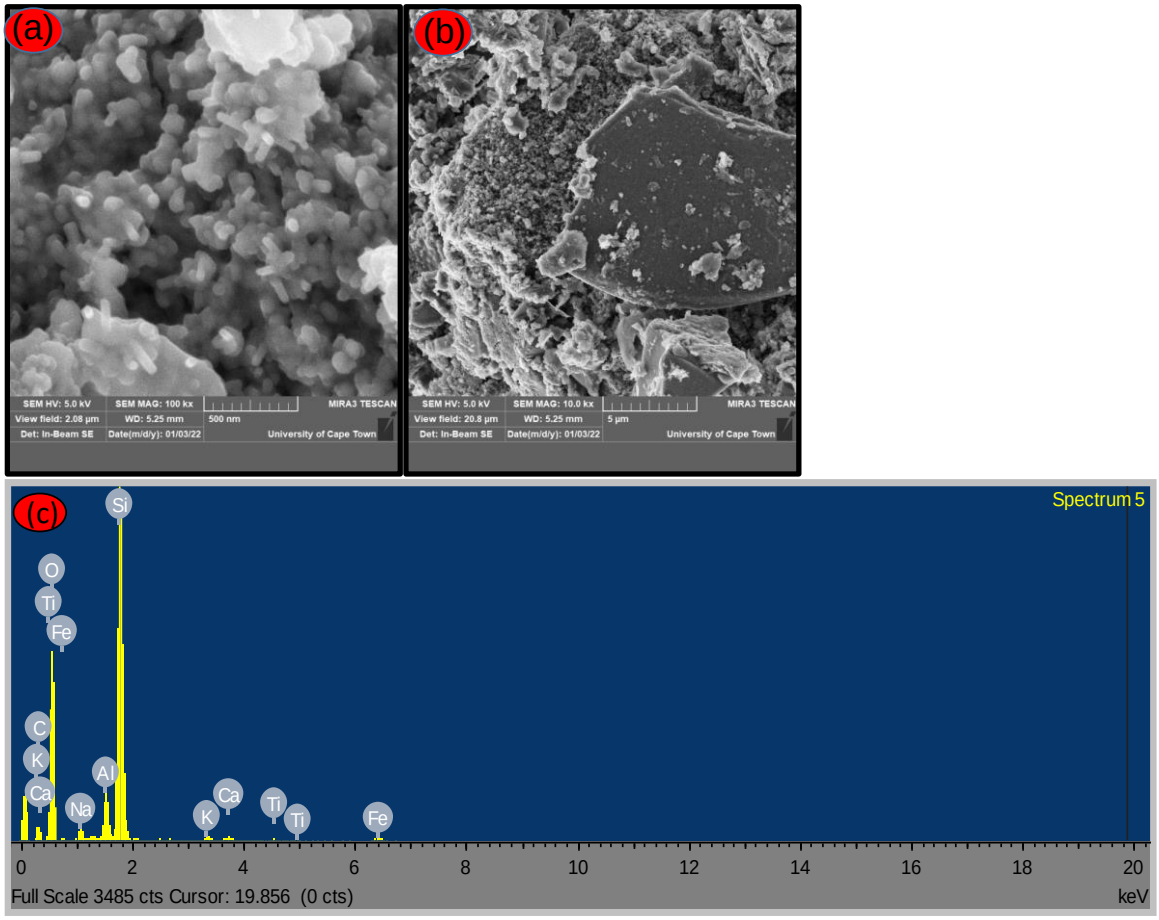

Figure 4.3. *SEM images presentation of (**a**) leached silica (low magnification), (**b**) leached silica (high magnification) and (**c**) SEM-EDX of as-synthesized CA-TPAH silica treated with citric acid.*

The SEM analysis was determined to be in the range of 200–500 nm, whereas the crystallite size estimated from XRD had an average diameter in the range 26–29 nm using the Scherrer formula.

SEM-EDS was conducted to study the composition of the synthesized silica using two different organic acids. Figure 4.3c, shows the EDS for the synthesized silica acid-treated with citric acid, the presence of metallic impurities beside the residual carbon and a more intense peak associated with silicon.

Table 4.1 below shows the elemental composition of bagasse ash, acid treated and silica. It is worth noting that the elemental Si composition in silica increases significantly, from raw-SCBA 1.78 wt% and 7.69 wt% for SCBA CA leached to 26.46 wt% and from 8.89 wt% to 34.7 wt% for SCBA L-cys leached.

Table 4.1*:* *Chemical analysis of sugarcane bagasse composition acid treated with citric acid (ca) and L-cysteine hydrochloride monohydrate (L-cys).*

Element	SCBA-raw (wt%)	SCBA-Leached@CA (wt%)	Silica@TPAH-CA (wt%)	SCBA-Leached@L-cys (wt%)	Silica@TPAH-Lcys (wt%)
Carbon (C)	74.92	51.85	10.83	46.12	10.24
Oxygen (O)	22.45	28.4	53.39	42.29	55.05
Silicon (Si)	1.78	7.69	26.46	8.89	34.7
Potassium (K)	0.26	-	0.69	0.06	-
Calcium (Ca)	0.59	0.15	0.96	-	-
Sodium (Na)	-	-	1.09	-	-
Iron (Fe)	-	-	2.25	-	-
Titanium (Ti)	-	-	0.47	-	-
Aluminum (Al)	-	0.3	3.84	2.53	-
Fluorine (F)	-	11.61	-	-	-

Sulfur (S)	-	-	-	0.1	
Element	SCBA-raw (wt%)	SCBA-Leached@CA (wt%)	Silica@TPAH-CA (wt%)	SCBA-Leached@L-cys (wt%)	Silica@TPAH-Lcys (wt%)

The tabulated results above exhibit the morphology of powders from the ash to the extracted silica. It can be observed that the selective removal of the synthesis residues using acid solution resulted in the formation of a silicon with high composition, most importantly for silica from ash-treated with L-cysteine hydrochloride monohydrate [30]. This may be due to the chloride present in the acid which was sufficient for the significant removal of metallic impurity as compared to the silica from ash-treated with citric acid. Additionally, Aluminum (Al) and Iron Fe were found to be predominant at approximately 3.84 wt% and 2.25 wt%, respectively.

Figure 4.4a,b presents SEM micrographs of leached silica with L-cysteine hydrochloride monohydrate. The images revealed that silica nanoparticles are randomly distributed and clustered with a non-uniform and rough surface. The SEM-EDS of the as-prepared L-cys-TPAH silica is shown in Figure 4.4c, with the elemental composition predominantly silicon and oxygen with a very considerable amount of carbon present in the material.

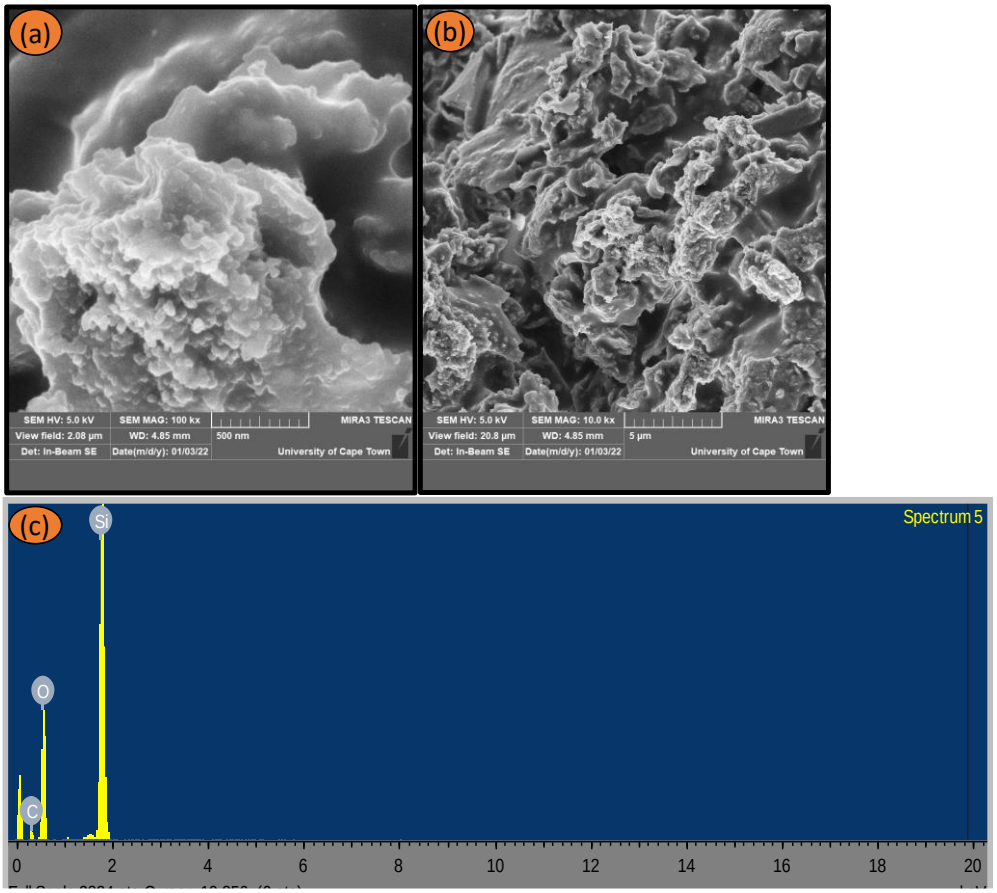

Figure 4.4. *SEM micrograph presentation of (a) leached silica (low magnification), (b) leached silica (high magnification) and (c) SEM-EDX of as-synthesized L-cys-TPAH silica treated with L-cysteine Hydrochloride.*

The SEM-EDS exhibited fewer impurities in the treated sample(s), for L-cysteine hydrochloride monohydrate, which indicates the efficacy of acid-pretreatment(s) in reducing these metallic impurities as reported in [30].

4.2.4. Thermal analysis

A thermogravimetric analysis (TGA) was conducted to investigate the thermal properties of the sugarcane bagasse ash from room temperature to 800 °C. This study essentially provided information on the pyrolysis/calcination temperatures and not the duration of the process. The thermogravimetric analysis in Figure 4.5 shows the thermal characteristics of (a) raw SCBA, (b) SCBA CA leached (c) SCBA L-cys leached respectively.

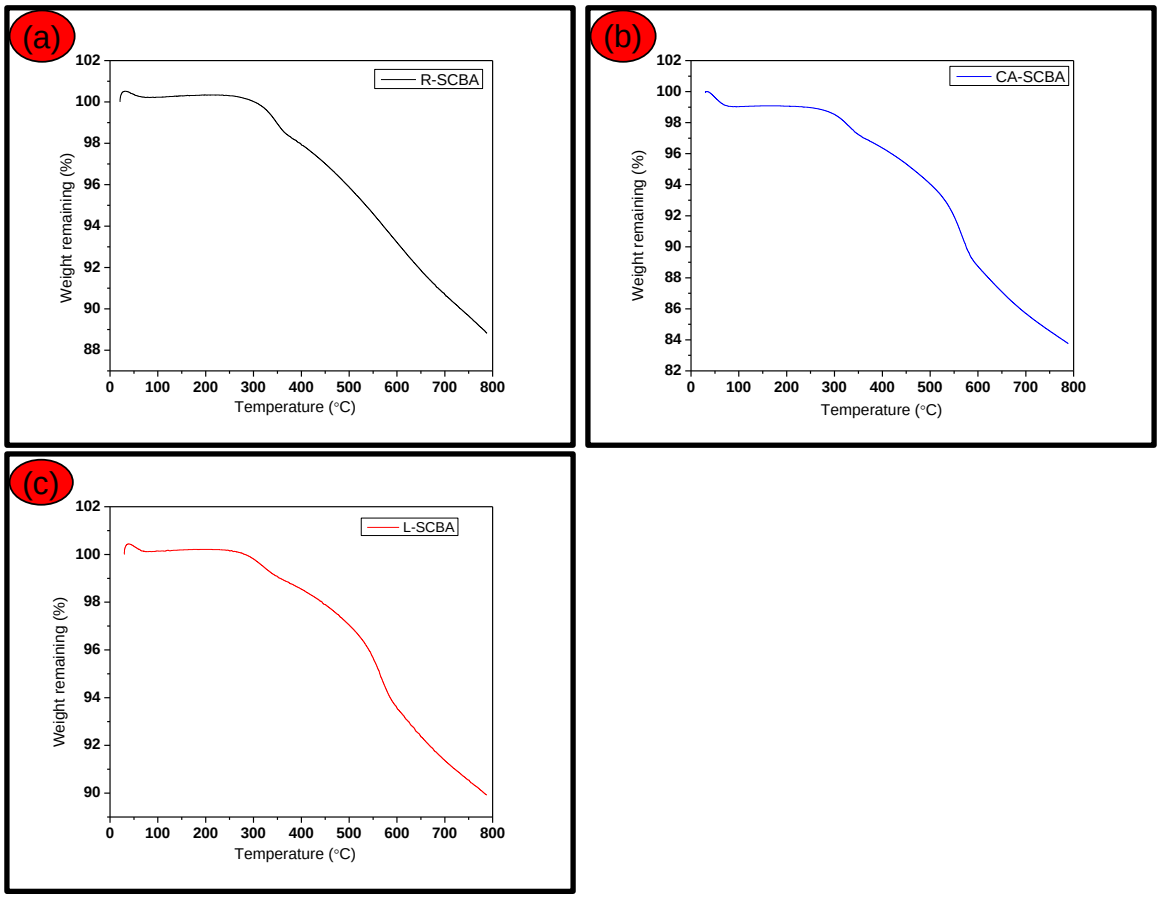

***Figure 4.5**: TGA distributions of (**a**) raw SCBA, (**b**) SCBA CA leached (**c**) SCBA L-cys leached respectively.*

The thermal characteristics of the sugarcane bagasse make it quite evident that the volatilization stage took place where hemicellulose, cellulose and lignin decomposition occurred [31,32]. Their weight loss, shown in figure 4.5, displays three main stages of dehydration, volatilization and carbonization, mostly for treated ash with CA and L-Cysteine, respectively. The TGA curves show that the evolution of thermal behavior started with the first stage of moisture drying occurring at 250 °C in all samples, owing to the crystallization in the interior part of the structures and light volatiles present in sugarcane bagasse ash [33].

The volatilization stage involves the decomposition of hemicellulose at approximately 180 °C and 340 °C, with the cellulosic breakdown occurring around 250 °C to 450 °C [34,35], whilst the lignin breakdown begins at 200 °C and goes to 800 °C [35]. Moreover, the rapid weight loss shown on the TGA curve (a) can be attributed to hemicellulose and cellulose

decomposition. Interestingly, TGA curves for the pretreated samples (b) and (c) reveal rapid weight loss with three distinctive stages, which is similar to the results reported in [36,37].

The TG curves revealed a total mass loss of 12%, 18% and 11%, respectively, making the pre-treatment with 5% citric acid solution the best organic acid for efficient leaching, as reported earlier in other studies. No further weight loss was observed, indicating the thermal stability of nanosilica present in the samples, which constitute about 84% in mass, as reported earlier in [38,39].

4.2.5. Nitrogen Physisorption Analysis

The textural properties of SCBA nano-silica(s) were evaluated using the N_2 adsorption-desorption method and the results are summarized in Table 4.2 below.

Table 4.2. *Textural properties of SCBA nano CA-Silica and L-cys Silica.*

Sample ID	BETSSA (m2/g)	Vp (cm3/g)	Dp (nm)
CA-Silica	21.6511	0.04312	8
L-cys Silica	116.005	0.1828	6

The BET_{SSA}, pore volume and pore diameter for SCBA for nano CA-Silica were 21.6511 m^2/g, 0.04312 cm^3 and 8 nm, respectively, while BET_{SSA}, pore volume and pore diameter for SCBA nano L-cys Silica is 116.005 m^2/g, 0.1828 cm^3/g and 6 nm, respectively. For CA-Silica displayed in Figure 6a, the amount of adsorbed gas increases steadily with increasing P/P_0 ratio at the lower P/P_0 regions, while it increases significantly for L-cys Silica with increasing P/P_0, as shown in Figure 4.6b. This is usually attributed to monolayer and multilayer adsorption, as reported in [38,39].

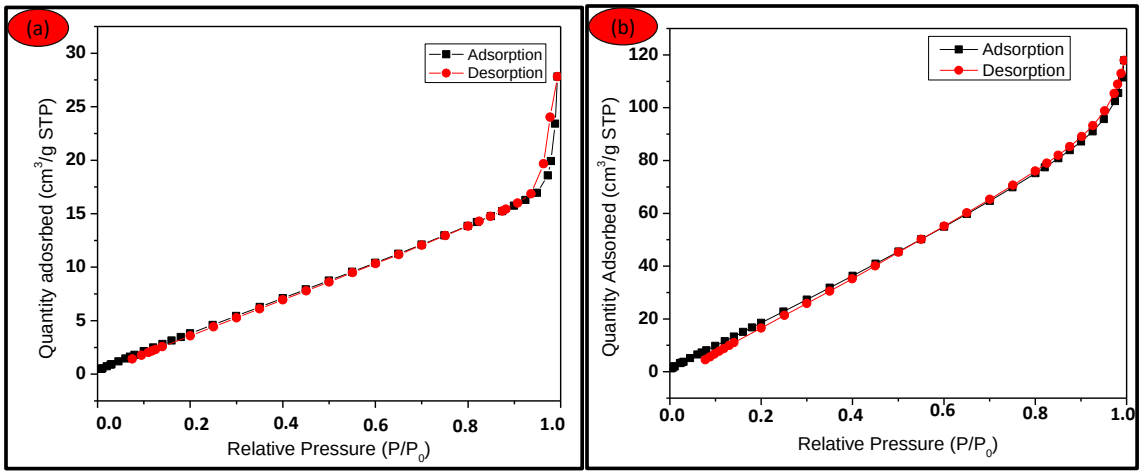

Figure 4.6. *N2 adsorption-desorption isotherm for (a) SCBA nano CA-Silica and (b) SCBA nano L-cys Silica.*

For the SCBA nano silica isotherm in Figure 4.6a, the hysteresis loop is observed at a range of $0.9 < P/P_0 < 1.0$, essentially associated with capillary condensation taking place in the mesopores. Furthermore, the loop at the high P/P_0 side has been reported to be related to large pores. The little loop at Figure 4.6b observed at range of $0.2 < P/P_0 < 0.4$ is also due to the capillary condensation inside the mesoporous structure, however no loop at the higher P/P_0 region is observed for this synthesized silica (SCBA nano L-cys Silica) [38,39,40].

4.3 Summary

Physical characteristics and quantitative elemental composition of silica produced from sugarcane bagasse ash were investigated using FTIR and SEM-EDS. Thermal properties were studied using TGA, and the crystalline nanostructure was studied by XRD analysis. The average diameter sizes were determined to be approximately 26 nm and 29 nm for silica acid-leached with CA and L-Cys, respectively.

This study has shown that sugarcane bagasse ash contains highly crystalline silica which could be affected by leaching. The as-synthesized ca-silica and L-cys-silica of the extracted crystallite size had an average diameter of 26 nm and 29 nm, respectively, in addition to a specific surface area of 21.6511 m^2/g and 116.005 m^2/g for ca-silica and L-cys silica, respectively. The FTIR spectra showed peaks at 461.231 cm^{-1}, 787.381 cm^{-1} and 1045.99 cm^{-1}, which corresponds to the Si~O~Si bending vibration, the Si~O~Si stretch vibration, and the Si~O~Si stretching vibration, respectively. It was established that acid pre-treatment of the bagasse was more affected by concentration and time than temperature.

Based on the findings of this experimental study, the major component of SCBA is SiO_2 from the elemental composition with the O and Si elements displaying very high percentages. The ash is a predominantly carbonaceous material. The methodology also showed that with higher calcination temperatures other metallic impurities form, whereby Al and Fe were found in minor quantities after Si. After the synthesis of bio-silica, the structural, morphological and thermal properties were studied. The advantage of this finding is the green method of utilizing citric acid, L-cysteine hydrochloride monohydrate for acid treatment. IN addition, TetraPropyl Ammonium Hydroxide monohydrate was used as an extraction solvent. Furthermore, the use of organic chemicals proved successful for the current study and are eco-friendly.

4.4 References

[1] Mohd, N.K., Wee, N.N.A.N. and Azmi, A.A., 2017, September. Green synthesis of silica nanoparticles using sugarcane bagasse. In *AIP conference proceedings* (Vol. 1885, No. 1, p. 020123). AIP Publishing LLC.

[2] Herzog, H. and Golomb, D., 2004. Carbon capture and storage from fossil fuel use. *Encyclopedia of energy*, *1*(6562), pp.277-287.

[3] Salem, S.S. and Fouda, A., 2021. Green synthesis of metallic nanoparticles and their prospective biotechnological applications: an overview. *Biological trace element research*, *199*(1), pp.344-370.

[4] Rodríguez-Félix, F., López-Cota, A.G., Moreno-Vásquez, M.J., Graciano-Verdugo, A.Z., Quintero-Reyes, I.E., Del-Toro-Sánchez, C.L. and Tapia-Hernández, J.A., 2021. Sustainable-green synthesis of silver nanoparticles using safflower (Carthamus tinctorius L.) waste extract and its antibacterial activity. *Heliyon*, *7*(4), p.e06923.

[5] Del-Toro-Sánchez, C.L., Rodríguez-Félix, F., Cinco-Moroyoqui, F.J., Juárez, J., Ruiz-Cruz, S., Wong-Corral, F.J., Borboa-Flores, J., Castro-Enríquez, D.D., Barreras-Urbina, C.G. and Tapia-Hernández, J.A., 2021. Recovery of phytochemical from three safflower (Carthamus tinctorius L.) by-products: antioxidant properties, protective effect of human erythrocytes and profile by UPLC-DAD-MS. *Journal of Food Processing and Preservation*, *45*(9), p.e15765.

[6] Rodríguez-Félix, F., Corte-Tarazón, J.A., Rochín-Wong, S., Fernández-Quiroz, J.D., Garzón-García, A.M., Santos-Sauceda, I., Plascencia-Martínez, D.F., Chan-Chan, L.H., Vázquez-López, C., Barreras-Urbina, C.G. and Olguin-Moreno, A., 2022. Physicochemical,

structural, mechanical and antioxidant properties of zein films incorporated with no-ultrafiltred and ultrafiltered betalains extract from the beetroot (Beta vulgaris) bagasse with potential application as active food packaging. *Journal of Food Engineering*, p.111153.

[7] Rodríguez-Félix, F., Graciano-Verdugo, A.Z., Moreno-Vásquez, M.J., Lagarda-Díaz, I., Barreras-Urbina, C.G., Armenta-Villegas, L., Olguín-Moreno, A. and Tapia-Hernández, J.A., 2022. Trends in Sustainable Green Synthesis of Silver Nanoparticles Using Agri-Food Waste Extracts and Their Applications in Health. *Journal of Nanomaterials*, *2022*.

[8] Farirai, F., Mupa, M. and Daramola, M.O., 2021. An improved method for the production of high purity silica from sugarcane bagasse ash obtained from a bioethanol plant boiler. *Particulate Science and Technology*, *39*(2), pp.252-259.

[9] Chung, I.M., Park, I., Seung-Hyun, K., Thiruvengadam, M. and Rajakumar, G., 2016. Plant-mediated synthesis of silver nanoparticles: their characteristic properties and therapeutic applications. *Nanoscale research letters*, *11*(1), pp.1-14.

[10] Dos Santos, R.M., Neto, W.P.F., Silvério, H.A., Martins, D.F., Dantas, N.O. and Pasquini, D., 2013. Cellulose nanocrystals from pineapple leaf, a new approach for the reuse of this agro-waste. *Industrial Crops and Products*, *50*, pp.707-714.

[11] Lauwers, A.M. and Heinen, W., 1974. Bio-degradation and utilization of silica and quartz. *Archives of Microbiology*, *95*(1), pp.67-78.

[12] Anuar, M.F., Fen, Y.W., Zaid, M.H.M., Matori, K.A. and Khaidir, R.E.M., 2020. The physical and optical studies of crystalline silica derived from the green synthesis of coconut husk ash. *Applied Sciences*, *10*(6), p.2128.

[13] Chruściel, J.J. and Leśniak, E., 2015. Modification of epoxy resins with functional silanes, polysiloxanes, silsesquioxanes, silica and silicates. *Progress in Polymer Science*, *41*, pp.67-121.

[14] Ndububa, E.E. and Nurudeen, Y., 2015. Effect of guinea corn husk ash as partial replacement for cement in concrete. *IOSR Journal of Mechanical and Civil Engineering (IOSR-JMCE)*, *12*(2), pp.40-45.

[15] Yi, D.K., Lee, S.S., Papaefthymiou, G.C. and Ying, J.Y., 2006. Nanoparticle architectures templated by SiO2/Fe2O3 nanocomposites. *Chemistry of Materials*, *18*(3), pp.614-619.

[16] Norsuraya, S., Fazlena, H. and Norhasyimi, R., 2016. Sugarcane bagasse as a renewable source of silica to synthesize Santa Barbara Amorphous-15 (SBA-15). *Procedia Engineering*, *148*, pp.839-846.

[17] Aprianti, E., Shafigh, P., Bahri, S. and Farahani, J.N., 2015. Supplementary cementitious materials origin from agricultural wastes–A review. *Construction and Building Materials*, *74*, pp.176-187.

[18] Katare, V.D. and Madurwar, M.V., 2017. Experimental characterization of sugarcane biomass ash–A review. *Construction and Building Materials*, *152*, pp.1-15.

[19] Thomas, B.S., Yang, J., Mo, K.H., Abdalla, J.A., Hawileh, R.A. and Ariyachandra, E., 2021. Biomass ashes from agricultural wastes as supplementary cementitious materials or aggregate replacement in cement/geopolymer concrete: A comprehensive review. *Journal of Building Engineering*, p.102332.

[20] Moayedi, H., Aghel, B., Nguyen, H. and Rashid, A.S.A., 2019. Applications of rice husk ash as green and sustainable biomass. *Journal of Cleaner Production*, *237*, p.117851.

[21] Khan, N.A., Ibrahim, S. and Subramaniam, P., 2004. Elimination of heavy metals from wastewater using agricultural wastes as adsorbents. *Malaysian journal of science*, *23*(1), pp.43-51.

[22] Falk, G., Shinhe, G.P., Teixeira, L.B., Moraes, E.G. and de Oliveira, A.N., 2019. Synthesis of silica nanoparticles from sugarcane bagasse ash and nano-silicon via magnesiothermic reactions. *Ceramics international*, *45*(17), pp.21618-21624.

[23] Rahmat, N., Sabali, M.A., Sandu, A.V., Sahiron, N. and Sandu, I.G., 2016. Study of calcination temperature and concentration of NaOH effect on crystallinity of silica from sugarcane bagasse ash (SCBA). *Rev Chim*, *67*(9), pp.1872-1875.

[24] Shinohara, Y. and Kohyama, N., 2004. Quantitative analysis of tridymite and cristobalite crystallized in rice husk ash by heating. *Industrial health*, *42*(2), pp.277-285.

[25] de Lima, V.M.E., Barros, L.C. and de Melo, A.A., 2021. Characterization of sugarcane bagasse ash (SBA) and its evaluation for use in alkali-activated slag mixtures. *Cerâmica*, *67*, pp.123-130.

[26] Maza-Ignacio, O.T., Jiménez-Quero, V.G., Guerrero-Paz, J. and Montes-García, P., 2020. Recycling untreated sugarcane bagasse ash and industrial wastes for the preparation of resistant, lightweight and ecological fired bricks. *Construction and Building Materials*, *234*, p.117314.

[27] Jagadesh, P., Ramachandramurthy, A., Murugesan, R. and Sarayu, K., 2015. Micro-Analytical studies on sugar cane bagasse ash. *Sadhana*, *40*(5), pp.1629-1638.

[28] El-Sayed, S.A. and Mostafa, M.E., 2015. Kinetic parameters determination of biomass pyrolysis fuels using TGA and DTA techniques. *Waste and Biomass Valorization*, *6*(3), pp.401-415.

[29] He, C., Giannis, A. and Wang, J.Y., 2013. Conversion of sewage sludge to clean solid fuel using hydrothermal carbonization: hydrochar fuel characteristics and combustion behavior. *Applied Energy*, *111*, pp.257-266.

[30] Trninić, M., Jovović, A. and Stojiljković, D., 2016. A steady state model of agricultural waste pyrolysis: A mini review. *Waste Management & Research*, *34*(9), pp.851-865.

[31] Çepelioğullar, Ö. and Pütün, A.E., 2013. Thermal and kinetic behaviors of biomass and plastic wastes in co-pyrolysis. *Energy conversion and management*, *75*, pp.263-270.

[32] Lv, G.J., Wu, S.B. and Lou, R., 2010. Kinetic study for the thermal decomposition of hemicellulose isolated from corn stalk. *BioResources*, *5*(2), pp.1281-1291.

[33] Abdullah, N. and Sulaiman, F., 2013. A comparison study on oven and solar dried empty fruit bunches. *technology*, *3*(2).

[34] Aboyade, A.O., Hugo, T.J., Carrier, M., Meyer, E.L., Stahl, R., Knoetze, J.H. and Görgens, J.F., 2011. Non-isothermal kinetic analysis of the devolatilization of corn cobs and sugar cane bagasse in an inert atmosphere. *Thermochimica Acta*, *517*(1-2), pp.81-89.

[35] Rafiee, E. and Shahebrahimi, S., 2012. Nano silica with high surface area from rice husk as a support for 12-tungstophosphoric acid: an efficient nano catalyst in some organic reactions. *Chinese Journal of Catalysis*, *33*(7-8), pp.1326-1333.

[36] Rafiee, E., Shahebrahimi, S., Feyzi, M. and Shaterzadeh, M., 2012. Optimization of synthesis and characterization of nanosilica produced from rice husk (a common waste material). *International nano letters*, *2*(1), pp.1-8.

[37] Yadav, A.L., Sairam, V., Srinivasan, K. and Muruganandam, L., 2020. Synthesis and characterization of geopolymer from metakaolin and sugarcane bagasse ash. *Construction and Building Materials*, *258*, p.119231.

[38] Mantoura, S., 2007. Reduce and replicate. *Nature Nanotechnology*, pp.1-1.

[39] Shen, L., Guo, X., Fang, X., Wang, Z. and Chen, L., 2012. Magnesiothermically reduced diatomaceous earth as a porous silicon anode material for lithium ion batteries. *Journal of Power Sources*, *213*, pp.229-232.

[40] Li, M., Dai, Y., Ma, W., Yang, B. and Chu, Q., 2017, November. Review of new technology for preparing crystalline Silicon solar cell materials by metallurgical method. In

IOP Conference Series: Earth and Environmental Science (Vol. 94, No. 1, p. 012016). IOP Publishing

Chapter 5: Synthesis of nanosilicon from sugarcane bagasse ash

Synopsis

Solar-energy material silicon has traditionally been obtained from quartz through a high-energy, carbothermal process that reaches temperatures of around 1,900 ℃. This was not feasible due to the high cost of the operational costs and, ultimately, the cost of the as-fabricated solar cells. Interestingly, magnesiothermic reduction of silica into silicon is more energy efficient than the counterpart reduction procedure because the reaction conditions occur at lower temperatures. This study emphasizes the cost-effectiveness of reducing silica production because the precursor is industrial agrowaste, sugarcane bagasse.

Abstract

This study presents the magnesiothermic reduction of silica into silicon. This reduction process occurs at a lower reaction temperature than its carbothermal counterpart. Furthermore, silica was extracted from sugarcane bagasse ash via a thermo-chemical treatment method using, for the first time, L-cysteine chloride monohydrate and used as a precursor in the production of silicon using magnesiothermic reduction. The as-synthesized nanocrystalline silicon's physicochemical properties were investigated using XRD, Raman, FTIR, BET, and SEM. A peak at 2θ of 28.2 with a crystallite size of 32 nm was discovered using X-ray diffraction spectroscopy. The pronounced peak around 518 cm^{-1} was observed from the Raman spectrum, characteristic of crystalline silicon. The FTIR analysis showed two sharp peaks at 446 cm^{-1} and 1056 cm^{-1}, indicative of the Si-O rocking mode and Si-O-Si stretching mode functional groups present. N_2 physisorption at 77 K reveals that the surface area, pore volume, and pore diameter of the as-synthesized silicon were 73 m^2/g, 0.23 cm^3/g, and 12 nm, respectively. In this study, we were able to produce silicon from silica extracted from SCBA using the magnesiothermic reduction method in a tube furnace, which has potential for thin-film solar cells.

5.1. Background

Sugarcane bagasse ash, a waste product from the sugarcane industry, was processed into silica (SiO2) powder in this study. An ideal process for sustainability is the production of

manufactured silica particles from low-cost renewable or waste resources. Sugarcane bagasse has emerged as a sustainable resource for both tailored silica particles and bioenergy production. Furthermore, the manufacture of engineered silica particles from sugarcane bagasse ash to produce nanosilicon. Silica is a significant raw material for industrial applications, and much research has been conducted to extract it from agricultural wastes such as sugarcane bagasse, rice husk, etc. [1,2].

Silicon is an inorganic material of great technological importance across many fields owing to its inherent set of physical, chemical, electronic, and optical properties [1–3]. Due to its application-specific and superior properties, the performance profile with its synergistic high surface area and small particle size makes it a good candidate for applications in a range of new technological advances, including functional nanomaterials, biotechnology, nanoelectronics, energy production, and storage devices. Another interesting feature is the application of silicon in thermoelectric materials via magnesium alloy technology [4,5].

Presently, the crystalline silicon used in solar cell production is produced from the traditional quartz source of silica. The synthetic route is high energy intensive (around 1900 ℃), which minimizes all process steps at a high operating cost, resulting in the production of highly expensive solar cells. Several studies report alternative methods with low operating costs, including the metallothermic method, which has gained great attention as a straightforward synthesis of porous Si [6,7].

A metal, such as magnesium, zinc, or aluminum, to name a few, is used in the reduction procedure. Furthermore, the ideal metal for a reduction reaction should be cheap, easy to work with, produce eco-friendly products with a low melting point, and, most importantly, have significant redox properties. Metal oxides may be produced as by-products of these processes, which is undesirable. Nonetheless, metal oxide removal can be hazardous due to a violent reaction with water [8]. Indeed, Zn readily reacts with Si halides; however, the reaction with silica is thermodynamically unfavourable. As a result, Mg and Al are the most-used metallothermic reduction agents for silica. The magnesiothermic reduction has demonstrated the ability to produce silicon from silica in the laboratory. In the temperature range between 500 and 950 °C, the magnesiothermic reduction has demonstrated the ability

to synthesize silicon from silica, enabling the template-assisted creation of silicon structures [8,9].

Among the many different natural resources at our disposal, sugarcane is one of the main potential sources for silica extraction and subsequent transformation to nanostructured silicon, as tabulated in Table 1. This feedstock is traditionally used for sugar and ethanol, and the residue from the process (bagasse) is utilized as the main source of energy. In this study, experiments were carried out to convert silica nanoparticles to nanosilicon using magnesiothermic reduction. Consequently, the nanopowders were analyzed and compared in terms of physical, chemical composition, morphology, and structural properties [10].

Table 5.1: *Recent studies reported the magnesiothermic reduction with their results.*

Precursor	Reaction Conditions	Properties of As-Produced Silicon
Algae	T = 650 °C	Nanocrystal silicon SSA-500 m^2/g, Pore Size Diameter-2 nm. [11]
SiO_2 (Stober Method)	T = 800 °C t-12 h Argon atm	Porous nanocrystalline Si [12]
Rice Husk (RH), Bamboo Culm (BC), and Sugarcane Bagasse (SCB)	T = 650 °C t = 30 min (MW-MR)	Porous Silicon, Pore diameter (50–80 nm) SSA [13]
RH	T = 650 °C t = 7 h	Porous silicon SSA 150 m^2/g [14]

2. Experimental

2.1. Materials Used

All chemicals were purchased from Sigma-Aldrich and used without further purification. L-cysteine hydrochloride monohydrate (98%) and tetrapropylammonium hydroxide (1.0 M) in H_2O were purchased from Sigma-Aldrich (St Louis, MO, USA). Sugarcane was procured from the Sugar Illovo South Africa Company (KwaZulu-Natal, South Africa). In a typical preparation procedure, sugarcane bagasse was soaked for a period of 24 h in double-deionized water to remove any dust and soil particles. The soaked sugarcane was then oven-dried for a period of 6 h. After being soaked and dried, the sugarcane was burned in the open air to produce black sugarcane bagasse ash (SCBA). The synthesis was done using deionized water from the Milli-Q water purification system (Millipore, Bedford, MA, USA).

The chemical composition test was done using X-ray fluorescence spectroscopy (XRF, (Malvern Panalytical, Malvern, UK) for major oxides present in the SCBA in Table 2. The XRF study reveal that the leaching process was efficient as the amount of silica was significantly reported to be 79.40 wt%. The pretreatment step was done using L-cysteine hydrochloride monohydrate as the leaching acid. The loss on ignition is also reported in Table 2.

Table 2. *Chemical composition of acid-leached SCBA from XRF.*

Component	Wt%
SiO_2	79.40
TiO_2	1.03
Al_2O_3	8.45
Fe_2O_3	2.39
MnO	0.04
MgO	0.61
CaO	1.06

Na_2O	1.06
K_2O	3.86
P_2O_5	0.22
SO_3	0.03
Cr_2O_3	0.04
NiO	0.02
H_2O	0.04
LOI	1.18

The significant improvement in the morphology of silica in the powders of the ash is due to the selective removal of the synthesis residues using L-cysteine hydrochloride monohydrate, essentially reducing metallic impurities in the sample. After acid-treatment, the sample was calcined in a muffle furnace and subsequent extraction of silica via hydro-thermal method using tetrapropylammonium hydroxide, thereby minimizing the other metal oxides impurities.

5.2. Results and discussion

5.2.1 X-ray diffraction (XRD) and Raman Spectroscopy

The XRD and Raman analyses were performed on the material prepared by magnesiothermic reduction to study the crystallinity and vibration as well as structural properties, respectively. The phase identification from XRD analysis was cross-examined on SCBA nano-Si, whose 2θ angle of 28.2 (Figure 5.1a) showed peaks of highly crystalline silicon, which can be compared with the JCPDS (No. 27–1402 Si XRD) reference pattern number. The crystallite size estimated by the Scherrer equation based on the peak (inset) at 2θ of 28.2 was 32 nm.

Scherrer equation: $\mathrm{Dp} = \frac{\mathrm{K}\lambda}{\beta \cos\theta}$, whereby Dp-Average crystallite size (nm), K-Scherrer constant. It varies from 0.68 to 2.08 and K = 0.94 for spherical crystallites with cubic symmetry, λ-X-ray wavelength. For mini XRD, $CuK\alpha$ average = 1.54178 A, B-FWHM (full Width at Half Maximum) of XRD peak, θ-XRD peak position, one half of 2θ. Even though

the as-synthesized silicon has a well-defined crystalline structure, the presence of a small halo centred at $2\theta = 22.5$, characteristic of an amorphous property in the material, is quite interesting; similar results have been reported by [15,16].

This confirms the successful reduction of silica into nano-silicon from sugarcane bagasse ash. The structural properties were carried out using Raman spectroscopy for the as-synthesized SCBA nano-silicon, as presented in Figure 5.1b. The Raman spectra with a peak at 518 cm^{-1}, characteristic of Si-Si stretching mode, shown in the inset, and the half-full width at half maximum (FWHM) of 6 cm^{-1} were observed; similar results were reported by Li et al. This was as a result of the scattering of the first-order optical phonon of nanosilicon. In their study of the Raman spectrum for crystalline silicon, they observed a peak at 520 cm^{-1} and a FWHM of 2.8 cm^{-1} [17,18].

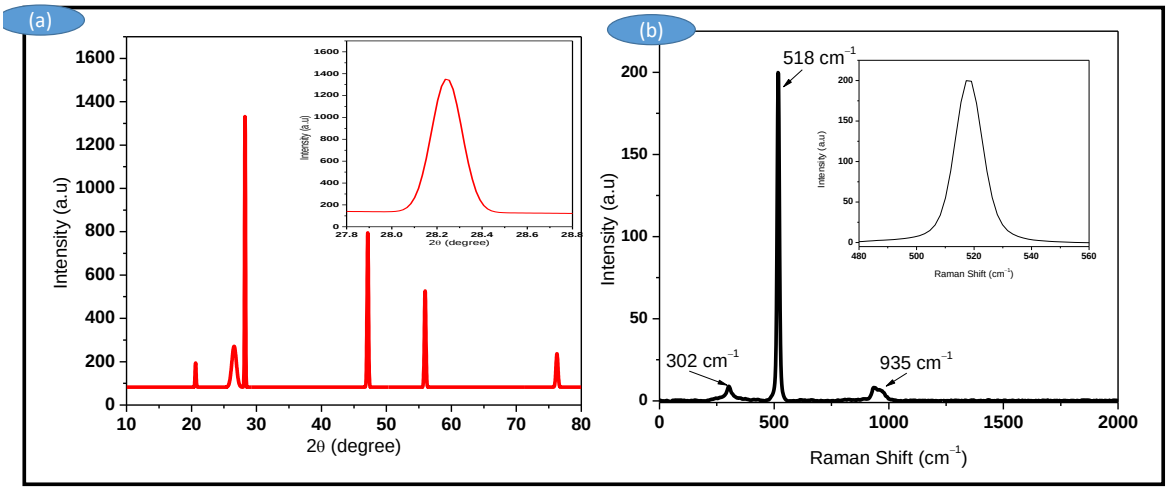

Figure 5.1. *XRD pattern (a) and Raman spectrum (b) of SCBA nano silicon prepared by magnesiothermic reaction.*

The other two peaks observed at 302 cm^{-1} and 935 cm^{-1}, respectively, were emanating from the scattering of two transverse acoustic (2TA) phonons and two optical (2TO) phonons, respectively. The peak at 935 cm^{-1} is reported in the literature due to the stretching mode of amorphous Si-Si. Interestingly, Li et al. [9] reported 300 cm^{-1} and 970 cm^{-1} as the observations for 2TA and 2TO, respectively [17,18].

As a result, Holzapfel et al. [19] reported a significant feature of silicon signals with the most desirable Raman characteristic at 518 cm^{-1} and a full width at half maximum (FWHM) of

6 cm^{-1}, similar to the current study's results. As a result, the scattering of first-order optical phonon mode (TO) was assigned. The two peaks at 300 cm^{-1}, and 900 cm^{-1} were notably assigned to the scattering of the second-order transverse acoustic phonon mode (2TA) and the second-order optical phonon mode (2TO), respectively [17–19].

5.2.2 FTIR spectroscopy

The evolution of the FT-IR spectra of nanosilicon prepared from the magnesiothermic reduction of silica extracted from sugarcane bagasse ash is presented in Figure 5.2, and the characteristic bond peaks that appeared in the spectra are tabulated in Table 3.

Table 3: *Typical bond peaks appearing in FTIR spectra for SCBA nano-Si.*

Wavelength (cm^{-1})	Bond	Type
1056	Si-O	Stretching mode
446	Si-O	Rocking vibration

The Si-O stretching mode (1056 cm^{-1}) and Si-O rocking vibration (446 cm^{-1}) are observed in the powder samples. A major contribution to the increase of the Si-O bond comes from the aging of the Si nanoparticles. It is highly probable that these bonds are formed by the combination of O_2 present in the DI water; a similar conclusion was made in the literature [20,21].

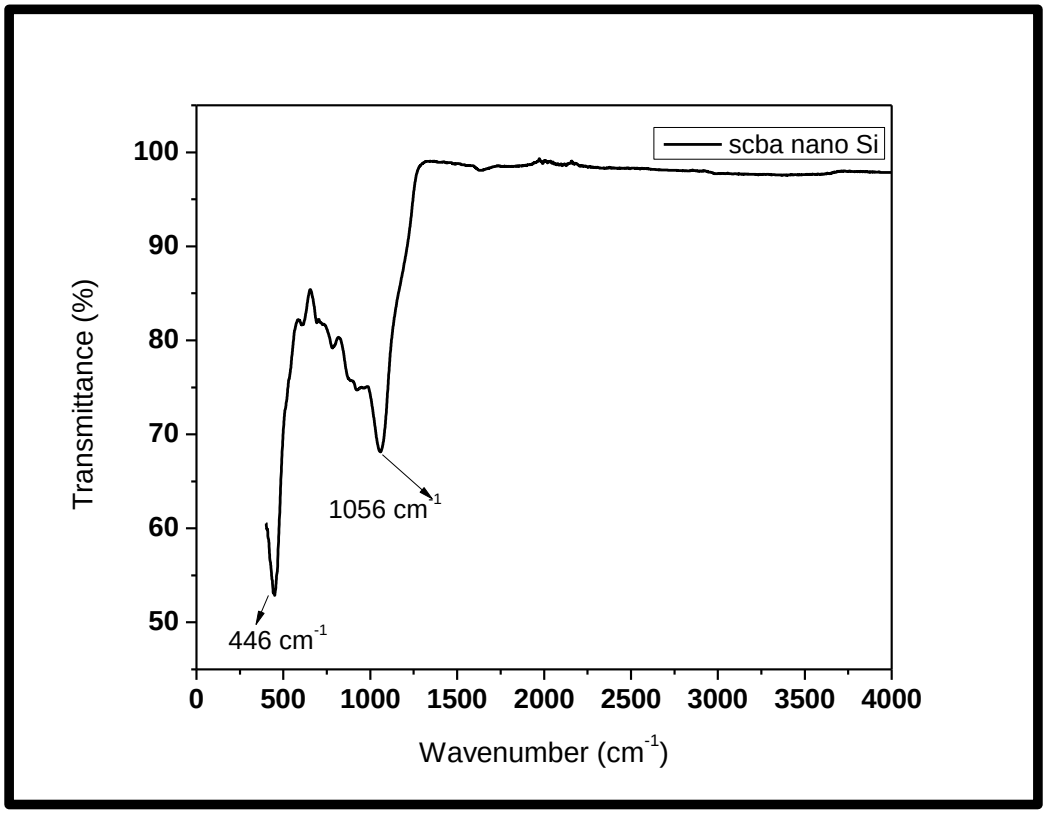

***Figure 5.2**: FTIR spectrum showing surface chemistry of SCBA nano silicon.*

5.2.3 Nitrogen Physisorption studies

The interfacial properties of the as-synthesized SCBA nanosilicon were studied via the N_2 adsorption–desorption method, and the results are reported in Table 5.2 below.

***Table 5.2**: Textural properties of sugarcane bagasse ash nano silicon.*

Sample ID	BET_{SSA} (m^2/g)	Vp (cm^3)	Dp (nm)
SCBA nano-silicon	74	0.23	12

The values for the specific surface area obtained by the BET analysis were 74 m^2/g, a pore volume of 0.23 cm^3, and a pore diameter of 12 nm for the SCBA nanosilicon. When the hysteresis loop was present at a range of $0.6 < P/P_0 < 1.0$ from the graph, the degree of porosity was observed. And the loop is associated with large pores [22]. It is interesting to note that the material prepared via the thermo-chemical treatment method was observed to have a moderate increase in specific surface area, porosity, pore volume, and average pore

diameter in relation to the increasing P/P_0 at the lower P/P_0 regions, as shown in Figure 5.3. Moreover, the adsorption isotherm of the as-prepared SCBA nanosilicon had similar features as those presented in [22–24].

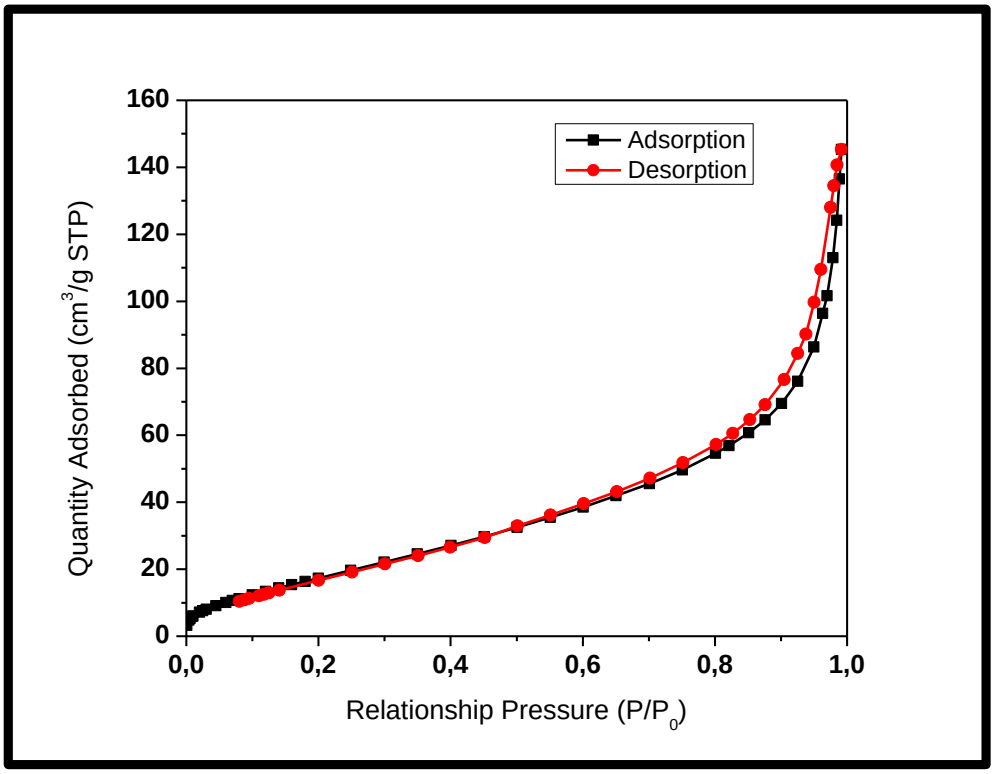

Figure 5.3: *N_2 adsorption-desorption isotherm for the powder SCBA nano silicon prepared by thermos-chemical method.*

It is interesting to note that the material prepared via the thermo-chemical treatment method had a relatively high specific surface area, porosity, pore volume, and average pore diameter in relation to the moderate increase with increasing P/P_0 at the lower P/P_0 regions. Moreover, the adsorption isotherm of the as-prepared scba nanosilicon had similar features as those presented in [23–25].

5.2.5 SEM-EDS analysis

The SEM images are presented in Figure 5.5 a,b at different magnifications. At higher magnifications, agglomerates of SCBA nanosilicon of irregular shapes can be seen, as well as the presence of some spherical particles distributed in a porous structure. This

transformation is as a result of the particles having sizes in the nanometric scale consistent with the XRD results, the grain size was in the range 30 nm to 500 nm [24].

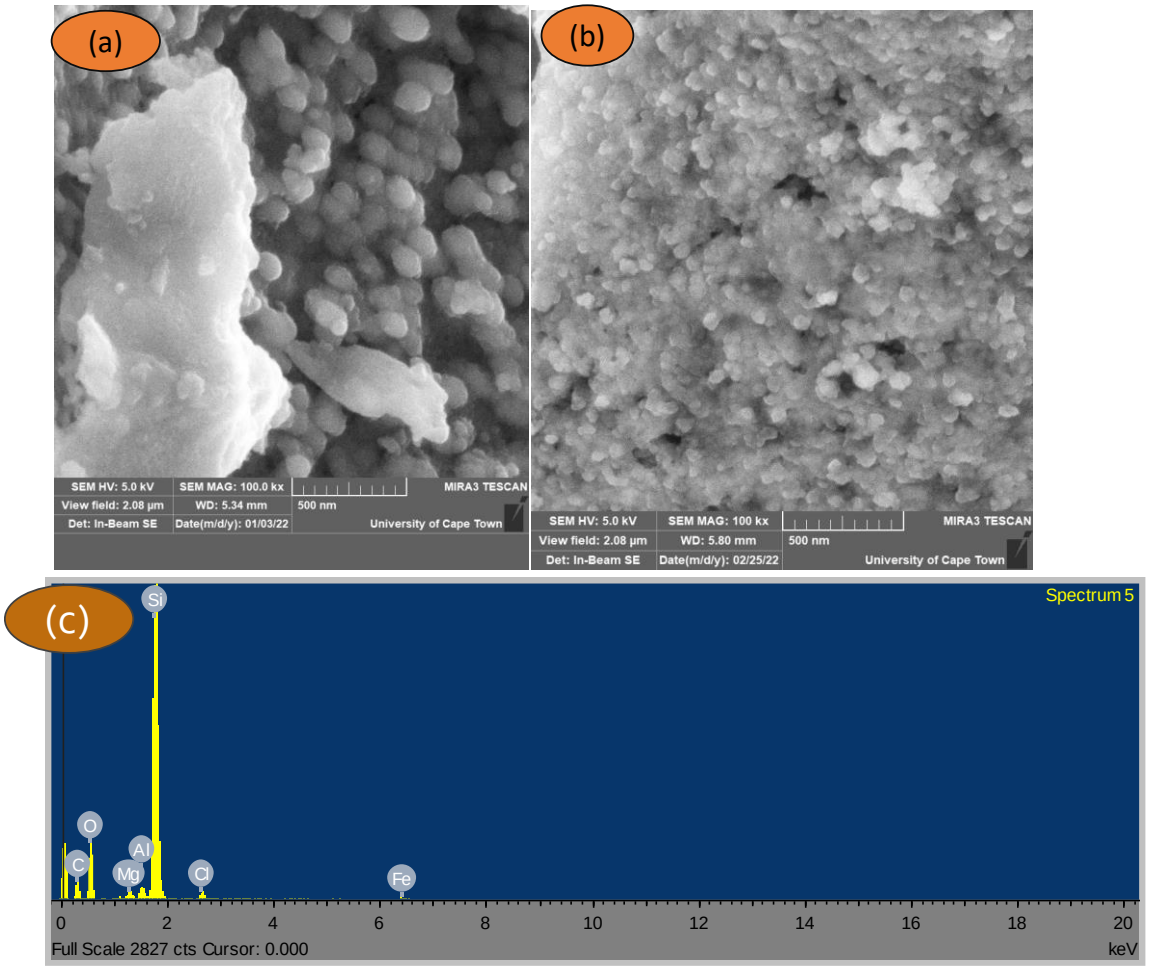

***Figure 5.5**: SEM images of (a), (b)SCBA nano silicon and (c) EDS spectrum of SCBA nano silicon.*

.

The surface morphologies of nano-silicon produced show nanoparticle agglomeration, which is favoured by the magnesiothermic reduction step. As shown in Figure 5c, the process efficacy was assessed using energy dispersive X-ray spectroscopy (EDX). The strong intensity of oxygen and silicon shown in the EDX spectra confirms the silica element is present in the sample. This is a negligible impurity commonly associated with the green method. This may be due to the resultant surface of highly active silicon upon exposure to the aqueous solution of HCl as well as the small presence of unreacted silica in the sample during the reduction method [24,25]. The morphological changes are in agreement with the surface chemistry discussed earlier in the FTIR analysis.

The SEM-EDX analysis presented in Figure 4c confirms that magnesiothermic reduction of silica into silicon is an effective tool in harnessing sugarcane bagasse ash for valuable materials such as silicon nanoparticles. The predominantly as-synthesized silicon content in the sample is indicative that the agro-waste SCBA is rich, useful, and cost-effective for the synthesis of silicon.

5.3. Summary

Based on the findings, silica extracted from sugarcane bagasse ash by L-cysteine chlorination-hydrothermal treatment was used as a precursor for the preparation of nano silicon by magnesium thermal reduction method. The nanosilicon nanoparticles were successfully synthesized from extracted biosilica from sugarcane bagasse ash (SCBA). The physical characteristics and quantitative elemental composition of nano-silicon were investigated. The surface area, pore volume, and pore diameter of the as-synthesized silicon were 74 m^2/g, 0.23 cm^{-1}, and 12 nm, respectively. According to Raman spectroscopy, a frequency downshift is caused by a decrease in particle size because of particle surface oxidation. The FTIR spectrum confirms the increase in oxidation of the particles during washing with deionized water, with peaks at 446 cm^{-1} and 1056 cm^{-1}, respectively, corresponding to rocking and stretching modes. The morphological, textural, and structural properties determined in this study indicated that the as-produced material exhibits highly rich silicon with a well-defined crystalline structure with a diameter of 32 nm. Moreover, these results showed that nanostructured silicon can be produced from sustainable sources of silica. Magnesiothermic process serves as a potential method for the production of silicon due to its low operating costs, and due to its high violent reactivity, sodium chloride is often used as a stabilizer for an efficient and stable process, and can rival a conventional carbothermal process.

5.4. References

[1] Yadav, M., Dwibedi, V., Sharma, S. and George, N., 2022. Biogenic silica nanoparticles from agro-waste: Properties, mechanism of extraction and applications in environmental sustainability. *Journal of Environmental Chemical Engineering*, p.108550.

[2] Praneetha, S. and Murugan, A.V., 2015. Development of sustainable rapid microwave assisted process for extracting nanoporous Si from earth abundant agricultural residues and

their carbon-based nanohybrids for lithium energy storage. *ACS Sustainable Chemistry & Engineering*, *3*(2), pp.224-236.

[3] Liu, N., Huo, K., McDowell, M.T., Zhao, J. and Cui, Y., 2013. Rice husks as a sustainable source of nanostructured silicon for high performance Li-ion battery anodes. *Scientific reports*, *3*(1), pp.1-7.

[4] Guo, M., Zou, X., Ren, H., Muhammad, F., Huang, C., Qiu, S. and Zhu, G., 2011. Fabrication of high surface area mesoporous silicon via magnesiothermic reduction for drug delivery. *Microporous and mesoporous materials*, *142*(1), pp.194-201.

[5] Jeong, J.H., Kim, K.H., Jung, D.W., Kim, K., Lee, S.M. and Oh, E.S., 2015. High-performance characteristics of silicon inverse opal synthesized by the simple magnesium reduction as anodes for lithium-ion batteries. *Journal of Power Sources*, *300*, pp.182-189.

[6] Zhou, Z., Han, G., Lu, X., Wang, G. and Zhou, X., 2022. High-performance magnesium-based thermoelectric materials: Progress and challenges. *Journal of Magnesium and Alloys*.

[7] Zhong, H., Zhan, H. and Zhou, Y.H., 2014. Synthesis of nanosized mesoporous silicon by magnesium-thermal method used as anode material for lithium ion battery. *Journal of Power Sources*, *262*, pp.10-14.

[8] Huang, Z.G., Gao, K., Wang, X.G., Xu, C., Song, X.M., Shi, L.X., Zhang, Y., Hoex, B. and Shen, W.Z., 2019. Large-area MACE Si nano-inverted-pyramids for PERC solar cell application. *Solar Energy*, *188*, pp.300-304.

[9] M. Li, Y. Dai, W. Ma, B. Yang, Q. Chu, IOP Conference Series, 94 (2017) 012016.

[10] Inasawa, S., Ono, Y., Mizuguchi, T., Sunairi, A., Nakamura, S.I., Tsuji, Y. and Yamaguchi, Y., 2017. Cross-sectional analysis of the core of silicon microparticles formed via zinc reduction of SiCl 4. *CrystEngComm*, *19*(19), pp.2681-2686.

[11] Shen, P., Uesawa, N., Inasawa, S. and Yamaguchi, Y., 2010. Characterization of flowerlike silicon particles obtained from chemical etching: visible fluorescence and superhydrophobicity. *Langmuir*, *26*(16), pp.13522-13527.

[12] Bao, Z., Weatherspoon, M.R., Shian, S., Cai, Y., Graham, P.D., Allan, S.M., Ahmad, G., Dickerson, M.B., Church, B.C., Kang, Z. and Abernathy Iii, H.W., 2007. Chemical reduction of three-dimensional silica micro-assemblies into microporous silicon replicas. *Nature*, *446*(7132), pp.172-175.

[13] Kim, K.H., Lee, D.J., Cho, K.M., Kim, S.J., Park, J.K. and Jung, H.T., 2015. Complete magnesiothermic reduction reaction of vertically aligned mesoporous silica channels to form pure silicon nanoparticles. *Scientific reports*, *5*(1), pp.1-7.

[14] Xing, A., Tian, S., Tang, H., Losic, D. and Bao, Z., 2013. Mesoporous silicon engineered by the reduction of biosilica from rice husk as a high-performance anode for lithium-ion batteries. *RSC advances*, *3*(26), pp.10145-10149.

[15] Seroka, N.S., Taziwa, R. and Khotseng, L., 2022. Green synthesis of crystalline Silica from Sugarcane Bagasse Ash: Physico-chemical properties. *Nanomaterials*, *12*(13), p.2184.

[16] Atkins, P. and Overton, T., 2010. *Shriver and Atkins' inorganic chemistry*. Oxford University Press, USA.

[17] Li, B., Yu, D. and Zhang, S.L., 1999. Raman spectral study of silicon nanowires. *Physical Review B*, *59*(3), p.1645.

[18] Xia, H., He, Y.L., Wang, L.C., Zhang, W., Liu, X.N., Zhang, X.K., Feng, D. and Jackson, H.E., 1995. Phonon mode study of Si nanocrystals using micro-Raman spectroscopy. *Journal of Applied Physics*, *78*(11), pp.6705-6708.

[19] Holzapfel, M., Buqa, H., Hardwick, L.J., Hahn, M., Würsig, A., Scheifele, W., Novák, P., Kötz, R., Veit, C. and Petrat, F.M., 2006. Nano silicon for lithium-ion batteries. *Electrochimica acta*, *52*(3), pp.973-978.

[20] Richter, H., Wang, Z.P. and Ley, L., 1981. The one phonon Raman spectrum in microcrystalline silicon. *Solid State Communications*, *39*(5), pp.625-629.

[21] Zhang, S.L., Wang, X., Ho, K.S., Li, J., Diao, P. and Cai, S., 1994. Raman spectra in a broad frequency region of p− type porous silicon. *Journal of applied physics*, *76*(5), pp.3016-3019.

[22] Kale, P.G. and Solanki, C.S., 2010, June. Synthesis of si nanoparticles from freestanding porous silicon (PS) film using ultrasonication. In *2010 35th IEEE Photovoltaic Specialists Conference* (pp. 003692-003697). IEEE.

[23] Lee, J.H., Kwon, J.H., Lee, J.W., Lee, H.S., Chang, J.H. and Sang, B.I., 2017. Preparation of high purity silica originated from rice husks by chemically removing metallic impurities. *Journal of Industrial and Engineering Chemistry*, *50*, pp.79-85.

[24] Gregg, S.J., Sing, K.S.W. and Salzberg, H.W., 1967. Adsorption surface area and porosity. *Journal of The electrochemical society*, *114*(11), p.279Ca.

[25] Falk, G., Shinhe, G.P., Teixeira, L.B., Moraes, E.G. and de Oliveira, A.N., 2019. Synthesis of silica nanoparticles from sugarcane bagasse ash and nano-silicon via magnesiothermic reactions. *Ceramics international*, *45*(17), pp.21618-21624.

CHAPTER 6: Novel nanostructured Silicon-doped thin films by e-beam PVD for solar energy materials

Synopsis

This chapter discusses the synthesis and application of p-type and n-type doped crystalline silicon materials in thin-film solar cells. The study was conducted as part of the requirements for the PhD degree in Chemistry at the Energy Lab, Department of Chemistry, University of the Western Cape, and Ithemba Lab (NRF). In the quest to find suitable solar energy materials, the immediacy of high demand for energy, and the depletion of fossil fuels as energy sources, the world has shifted focus to renewable energy sources. This research focuses on the development of low-cost silicon sources that contain a significant amount of silica from sugarcane bagasse.

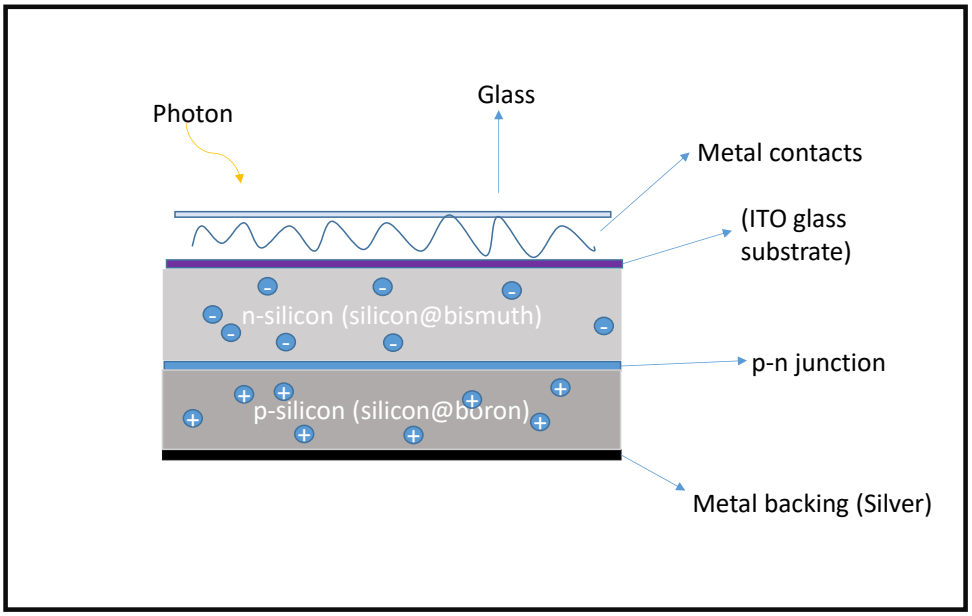

Figure 6.1: *Representation of the solar cell architecture that will be of focus in this study*

Abstract

The utilization and depletion of fossil fuels, global warming, an ever-increasing population, and industrial advancements all encourage the world to find alternative sources of energy. Solar technology has the potential to be an ideal alternative compared to other renewable energy sources given the geographical location of the current study. The materials prepared

in Chapter 4 and their subsequent transformation to silicon in Chapter 5 were used to fabricate a solar cell in this study. The fabrication and testing of solar cell devices has resulted in a worldwide desire for scientists to improve and reduce the costs of the materials that already dominate the photovoltaic market. This chapter will focus on the development of photovoltaic cells and evaluate their optical and electrical properties, as well as the efficacy of the cell. The device will be fabricated using ITO glass substrates with silicon, bismuth, boron, and silver as the rear contacts. The impurities were introduced in the layers to significantly improve the solar energy conversion to electrical energy. The results show that the introduction of foreign molecules is a beneficial tool to enhance the charge transport processes in the preparation of a photovoltaic cell.

6.1. Background

Energy consumption has steadily increased alongside civilization. The compounding energy crisis due to a decrease in fossil fuel stocks and rapidly increasing carbon dioxide emissions that are causing global warming has poked interest in the development of clean, renewable sources of energy. The quality of human development and life itself makes it necessary to sustain the projected electrical energy consumption in the future [1].

Solar energy holds enormous promise as an economically viable and environmentally friendly renewable energy source. To date, silicon-based solar cells dominate the market owing to their rapid and wide development. They have attracted not only much theoretical research but also technological applications in scaled-up manufacturing. Various commercial crystalline Si solar cells with conversion efficiencies of 14%–17% have been steadily developed in the last decade. In addition, the cost performance of crystalline Si-based solar cells exhibiting conversion efficiencies above 18% to 20% is poised to advance the green energy industry [1-4].

Despite, the conversion efficiency thus far realized falls short of the theoretical target of 29.8% for crystalline Si. This implies that a thorough understanding of these crystalline Si is required; consequently, solar cell fabrication technologies inspire further development. In the quest to achieve this goal, it does not necessitate individual consideration of the spatially distributed foreign substances and defects in crystalline Si; however, a comprehensive, in-depth knowledge of the various problems associated with crystalline Si and the numerous

thermal processes used during the fabrication of a solar cell is necessary to clearly state the reasons for the decline in the conversion efficiency of crystalline Si solar cells [5,6].

Transparent conducting indium tin oxide (ITO) materials are widely used in various types of solar cells due to their excellent optical transparency and electrical conductivity. Moreover, crystalline silicon solar cells are doped to form the p-n junction (emitter/bulk junction) and/or to preserve the minority carriers from recombination near the contacts (back surface field or front surface field) [7].

The doping process can be achieved through various techniques such as ion implantation, dopant diffusion in the gas phase, the growth of doped epitaxial layers, or the diffusion of dopants from dielectric layers. The processes normally depend on the atomic diffusivity of impurities in Si, but it has been revealed that a thermal budget as high as 1000 ℃ is required to diffuse the dopant source (boron in this instance) inside the crystalline silicon substrate [7-9].

6.2. Material characterization

6.2.1. Raman characterization

In order to study the microstructural properties of crystalline silicon thin films doped with bismuth and boron, respectively, Raman spectra were conducted. The crystalline Si thin films were prepared with the e-beam technique and deposited on glass substrates covered with a thin indium tin oxide (ITO) layer. Figure 6.2 shows the Raman spectra of Si thin films prepared at different working vacuum pressures [10].

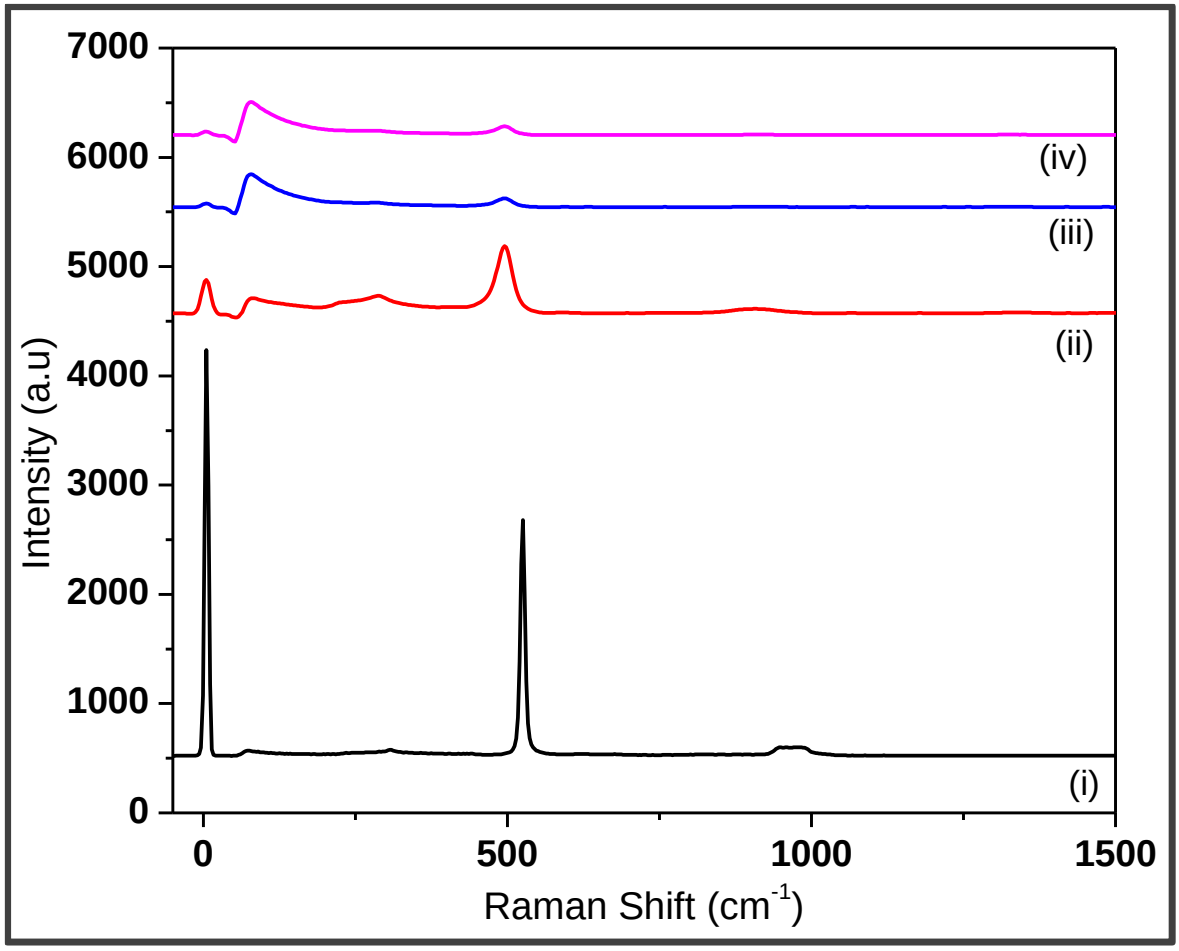

Figure 6.2: *Raman thin films of (i) pristine silicon, and (ii), (iii), (iv) nanocrystalline silicon thin films deposited on ITO glass substrates using e-beam PVD at vacuum pressures of $1.2x10^{-6}$, $2.4x10^{-6}$ and $7.2x10^{-6}$ Torr, respectively.*

All the samples displayed a strong peak near 520 cm^{-1}, confirming the large crystallinity of those Si thin films. Concurrently, at lower pressures, the peak intensity became gradually larger for the samples. As a result, at lower pressures, Si thin films are aided in crystallization. The peak at near 520 cm^{-1} corresponds to crystalline silicon. They are not at their usual peak position, possibly due to the mixed state of the grain boundary, and foreign atoms present in the silicon matrix [10].

6.2.2. Optical properties

The optical properties of Si thin films were investigated with a UV/Vis spectrophotometer. The samples were deposited on ITO-coated glass substrates and all annealed at 200 ℃, for 2 h in a tube furnace under nitrogen atmosphere.

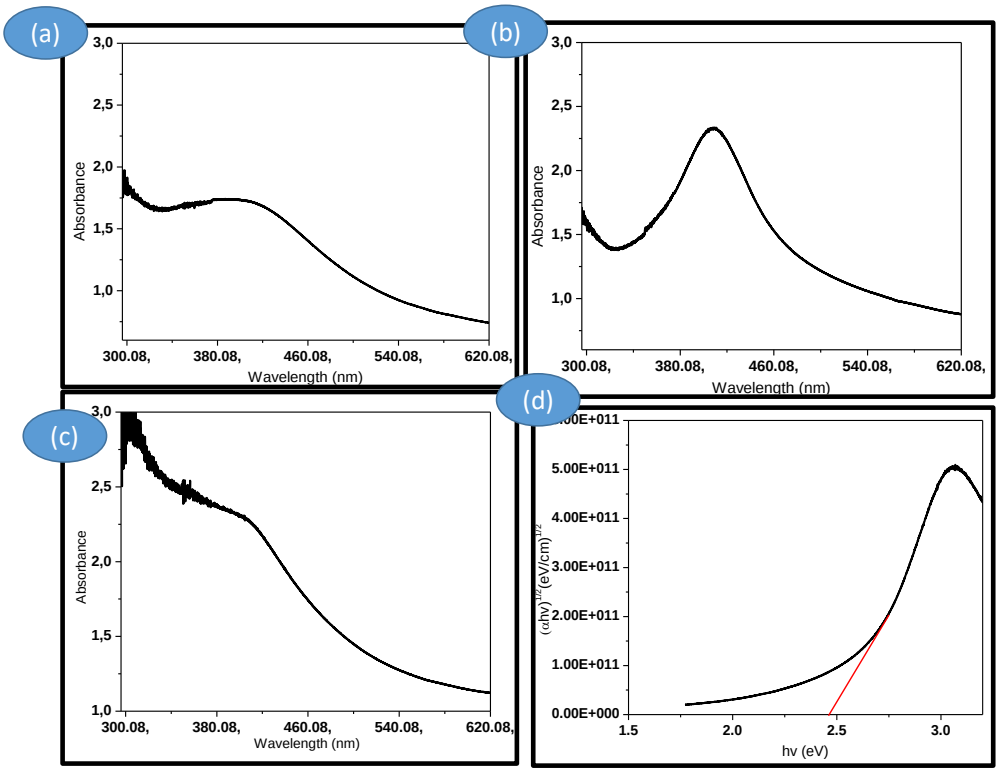

***Figure 6.3**: UV/Vis spectra of nanostructured silicon thin films deposited on ITO glass substrates using e-beam PVD at vacuum pressures (a) 1.2 x 10^{-6}, (b) 2.4 x 10^{-6} (c) 7.2 x 10^{-6}, (d) Tauc-plot*

The optical properties were cross-examined UV/Vis spectroscopy, shown in figure 6.3 (a)-(d). Notably, the absorption wavelength is affected by film thickness, and it was determined for figure 6.3 (b) the optical band gap to be ($\lambda = \frac{1240}{420} = 2.95\ eV$), which is slightly higher than the desired band gap for solar cells in the range $1 - 2\ eV$. Interestingly, the other films showed positive and broad absorption band in the range 300-500 nm [11-14]. The intersection on hv-axis, shown in figure 6.3 d, is 2.46 eV which is coincidently higher than the crystalline-silicon.

6.2.3. AFM analysis

The surface roughness of silicon-doped thin films produced on ITO substrates was assessed using the AFM technique. Figure 6.4a depicts an 2D AFM image of the surface of a crystalline silicon thin film solar cell as it was after deposition and 200 ℃ annealing. Surface roughness that corresponds to this is 35.9 nm. In figure. 41a and c, the surface roughness is

depicted. The surface of these samples underwent a thermo-chemical treatment, which is what gave rise to the final surface roughness value [15].

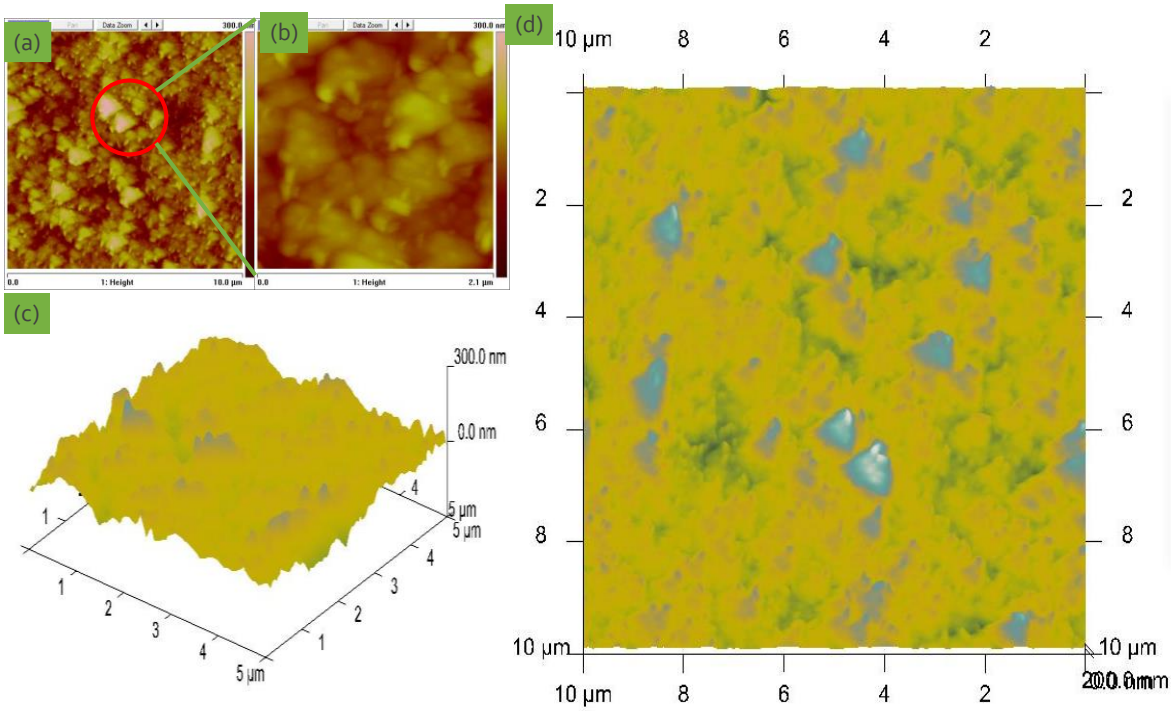

***Figure 6.4**: AFM images of the nanostructured silicon thin films surfaces (a) top view, (b) zoom-section in a, (c) 3D image and (d) 2D image.*

Figures 6.4 c and d show 3D and top view images of nc-SiOx:Bi:nc-SiOx:B:Ag deposited on an ITO glass substrate. In addition, I was able to estimate the surface roughness and density from the latter. The estimated values are the root-mean-square roughness (Rq) = 45.4 nm, the average roughness (Ra) = 35.2 nm, and the maximum height (Rz) = 37.4 nm. Interestingly the roughness evens out by reducing to Rq = 13.2 nm and Ra = 10.8 throughout the film [15].

6.3. Material application (Photovoltaic efficiency)

The prepared materials were used to obtain the I-V characteristics of the fabricated solar cells shown in; figure 6.5 -a and b; silicon powder into pellets, metallic bismuth, boron powder into pellets, and silver powder into pellets. The n-type layer was achieved through doping silicon thin film with bismuth film; the p-type layer was obtained by doping silicon thin film with boron thin film. As a result, n-type and p-type thin films with distinct properties are produced, the former as an electron transporting film and the latter as a hole

transporting film. Because Ag tends to diffuse easily into the p-type film, making it more positive and thus heavily doped, it was chosen as the rear contact for this typical nanocrystalline silicon-based cell rather than Aluminium (Al) [16,17].

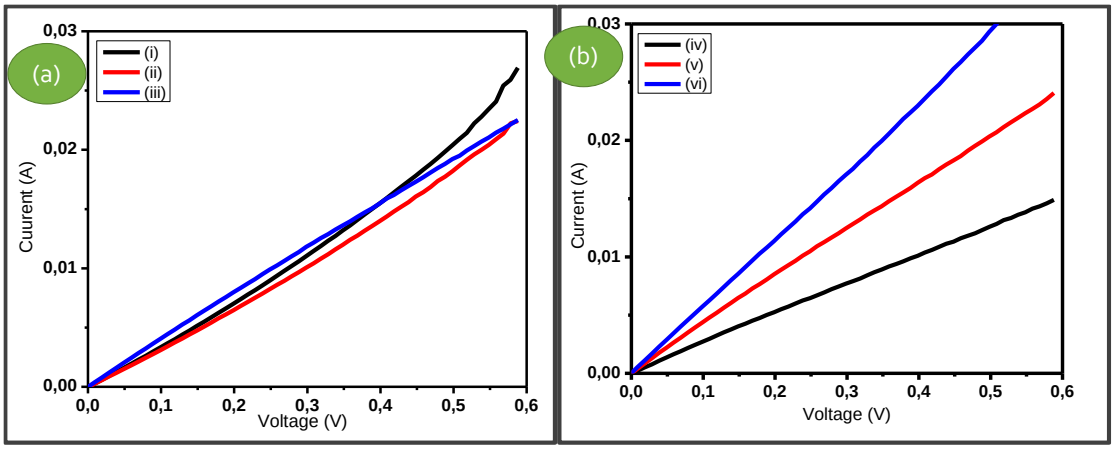

***Figure 6.5**: Solar-to-electricity conversion capabilities of nanostructured crystalline silicon thin films prepared at (a) 250 ℃ and (b) room temperature deposited on ITO glass substrates.*

The prepared solar cells were evaluated for their power conversion efficiencies, and the results are presented in tables 6.1 and 6.2, which give a summary of the obtained results on the photovoltaic efficiencies of the prepared thin films of the same thickness. The devices were prepared at various temperatures; for example, the results in Table 6.1 were prepared at temperatures around 250, whereas the results in Table 6.2 were prepared at room temperature of 19°C [17-20].

***Table 6.1**: Photovoltaic efficiencies of nc-Si/Bi@nc-Si/B@Ag deposited at 250 ℃.*

Obtained results	e-beam Vacuum (Torr)	e-beam Vacuum (Torr)	e-beam Vacuum (Torr)
Parameters	*1.2x10^{-6}*	*2.4x10^{-6}*	*7.2x10^{-6}*
J_{sc}(μA)	0.181	0.0025	0.0035
V_{oc}(mV)	0.0788	-0.0016	-2.54 x 10^{-5}
P_{max} (μmW)	3572	50.28	584.80
FF (%)	23.2	15.0	30.0
PCE (%)	0.0042	1.19 x 10^{-5}	7.2 x 10^{-5}

Among all the prepared devices at different temperatures, the room temperature was found to possess the optimal photovoltaic efficiency. Although the very low power conversion efficiencies might arise from the boron content in the p-type silicon thin film, E-beam is a poor technique for boron deposition, lowering the quality of the thin film layer. All the devices were annealed at 200 in a tube furnace for 2 hours.

***Table 6.2**: Photovoltaic efficiencies of nc-Si/Bi@nc-Si/B@Ag deposited at room temperature.*

Obtained results	e-beam Vacuum (Torr)	e-beam Vacuum (Torr)	e-beam Vacuum (Torr)
Parameters	$1.2x10^{-6}$	$2.4x10^{-6}$	$7.2x10^{-6}$
J_{sc}(μA)	0.498	0.018	0.019
V_{oc}(mV)	0.310	0.0080	0.0081
P_{max} (μmW)	4883	446	225
FF (%)	29.6	23.6	20.0
PCE (%)	0.0145	1.6×10^{-5}	3.5×10^{-5}

The corresponding photovoltaics parameter summarized in tables 6.1 and 6.2 reveals that thin film solar cells are thickness-dependent, and finding the optimal thickness will result in the optimization of the solar conversion to electricity. The open circuit voltage (V_{oc}) and short circuit current density (J_{sc}) were too low to give rise to significant PCE.

6.4. Summary

In this chapter, the crystalline silicon-doped thin films were deposited at different vacuum pressures in the range of 1.2×10^{-6} to 7.2×10^{-6} for solar energy materials. The ITO glass substrates were preheated to 250 to aid in the deposition process. Silicon was stored first in tangulum e-beam liners because it melts efficiently there, followed by bismuth in an alumina crucible, boron in a glassy-graphite coated e-beam liner, and metallic silver in an alumina crucible.

The thin films were deposited at 250 and annealed at 200 for 2 hours in a tube furnace. The cells were then prepared with the same thickness, but the deposition was carried out at room temperature. Consequently, they were annealed at 200 ℃ for 2 hours in a tube furnace. The

optical, structural, and electrical properties of these cells were cross-examined using Raman, AFM, UV/Vis, and the AM1.5 testing station.

The results obtained in this study (0.01%) were considerably low for crystalline silicon solar cells with over 25% efficiency. This is experiential learning, and there is potential for solar energy materials. The cells showed they are capable of generating photo-carriers under illumination, and this is the first time fabricating crystalline silicon solar energy materials on ITO glass substrates, which proves to be a good contribution to knowledge.

6.5. References

[1] Glunz, S.W. and Feldmann, F., 2018. SiO2 surface passivation layers–a key technology for silicon solar cells. *Solar Energy Materials and Solar Cells*, *185*, pp.260-269.

[2] El Chaar, L. and El Zein, N., 2011. Review of photovoltaic technologies. *Renewable and sustainable energy reviews*, *15*(5), pp.2165-2175.

[3] Liu, J., Yao, Y., Xiao, S. and Gu, X., 2018. Review of status developments of high-efficiency crystalline silicon solar cells. *Journal of Physics D: Applied Physics*, *51*(12), p.123001.

[4] Essig, S., Allebé, C., Remo, T., Geisz, J.F., Steiner, M.A., Horowitz, K., Barraud, L., Ward, J.S., Schnabel, M., Descoeudres, A. and Young, D.L., 2017. Raising the one-sun conversion efficiency of III–V/Si solar cells to 32.8% for two junctions and 35.9% for three junctions. *Nature Energy*, *2*(9), pp.1-9.

[5] Allen, T.G., Bullock, J., Yang, X., Javey, A. and De Wolf, S., 2019. Passivating contacts for crystalline silicon solar cells. *Nature Energy*, *4*(11), pp.914-928.

[6] Chopra, K.L., Paulson, P.D. and Dutta, V., 2004. Thin-film solar cells: an overview. *Progress in Photovoltaics: Research and applications*, *12*(2-3), pp.69-92.

[7] Liu, Y., Li, Y., Wu, Y., Yang, G., Mazzarella, L., Procel-Moya, P., Tamboli, A.C., Weber, K., Boccard, M., Isabella, O. and Yang, X., 2020. High-efficiency silicon heterojunction solar cells: materials, devices and applications. *Materials Science and Engineering: R: Reports*, *142*, p.100579.

[8] Avrutin, V., Izyumskaya, N. and Morkoç, H., 2011. Semiconductor solar cells: Recent progress in terrestrial applications. *Superlattices and Microstructures*, *49*(4), pp.337-364.

[9] Rimini, E., 1994. *Ion implantation: basics to device fabrication* (Vol. 293). Springer Science & Business Media.

[10] Dhar, S., Mandal, S., Das, G., Mukhopadhyay, S., Ray, P.P., Banerjee, C. and Barua, A.K., 2015. Silicon heterojunction solar cells with novel fluorinated n-type nanocrystalline

silicon oxide emitters on p-type crystalline silicon. *Japanese Journal of Applied Physics*, *54*(8S1), p.08KD03.

[11] Gaponenko, S.V., 1998. *Optical properties of semiconductor nanocrystals* (No. 23). Cambridge university press.

[12] Bakry, A.M., 2008. Influence of film thickness on optical properties of hydrogenated amorphous silicon thin films. *Egypt. J. Solids*, *31*(1), p.11566.

[13] Pankove, J.I., 1975. *Optical processes in semiconductors*. Courier Corporation.

[14] Shaaban, E.R., Soraya, M.M., Shapaan, M., Hassan, H.S. and Samar, M.M., 2017. Applying wedge shape model for calculating both film thickness and optical constants of SeSZn films with high precision for optoelectronic devices. *Journal of Alloys and Compounds*, *693*, pp.1052-1060.

[15] Dhar, S., Mandal, S., Das, G., Mukhopadhyay, S., Ray, P.P., Banerjee, C. and Barua, A.K., 2015. Silicon heterojunction solar cells with novel fluorinated n-type nanocrystalline silicon oxide emitters on p-type crystalline silicon. *Japanese Journal of Applied Physics*, *54*(8S1), p.08KD03.

[16] He, B., Wang, H., Li, Y., Ma, Z., Xu, J., Zhang, Q., Wang, C., Xing, H., Zhao, L. and Wang, D., 2013. Fabrication and characterization of amorphous ITO/p-Si heterojunction solar cell. *Science China Technological Sciences*, *56*(8), pp.1870-1876.

[17] Bae, S., Oh, W., Lee, K.D., Kim, S., Kim, H., Park, N., Chan, S.I., Park, S., Kang, Y., Lee, H.S. and Kim, D., 2017. Potential induced degradation of n-type crystalline silicon solar cells with p+ front junction. *Energy Science & Engineering*, *5*(1), pp.30-37.

[18] Ryu, K., Lee, Y.J., Ju, M., Choi, H., Kim, B., Lee, J., Oh, W., Choi, K., Balaji, N. and Yi, J., 2012. Optimal indium tin oxide layer as anti reflection coating for crystalline silicon solar cell with shallow emitter. *Thin Solid Films*, *521*, pp.50-53.

[19] Glunz, S.W. and Feldmann, F., 2018. SiO2 surface passivation layers–a key technology for silicon solar cells. *Solar Energy Materials and Solar Cells*, *185*, pp.260-269.

[20] Feldmann, F., Simon, M., Bivour, M., Reichel, C., Hermle, M. and Glunz, S.W., 2014. Efficient carrier-selective p-and n-contacts for Si solar cells. *Solar Energy Materials and Solar Cells*, *131*, pp.100-104.

Chapter 7

7.1. Summary of major findings

The study was effective, according to the results that were reported. The thesis' goals and objectives were achieved, and significant advances were found. The study's major objective was to prepare silicon semiconductor thin films for solar energy materials principally from sugarcane bagasse ash. As described earlier in Chapter 3, sugarcane bagasse was burned insufficiently to produce ash. After that, silica was extracted using an organic base as an extracting agent and an organic acid as a pre-treatment. Then, using a metallothermic (magnesiothermic reaction) reduction technique, nanosilica was converted into nanostructured silicon in a tube furnace to create nanosilicon from sugarcane bagasse ash.

All of the prepared materials were thoroughly examined using FTIR, XRD, TGA, XRF, Raman, BET, TEM, SEM, AFM, and UV/VIS. The extracted crystallite size ca-silica and L-cys-silica had an average diameter of 26 nm and 29 nm, respectively, as well as specific surface areas of 21.6511 m^2/g and 116.005 m^2/g for ca-silica and L-cys-silica, respectively. Peaks in the FTIR spectra were found at 461.231 cm^{-1}, 787.381 cm^{-1}, and 11045.99 cm^{-1}, which correspond to the $Si-O-Si$ bending vibration, $SiO-S-$i stretch vibration, and $Si-O-Si$ stretching vibration, respectively. The nanosilicon nanoparticles were successfully synthesized from extracted biosilica from sugarcane bagasse ash (SCBA), with the as-synthesized silicon having surface area, pore volume, and pore diameter of 73.58 m^2/g, 0.23 cm^{-1}, and 12 nm, respectively. The FTIR spectrum confirms the increase in particle oxidation during deionized water washing, with peaks at 446 cm^{-1} and 1056 cm^{-1}.

The e-beam PVD process was used to create the silicon-doped thin films, which are essentially perfect for the solar spectrum's visible range. In Chapter 6, nanostructured materials are used to increase the power conversion efficiency of the solar-to-electricity ratio or relationship by focusing practically all of the energy from the visible portion of the solar spectrum. For crystalline silicon solar cells with an efficiency of over 25%, the results from this study (0.01%) were noticeably low. There is a chance for solar energy materials in this type of practical learning. This is the first time producing crystalline silicon solar energy materials on ITO glass substrates, which proved to be a good contribution to knowledge. The cells demonstrated their ability to generate photo-carriers under illumination.

7.2. Conclusion

The study showed that an agricultural residue, sugarcane bagasse, can be harnessed for industrial purposes in South Africa for a range of applications, including functional nanomaterials, polymers, biotechnology, and solar energy materials. Most importantly, the results reported indicate that nanostructured silicon can be produced from sustainable sources.

The objectives were met satisfactorily, comprehensive literature review was done and were able to extract silica from sugarcane bagasse ash. Despite the availability of numerous studies on the synthesis and application of nano silicon, there is little information available on its production from natural resources. as well as its commercial applications. Thus, the goals of this research were to create silicon nanoparticles from nano silica produced by magnesiothermic reduction of SCBA, and to use the resulting material in solar cell applications. Every single sample, the products were thoroughly characterized at neutral pH and 700°C. Lastly, the silicon thin films solar cells were fabricated using e-beam PVD technique.

7.2. Recommendations and future work

Crystalline silicon thin films have proven and showed hope for improved efficiencies over the years and potential reduction in manufacturing costs.

An ideal solar cell, it is expected to exhibit high conversion rate of solar energy to electrical energy from low cost materials.

- Study and determine the high quality of waste to valuable materials after purification
- Investigate the power conversion efficiency of valuable products from biomass

Study and report on the opto-electronic properties of solar suitable materials in testing conditions. The optimal efficiency for crystalline silicon thin film reported thus far in literature show a distinct architecture from the one reported in this study. The recently reported silicon thin film solar cells utilize crystalline silicon therefore; I would recommend the introduction of nanostructured silicon derived from industrial agro-waste on the solar cell design.

Finally, future research should prioritize waste material research and development for solar energy materials among electronic applications. Nonetheless, utilization of waste to valuable materials can potentially bring about various benefits to solar cell materials and manufacturing, including simplified and low-cost fabrication processes, ideally without impurities, while enabling high solar-to-electricity conversion efficiencies.